PHENOMENOLOGICAL CONSEQUENCES OF NEUTRINO OSCILLATIONS

by

Mohan Narayan

A THESIS IN PHYSICS

Presented to the University of Madras in partial fulfillment of
the requirements for the degree of Doctor of Philosophy

SEPTEMBER 1998

THE INSTITUTE OF MATHEMATICAL SCIENCES

C.I.T. Campus, Taramani
CHENNAI–600 113, INDIA

DEDICATED TO

MY PARENTS

Acknowledgments

THE INSTITUTE OF MATHEMATICAL SCIENCES

C I T CAMPUS, TARAMANI, MADRAS 600 113, INDIA

Prof. M. V. N. Murthy

Phone: (044)235 1856, (044)235 0588
(044)235 1049, (044)235 1050
Fax: (044)235 0586; Grams: MATSCIENCE
Telex: 041 8960 PCO IN PP WDT 20
E-Mail: murthy@imsc.ernet.in
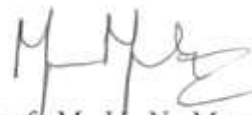
CERTIFICATE

This is to certify that the Ph.D. thesis submitted by Mohan Narayan to the University of Madras, entitled **Phenomenological Consequences of Neutrino Oscillations** is a record of bonafide research work done by him under my supervision. The research work presented in this thesis has not formed the basis for the award to the candidate of any Degree, Diploma, Associateship, Fellowship or other similar titles.

It is further certified that the thesis represents independent work by the candidate and collaboration when existed was necessitated by the nature and scope of problems dealt with.

Prof. M. V. N. Murthy

September, 1998.

Thesis Supervisor

ii

Contents

Chapter 0

Abstract

0.1 Introduction

Neutrinos are electrically neutral spin half particles which interact only via weak interactions with other particles. Historically the neutrino was first postulated by Wolfgang Pauli to explain apparent violation of energy momentum conservation in nuclear beta decay. The particle first proposed by Pauli is what we call today the electron antineutrino denoted as $\bar{\nu}_e$, the particle which accompanies the electron in weak interaction processes. Its antiparticle the electron neutrino denoted as ν_e accompanies the positron in weak interactions. Today we know that there are three types or flavors of neutrinos, the electron type ν_e, the muon type ν_μ which accompanies the muon in weak interactions, and the tau type denoted by ν_τ, which accompanies the tau lepton in weak processes.

Presently neutrinos form one of the building blocks of the GSW (Glashow, Weinberg, and Salam) model of weak and electromagnetic interactions. In this model the neutrino is assumed to be a massless particle paticipating only in the weak interactions. This model is consistent with all the laboratory data examined so far, and, there is no irrefutable evidence for neutrino mass.

A problem however arises when one considers neutrinos from extraterrestrial sources, specifically neutrinos from the sun and neutrinos from the atmosphere.

The first major discrepancy between theory with massless neutrinos and data came with respect to neutrinos from the sun, i.e solar neutrinos. The mechanism which is responsible for energy release in the sun is nuclear fusion. A byproduct of the fusion reactions are the electron type of neutrinos. Astrophysical models of the sun, called as the standard solar model of the sun (SSM) predict a definite flux of these electron neutrinos which should reach the earth. Experiments which have measured the flux of these neutrinos have consistently found less number of neutrinos vis a vis the SSM. This is called the solar neutrino problem, and it has been with us for over thirty years. It is also extremely difficult to reconcile data with theory by changing the parameters of the SSM, as the SSM has to satisfy other conditions like for example the luminosity constraint.

However, there exists another attractive alternative by which the Solar Neutrino problem may be resolved, and that is the idea of neutrino oscillations. If neutrinos are massive, then they may mix with each other, i.e the flavor states could be different from the mass eigenstates, and they can be linear combinations of the mass eigenstates. These mass eigenstates have masses, μ_1 and μ_2 say in the framework of only two flavors. One can now have the phenomenon of flavor oscillations, i.e., a neutrino of one flavor can get converted into a neutrino of another flavor after propagating for some time. This conversion process is basically controlled by the mixing angle θ between the two neutrinos, and the difference between the masses of the two mass eigenstates $\delta_{21} = \mu_2^2 - \mu_1^2$. Also the conversion can be drastically different in matter, as compared to conversion in vacuum, due to what is known as the Mikhail, Smirnov and Wolfenstein effect or the MSW effect. It is immediately obvious that oscillations via mixing is possible only for massive neutrinos, therefore any positive signal of oscillations, is also a signal for new physics beyond the GSW model.

Another problem that has emerged recently is the so called atmospheric neutrino problem. The atmosphere is a source of electron as well as muon type of neutrinos and antineutrinos. These neutrinos are the end product of a cascade process which is triggered by cosmic rays interacting with nuclei in the earth's atmosphere. There are Monte carlo predictions for these fluxes, and experiments have measured these

respect to the monte carlo predictions, while the electron type of neutrinos are in reasonable agreement with the Monte carlo predictions.

More importantly if one analyzes the solar and atmospheric neutrino problems with massive neutrinos, then it may be possible to reconcile experiment with theoretical predictions. There have been many analyses of the solar and atmospheric neutrino problems, in a scenario where one flavor of neutrino mixes with the other flavor, and it has been demonstrated that one can reconcile theory with either the solar or the atmospheric neutrino experiment depending on which experiment one analyzes, and that there is a region in the two flavor parameter space, i.e in the θ and δ_{21} space where one gets agreement with experiment. But the crucial point to be noted is that, the mass scale (i.e the δ) that is required for these two problems are drastically different. This immediately tells us that one needs two independent mass squared differences, and hence at least three mass eigenstates. This in turn implies that we need at least three flavors of neutrinos. Now a major drawback of a two flavor analysis is that the influence of the third flavor on the two flavor results are unknown. The inclusion of the third flavor could lead to significantly different results. Also independently we know from LEP data, that the number of light neutrino species is three. So any realistic analysis of these problems with neutrinos must take all the three flavors into account.

This thesis makes a systematic analyses of the solar and the atmospheric neutrino problems in a single framework in which all the three flavors of neutrinos can mix with each other. The region which is allowed by solar and atmospheric neutrino data in the three neutrino parameter space is mapped out. It is shown that one gets bounds on all the five parameters which control the oscillations. Novel effects of neutrino oscillations such as the day- night asymmetry observable in the real time solar neutrino detectors. The possible enhancement of the solar neutrino counting rate during a solar eclipse is analyzed. It shown how these can constrain the neutrino parameter space mapped out previously. It is pointed out that these effects can establish, in a model independent way, the fact that neutrinos are massive as these effects can occur only if neutrinos oscillate. These effects can be probed efficiently by the high statistics detectors like Super-Kamiokande, Borexino , SNO etc. Lastly

by the high statistics detectors like Super-Kamiokande, Borexino , SNO etc. Lastly
we take the constraints coming from terrestrial experiments into account, and show
that this can drastically reduce the allowed region in the three flavor parameter
space, and also give an estimate of the contribution of various channel of oscillations
to different experiments.

A summary of the mail results of this thesis is as follows.

0.2   The solar neutrino problem

We describe the salient features of the solar neutrino problem. The point is em-
phasised that the suppression seen by the various detectors is an energy dependent
quantity. Because of this it is extremely difficult to explain the solar neutrino prob-
lem through modifications to the SSM. Therefore neutrino oscillations provides a
very attractive alternative as a possible solution to the solar neutrino problem. The
solar neutrino problem is then analyzed in the context of three flavor neutrino oscil-
lations. We assume a mass heirarchy in the vacuum mass eigenvalues $\mu_3^2 \gg \mu_2^2 \geq \mu_1^2$,
but make no approximation regarding the magnitudes of the mixing angles. It is
shown that the solar neutrino problem involves only three of the five parameters rele-
vant to three flavor oscillations, viz δ_{21}, the (12) mixing angle ω, and the (13) mixing
angle ϕ. We develop a perturbative analysis of the neutrino evolution equations in
the sun, and obtain a three flavor expression for the MSW resonance condition in
the sun. Finally we develop an analytic expression for the electron neutrino survival
probability on the surface of the earth. Using this expression we compute the solar
neutrino detection rates for the various detectors. We map out the allowed region
in the three parameter space using the constraints coming from the available data,
i.e from the solar neutrino experiments. We also compute the recoil electron energy
spectrum in detectors that use $\nu_e - e$ scattering (mainly the high statistics detectors
like Super-Kamiokande, The Sudbury Neutrino Observatory(SNO) and Borexino),
and show that it can distinguish between some regions in the parameter space.

0.3   The atmospheric neutrino problem

We introduce the atmospheric neutrino problem and then analyze the atmospheric neutrino data in the context of three flavor neutrino oscillations. With the hierarchy among the vacuum mass squares, $\mu_3^2 \gg \mu_2^2 \geq \mu_1^2$, we show that the solution of the atmospheric neutrino problem depends on $\delta_{31} = \mu_3^2 - \mu_1^2$ and the (13) and (23) mixing angles ϕ and ψ. Therefore the atmospheric neutrino problem is also a three parameter problem with the parameter ϕ being the common parameter between the two problems. We first analyze the sub-GeV data on atmospheric neutrinos and find that a lower limit on $\delta_{31} > 10^{-3}$ eV^2 can be got. We then analyze the zenith angle dependent suppression observed in the multi-GeV data and find that it limits δ_{31} from above also. The allowed regions of the three parameter space are strongly constrained by the multi-GeV data. Consistent with our earlier solution to the solar neutrino problem which depends on $\delta_{21} = \mu_2^2 - \mu_1^2$ and the (12) and (13) mixing angles ω and ϕ, we obtain the ranges of values of the five neutrino parameters which solve both the solar and the atmospheric neutrino problems simultaneously. Therefore the two problems together give us bounds on all the three mixing angles of the neutrino mixing matrix. Note that this is possible only in a three flavor framework where both the problems are addressed simultaneously unlike two flavor analyses where only one problem can be addressed at a time.

0.4   Novel effects of neutrino oscillations

If neutrino oscillations are indeed the solution to the solar and atmospheric neutrino problems, then are there other signals for this phenomenon which unlike the solar and atmospheric neutrino problems do not depend on astrophysical predictions of the solar neutrino fluxes, and the monte-carlo predictions of the atmospheric neutrino fluxes? The one effect which was realised quite some time ago which could demonstrate such a signal is the so called day-night effect. It is possible to see this effect in the real time solar neutrino detectors. This effect has been analyzed in the literature for the case of two flavor mixing. We do the analysis of the day-night effect

in a genuine three flavor case, and demonstrate that the third flavor distinctly alters the two flavor results. We believe ours is the first calculation of this kind with three neutrinos included. We also develop an analytic way of handling the night regeneration effect, whereas previous efforts were based on brute force numerical integration. We show that this analytic formula agrees very well with the previous two flavor results (which we get as a limiting case) which were based on numerical integration. Most importantly absence of day-night effect is instrumental in constraining a part of the solar neutrino parameter space.

If the earth can affect the solar neutrinos on their way to the detector in the night, then it is quite likely that during a solar eclipse, the moon too could affect the neutrinos on their way to the detector, especially since the Wolfenstein term due to the moon is of the same magnitude as that of the earth. And this effect again could be monitored by the real time detectors, since they continue taking data during the eclipse also, and most importantly they can measure the rate during the specific duration of the eclipse. If a change in the counting rate is seen during an eclipse as compared with the no eclipse rate, it would be a spectacular demonstration of the phenomenon of neutrino mixing and oscillations. This however requires a real time detector with high statistics. We do a three flavor analysis of such an effect, and show that such an effect can be measured by the high statistics real time detectors. Hence the eclipse effect is another spectacular signal of neutrino oscillations. Even the absence of such an effect constrains part of the solar neutrino parameter space, hence the eclipse effect is yet another window on neutrino physics.

0.5 Terrestrial experiments and future experiments

Up to now now the reactor and accelerator experiments which looked for signals of neutrino oscillations, were short baseline experiments, and hence were not capable of probing the actual three flavor parameter space allowed as fits to solar and atmospheric neutrino data. But the recent CHOOZ result is the first of the longbaseline experiments to probe the neutrino parameter space. We analyze the CHOOZ result

in a three flavor framework, and show that it has a dramatic influence in the three flavor parameter space when included as a constraint. As a spin off of this result, we show that the atmospheric neutrino anomaly is dominantly due to $\nu_\mu \leftrightarrow \nu_\tau$ oscillations, and hence the atmospheric neutrino problem is mainly due to vacuum oscillations. Therefore zenith dependence is a strong indication of the oscillating term which comes in the neutrino survival probabilities, which ultimately is a signal of neutrino oscillations. Also future long baseline experiments will be able to confirm the CHOOZ result.

Among the high statistics detectors which will start operating in the near future (Super-Kamioka has already started operating), one of the most important experiments will be the Borexino detector. We analyze the physics prospects of Borexino in the context of three flavor neutrino oscillations and show that Borexino measurements can focus on a very small region in the three flavor parameter space , and hence it is a powerful tool to distinguish between the various solutions to the solar neutrino problem. Because of its very high statistics, Borexino is an ideal tool to look for day-night effects in solar neutrino signals (which could be a very small effect for some values of the neutrino parameters). Therefore Borexino can probe an appreciable part of the neutrino parameter space, with no dependence at all on the absolute prediction of the ^7Be flux which is unique to this detector. An evidence for day-night effect from Borexino will be an unambiguos signal for neutrino mixing and oscillations.

0.6 Conclusions

In this chapter we summarize the main results of the thesis, and offer a few remarks. We also list some possibilities for future research.

This thesis is based on the following papers.

(1) "Solar and atmospheric neutrino oscillations with three flavors. "
Authors: Mohan Narayan, M.V.N. Murthy, G.Rajasekaran,
and S. Uma Sankar.

Phys. Rev. **D53** (1996) 2809

(2) "Atmospheric neutrino oscillations with three flavors. "
Authors: Mohan Narayan, G.Rajasekaran, and S. Uma Sankar.
Phys. Rev. **D56** (1997) 437

(3) "Solar eclipse and neutrinos . "
Authors: Mohan Narayan, G.Rajasekaran, and
Rahul Sinha.
Current Science. **70** (1996) 848,
ibid **72** (1997) 417E

(4) "Time-of-night variation of solar neutrinos. "
Authors: Mohan Narayan, G.Rajasekaran,
and Rahul Sinha.
Mod Phys Letters. **A 13** (1998) 1915

(5) "Solar neutrinos : Eclipse effect. "
Authors: Mohan Narayan, G.Rajasekaran,
and Rahul Sinha.
Preprint IMSc-97/03/07 (astro-ph/9702395)

(6) "Three flavor implications of CHOOZ result. "
Authors: Mohan Narayan, G.Rajasekaran, and S. Uma Sankar
Phys. Rev. **D58** (1998) R031301

Chapter 1

Review of neutrino masses and oscillations

1.1 Introduction to neutrinos

Neutrinos are electrically neutral spin half particles. Historically, neutrino was first postulated by Wolfgang Pauli to explain the continous electron spectrum, which was observed in nuclear beta decay of the neutron. This decay was thought to be the following process

$$n \rightarrow p + e^-.$$

Since the final state contains only two particles the electron energy must be a line spectrum, in contradiction to what was observed.

Pauli proposed that, the above process is actually a three body decay, and that a third massless, spin half neutral particle is emitted along with the electron. This particle was called the neutrino, and was denoted as ν. Further more it was assumed to interact only weakly with matter. This particle which accompanies the electron in beta decay is what we call today the electron antineutrino denoted as $\bar{\nu}_e$. Therefore the above reaction is properly written as

$$n \rightarrow p + e^- + \bar{\nu}_e.$$

Its antiparticle the electron neutrino denoted as ν_e accompanies the positron in weak interactions. The subscript e tells us that this is the neutrino that accompanies the electron in weak interaction processes.

Soon after this Fermi proposed his theory of beta decay (which was later extended by Gamow and Teller), in which the neutrinos were an essential component. In this theory the interaction Lagrangian for the beta decay of the neutron is of the form.

$$\mathcal{L} = -\frac{G_F}{\sqrt{2}} \bar{\Psi}_p \gamma_\mu \Psi_n(x) \bar{\Psi}_e \gamma_\mu \Psi_\nu(x).$$

This was modelled after the current current interaction of quantum electrodynamics (QED), the quantum field theory of electromagnetic interactions. In the above equation G_F is a coupling constant, which is experimentally found to be $1.16639 \times 10^{-5} GeV^{-2}$ in natural units ($\hbar = c = 1$). Ψ denotes the quantized fermion field, and $\bar{\Psi}$ its conjugate field. Positron emission along with a electron neutrino is described by adding to the Lagrangian the hermitian conjugate of the above term. The Fermi theory was extremely successful in explaining nuclear beta decay, and the idea of neutrino gained universal acceptance. The first experimental demonstration of the electron neutrino, was done in a classic experiment by Reines and Cowan [1]. Today we know that there are three types or flavors of neutrinos, the electron type ν_e, the muon type ν_μ which accompanies the muon in weak interactions, and the tau type denoted by ν_τ, which accompanies the tau lepton in weak processes. The existence of the second type of neutrino (viz the muon type) was demonstrated at Brookhaven National Laboratory by Danby et al [2]. The existence of the ν_τ, is inferred by experiments at the electron positron collider (LEP) at CERN, via what is called "the invisible width" of the Z boson. This quantity directly gives the number of light neutrino species. The experimental value of this number is [3] 2.987 ± 0.016. So even though the number of neutrino species is fixed by experiment, the question of whether the neutrino is massless or not is still unresolved.

1.2 Present status of neutrino masses

Laboratory experiments try to measure neutrino mass by studying weak decays involving neutrinos as one of the final products. Today we only have upper limits

on the masses of the three types of neutrinos. The upper limit on the electron neutrino mass comes from studying the beta decay of tritium.

$$^3H \rightarrow {}^3He + e^- + \bar{\nu}_e.$$

The present experimental result is [4]

$$m(\nu_e) < 7.3eV. \tag{1.1}$$

The upper limit on the muon neutrino mass comes from studying the decay

$$\pi^- \rightarrow \mu^- + \bar{\nu}_\mu.$$

The present result is [5]

$$m(\nu_\mu) < 270KeV. \tag{1.2}$$

The limit on the tau neutrino mass comes from study of the 5 π invariant mass distribution in the reaction

$$e^+ + e^- \rightarrow \tau^+ + \tau^-,$$

followed by

$$\tau^- \rightarrow 2\pi^+ + 3\pi^- + \nu_\tau.$$

The present result is [6]

$$m(\nu_\tau) < 35MeV. \tag{1.3}$$

The point to be emphasised at this juncture is that since we only have upper bounds on the masses, they could be zero also. So at present there is no irrefutable evidence of neutrino mass.

Since neutrino is electrically neutral, there also exists the possibility that the antineutrino is the same particle as the neutrino. Such a self conjugate spin $\frac{1}{2}$ particle is called a Majorana particle. In this case the lepton number is not a good quantum number, i.e lepton number is violated. If the neutrino is indeed a Majorana particle, then one can have the process of neutrinoless double beta decay. This process is described by the following reaction

$$(A, Z) \rightarrow (A, Z + 2) + 2e^-,$$

where a nucleus decays into another nucleus with the emission of two electrons. This process requires that, in addition to being Majorana type, the neutrino must also be massive. There has been lot of experimental effort to look for neutrinoless double beta decay. But no positive signal is found for this effect till now. The present experimental limit on the electron neutrino mass coming from a study of neutrinoless double beta decay is [7]

$$m(\nu_e) < 0.68 eV. \tag{1.4}$$

Thus all the laboratory experiments examined so far are consistent with *zero neutrino mass.*

At present the GSW model of particle physics forms the basis of our understanding of the electromagnetic and the weak interactions of elementary particles. Neutrinos along with the other leptons and quarks form the basic building blocks of the model. The quarks and leptons are arranged into three families, where each family consists of one doublet of leptons and one doublet of quarks. The doublets are as follows. The three lepton doublets are

$$\begin{pmatrix} \nu_e \\ e^- \end{pmatrix}, \begin{pmatrix} \nu_\mu \\ \mu^- \end{pmatrix} and \begin{pmatrix} \nu_\tau \\ \tau^- \end{pmatrix}.$$

The three quark doublets are

$$\begin{pmatrix} u \\ d \end{pmatrix}, \begin{pmatrix} c \\ s \end{pmatrix} and \begin{pmatrix} t \\ b \end{pmatrix}.$$

The first family consists of the first of the lepton doublets and the first of the quark doublets written above. For the neutrinos it is only the left handed components of these doublets that are present in the model. Therefore the neutrino is massless in the GSW model. The GSW model with the inclusion of QCD, which is the theory of strong interactions is called the standard model of particle physics. The standard model has been extremely successful in explaining almost all the observed phenomena in particle physics. However it should be remarked that today there is a general consenses that the standard model may not be the final theory of the strong, weak and the electromagnetic interactions, and it is only part of a more complete theory. There are quite a few candidates today for the other theories. Examples are

Supersymmetry, Left-Right symmetric models, Grand Unified theories etc. In all these theories neutrinos are massive particles. Also neutrinos are one of the favoured candidates for hot dark matter of the universe, which in turn demands neutrinos to be massive. So massive neutrinos are quite a natural possibility.

1.3 Consequences of massive neutrinos

Experimentally it is known that there is mixing in the quark sector of the GSW model. This means that the quarks which participate in the weak interactions are linear combinations of the quarks with definite flavor. This can be expressed as follows. Let d', s', and b' be the quark states which participate in the weak interactions. Then one can write

$$\begin{bmatrix} d' \\ s' \\ b' \end{bmatrix} = U \begin{bmatrix} d \\ s \\ b \end{bmatrix}, \tag{1.5}$$

where U is a three by three unitary matrix, and is known as the mixing matrix, or the Cabbibo-Kobayashi-Maskawa matrix. As stated before, mixing arises because quarks are massive and the quark mass eigenstates are not the same as the weak interaction eigenstates. If neutrinos are massive, then in a manner similar to the quark mixing, there could be mixing in the neutrino sector also. This possibility was raised long ago by B. Pontecorvo [8]. The three neutrino flavor eigenstates, i.e the states that are produced in weak decays, would then be related to three mass eigenstates through a unitary transformation in general. So we can write

$$\begin{bmatrix} \nu_e \\ \nu_\mu \\ \nu_\tau \end{bmatrix} = U^v \begin{bmatrix} \nu_1^v \\ \nu_2^v \\ \nu_3^v \end{bmatrix}, \tag{1.6}$$

where the superscript v on r.h.s. stands for vacuum. The 3×3 unitary matrix U^v can be parametrized by three Euler angles (ω, ϕ, ψ) and a phase. The form of the unitary matrix can therefore be written in general as,

$$U^v = U_{23}(\psi) \times U_{phase} \times U_{13}(\phi) \times U_{12}(\omega),$$

where $U_{ij}(\theta_{ij})$ is the mixing matrix between ith and jth mass eigenstates with the mixing angle θ_{ij}.

This can lead to the novel phenomenon of neutrino oscillations. Since there are three flavors of neutrinos, one must in general consider oscillations between all the three flavors. However the basic features of neutrino oscillations can be illustrated even in a two flavor framework. So let us first consider the case when there are only two flavors of neutrinos, ν_e and ν_μ. These two flavor states will then be related to two mass eigenstates ν_1 and ν_2. We will first consider oscillations in vacuum. We can write

$$\begin{pmatrix} \nu_e \\ \nu_\mu \end{pmatrix} = \begin{pmatrix} \cos\theta & \sin\theta \\ -\sin\theta & \cos\theta \end{pmatrix} \begin{pmatrix} \nu_1 \\ \nu_2 \end{pmatrix}. \tag{1.7}$$

(Here we suppress the superscript v on the mass eigenstates). θ is known as the vacuum mixing angle. In general we can write

$$|\nu_a\rangle = \sum_i U_{ai}|\nu_i\rangle,$$

where $\alpha = e, \mu, ..$, and the sum runs over the various mass eigenstates. Now suppose that at time $t = 0$, a neutrino of flavor α is born in a weak interaction process. Also for the sake of definitiness let α be the electron flavor. Then we can write

$$|\nu_e(0)\rangle = \cos\theta|\nu_1(0)\rangle + \sin\theta|\nu_2(0)\rangle.$$

After a time t the state will be

$$\begin{aligned} |\nu_e(t)\rangle &= \cos\theta|\nu_1(t)\rangle + \sin\theta|\nu_2(t)\rangle \\ &= e^{-iE_1 t}\cos\theta|\nu_1(0)\rangle + e^{-iE_2 t}\sin\theta|\nu_2(0)\rangle \\ &= (e^{-iE_1 t}\cos^2\theta + e^{-iE_2 t}\sin^2\theta)|\nu_e(0)\rangle \\ &\quad + \sin\theta\cos\theta(e^{-iE_2 t} - e^{-iE_1 t})|\nu_\mu(0)\rangle, \end{aligned}$$

where

$$E_i = \sqrt{p^2 + m_i^2}.$$

Here $\vec{p}$ is the three momentum of the neutrino, and m is the mass of the mass eigenstate. Here we assume that all the mass eigenstates have the same momentum.

One sees that at time t there is a finite probability, that the neutrino of flavor α (in this case of flavor e) has oscillated into a neutrino of another flavor (the μ flavor). The probability that a neutrino of flavor e, has oscillated into a neutrino of flavor μ is given by

$$
\begin{aligned}
P(\nu_e \rightarrow \nu_\mu) &= |\langle \nu_\mu(0)|\nu_e(t)\rangle|^2, \\
&= \sin^2 2\theta \sin^2(E_2 - E_1)t.
\end{aligned}
$$

Now since neutrinos are ultrarelativistic, we can write

$$
E = \sqrt{p^2 + m^2} \approx p + \frac{m^2}{2p},
$$

assuming $m << p$. Using the above equation we get

$$
E_2 - E_1 \approx \frac{\delta m^2}{2p}, \tag{1.8}
$$

where $\delta m^2 = m_2^2 - m_1^2$.

Hence our expression for the conversion probability becomes

$$
P(\nu_e \rightarrow \nu_\mu) = \sin^2 2\theta \sin^2(\frac{\delta m^2}{4E}x).
$$

Here t has been replaced by x, and p by E as the neutrinos are ultrarelativistic. This probability is also called the conversion probability , and is denoted by $P_{e\mu}$. It gives the probability of conversion of one flavor to another. Note that the conversion probability depends on two parameters, the mixing angle θ and the vacuum mass squared difference δm^2. Therefore to have oscillations, one needs non zero mixing, as well as non degenerate masses. The survival probability, i.e the probability that the neutrino retains its original flavor denoted by P_{ee} is given by

$$
\begin{aligned}
P_{ee} &= 1 - P(\nu_e \rightarrow \nu_\mu) \\
&= 1 - \sin^2 2\theta \sin^2(\frac{\delta m^2}{4E}x).
\end{aligned}
$$

Define a quantity called the oscillation length as

$$
L \equiv \frac{4\pi E}{\delta m^2}. \tag{1.9}
$$

In the above equation, L is in meters provided, E is in MeV, and δm^2 is in eV^2. We get

$$
P_{ee} = 1 - \sin^2 2\theta \sin^2(\frac{\pi x}{L}), \tag{1.10}
$$

and the conversion probability becomes

$$P_{e\mu} = \sin^2 2\theta \sin^2(\frac{\pi x}{L}). \tag{1.11}$$

Observe that in order to have appreciable conversion, the distance travelled must be comparable to the oscillation length. On the other hand if one can average out the oscillating term then one gets

$$P_{e\mu} = \frac{1}{2}\sin^2 2\theta. \tag{1.12}$$

So the conversion probability can be very small, if the mixing angle is small. At this point it is instructive to note a very important aspect of neutrino oscillations. Let us write down the evolution equation of the two mass eigenstates. We can write

$$i\frac{d}{dt}\left[\begin{array}{c} |\nu_1(t)\rangle \\ |\nu_2(t)\rangle \end{array}\right] = \left(\begin{array}{cc} E_1 & 0 \\ 0 & E_2 \end{array}\right)\left[\begin{array}{c} |\nu_1(0)\rangle \\ |\nu_2(0)\rangle \end{array}\right].$$

Note that here we have written the evolution in the mass eigenstate basis. The matrix is diagonal as each mass eigenstate in vacuum propagates independently. The expressions for the oscillation probabilities (both conversion and survival) derived earlier, depends as stated before, on the weak mixing angle and the oscillation length. The oscillation length defined in (1.9) can be written in the form

$$L = \frac{2\pi}{E_2 - E_1}.$$

Notice that the denominator is the difference between the diagonal elements of the evolution matrix. Hence any element which is common to both the diagonal elements, does not matter for neutrino oscillations. In other words any multiple of the identity matrix is redundant for oscillations.

1.4 Neutrino oscillations in matter

So far, we have studied neutrino oscillations in vacuum, and derived expressions for conversion and survival probabilities. However, when neutrinos propagate in matter, these results can change significantly. When neutrinos propagate through matter, the forward scattering of neutrinos in matter will alter the propagation of the mass

17

eigenstates. Using the GSW model of neutrino interactions with matter, neutrinos will scatter off the background matter via the charged current and the neutral current. The neutral current interaction influences all neutrino flavors equally. But the electrons in the matter will interact via the charged current with the electron neutrinos only. The interaction term for the charged current interaction can be written as

$$H = \frac{G_F}{\sqrt{2}}\bar{e}\gamma^\mu(1-\gamma^5)\nu_e\bar{\nu}_e\gamma_\mu(1-\gamma^5)e,$$

where G_F is the Fermi constant, e and ν are the quantized electron and electron neutrino fields. Fierz reordering the above term one gets

$$H = \frac{G_F}{\sqrt{2}}\bar{\nu}_e\gamma^\mu(1-\gamma^5)\nu_e\bar{e}\gamma_\mu(1-\gamma^5)e.$$

For forward scattering of neutrinos off electrons, the electron momentum is unchanged. Also for electrons at rest only the γ^0 component of the electron density can contribute. The $\gamma^\mu\gamma^5$ term mixes "small" and "large" components of the electron spinor, so it does not contribute. The term involving the electron fields becomes

$$\bar{e}\gamma_\mu(1-\gamma^5)e = \delta_{\mu0}N_e,$$

where N_e is the number density of electrons in the medium. The net result of the interaction term is [9]

$$V = G\sqrt{2}N_e$$

as the interaction resembles an external potential for the neutrino. The effective energy of the electron neutrino will be given by (to order V)

$$E_{eff} \approx p + \frac{m^2}{2p} + \langle e\nu_e|H|e\nu_e\rangle.$$

This can be written as

$$\begin{aligned}E_{eff} &= p + \frac{m^2}{2p} + V \\ &= p + \frac{1}{2p}(m^2+2pV) \\ &\approx p + \frac{1}{2E}(m^2+2EV).\end{aligned}$$

Thus V is equivalent to an addition to m^2 of

$$\delta m_e^2 = 2EV = 2\sqrt{2}(\frac{GY_e}{m_n})\rho E = A. \qquad (1.13)$$

A is known as the Wolfenstein term [10]. In the above equation m_n is the mass of the nucleon, Y_e the number of electrons per nucleon in the matter which is $\approx \frac{1}{2}$, and ρ is the density of matter in gm/cc. Let us look at the evolution equation of the neutrino mass eigenstates in vacuum, which we wrote down previously.

$$i\frac{d}{dt}\begin{bmatrix} |\nu_1(t)\rangle \\ |\nu_2(t)\rangle \end{bmatrix} = \left[\begin{pmatrix} p & 0 \\ 0 & p \end{pmatrix} + \frac{1}{2p}\begin{pmatrix} m_1^2 & 0 \\ 0 & m_2^2 \end{pmatrix} \right] \begin{bmatrix} |\nu_1(0)\rangle \\ |\nu_2(0)\rangle \end{bmatrix}.$$

Neglecting the terms proportional to the identity matrix we can write

$$i\frac{d}{dt}\begin{bmatrix} |\nu_1(t)\rangle \\ |\nu_2(t)\rangle \end{bmatrix} = \frac{1}{2E}\begin{pmatrix} m_1^2 & 0 \\ 0 & m_2^2 \end{pmatrix} \begin{bmatrix} |\nu_1(0)\rangle \\ |\nu_2(0)\rangle \end{bmatrix}.$$

The two by two matrix

$$\begin{pmatrix} m_1^2 & 0 \\ 0 & m_2^2 \end{pmatrix} = M^2$$

is known as the mass squared matrix in the mass eigenbasis, as the diagonal terms give the squared masses of the mass eigenstates. Since interactions are specified in the flavor basis, to study neutrino propagation in matter, we first look at the evolution in the flavor basis. This will be given by

$$i\frac{d}{dt}\begin{bmatrix} |\nu_e(t)\rangle \\ |\nu_\mu(t)\rangle \end{bmatrix} = \frac{1}{2E}M_f^2\begin{bmatrix} |\nu_e(0)\rangle \\ |\nu_\mu(0)\rangle \end{bmatrix},$$

where M_f^2 is the mass square matrix in the flavor basis, and is given by

$$M_f^2 = U\begin{pmatrix} m_1^2 & 0 \\ 0 & m_2^2 \end{pmatrix} U^\dagger + \begin{pmatrix} A & 0 \\ 0 & 0 \end{pmatrix}.$$

Here U is the two by two unitary matrix which relates the flavor to the mass eigenstates defined earlier. Note that in the flavor basis the interaction term appears only in the ee position in the mass squared matrix. On using the form of U, we get

$$M_f^2 = \frac{1}{2}(m_1^2 + m_2^2 + A)\begin{bmatrix} 1 & 0 \\ 0 & 1 \end{bmatrix} + \frac{1}{2}\begin{bmatrix} A - \Delta\cos 2\theta & \Delta\sin 2\theta \\ \Delta\sin 2\theta & -A + \Delta\cos 2\theta \end{bmatrix},$$

where $\Delta = m_2^2 - m_1^2$.

M_f^2 can be diagonalized to find the instantaneous eigenvalues and eigenstates. Let us define U^m to be mixing matrix in matter, and $M_{2,1}^2$ to be the two mass

eigenvalues in matter. So one can write

$$(U^m)^\dagger M_f^2 U^m = \begin{bmatrix} M_1^2 & 0 \\ 0 & M_2^2 \end{bmatrix}. \tag{1.14}$$

The eigenvalues of M_f^2 are

$$M_{2,1}^2 = \frac{(\Sigma + A) \pm \sqrt{[(A - \Delta \cos 2\theta)^2 + (\Delta \sin 2\theta)^2]}}{2}, \tag{1.15}$$

where $\Sigma = m_1^2 + m_2^2$ The mixing matrix in matter can be defined analogous to the vacuum mixing matrix as

$$\begin{aligned} \begin{pmatrix} \nu_e \\ \nu_\mu \end{pmatrix} &= \begin{pmatrix} \cos \theta_m & \sin \theta_m \\ -\sin \theta_m & \cos \theta_m \end{pmatrix} \begin{pmatrix} \nu_1^m \\ \nu_2^m \end{pmatrix}, \\ &= U^m \begin{pmatrix} \nu_1^m \\ \nu_2^m \end{pmatrix}. \end{aligned} \tag{1.16}$$

The mass eigenstates are ν_1^m and ν_2^m. θ_m which is the mixing angle in matter is given by

$$\sin 2\theta_m = \frac{\Delta \sin 2\theta}{\sqrt{[(A - \Delta \cos 2\theta)^2 + (\Delta \sin 2\theta)^2]}}. \tag{1.17}$$

One observes that the mixing angle in matter can be substantially different from the vacuum mixing angle. However, the most interesting feature of θ_m is its resonance behaviour as a function of A. That is if the condition

$$A = \Delta \cos 2\theta \tag{1.18}$$

is satisfied, then we get

$$\sin 2\theta_m = 1$$

i.e., the neutrino mixing angle reaches a value of $\frac{\pi}{4}$ *independent* of the vacuum mixing angle. So even a small mixing angle can be amplified to maximal mixing due to matter effects. Note that the resonance can occur only if the vacuum mixing angle θ is less than $\frac{\pi}{4}$, i.e., the electron neutrino is dominantly coupled to the lighter of the two mass eigenstates.

Let us now compute the electron neutrino survival probability P_{ee}, after the neutrino propagates in matter.

Case (1) Medium with constant density

Suppose the neutrino is produced as well as detected in a medium of constant density, then P_{ee} is the same as the vacuum case, with the difference that the vacuum parameters are replaced by the matter dependent parameters. The vacuum mixing angle θ gets replaced by θ_m and the vacuum oscillation length L is replaced by L_m. The survival probability is given by

$$P_{ee} = 1 - \sin^2 2\theta_m \sin^2(\frac{\pi x}{L_m}) \tag{1.19}$$

and the conversion probability becomes

$$P_{e\mu} = \sin^2 2\theta_m \sin^2(\frac{\pi x}{L_m}), \tag{1.20}$$

where

$$
\begin{aligned}
L_m &= \frac{4\pi E}{M_2^2 - M_1^2} \\
&= \frac{4\pi E}{\sqrt{[(A - \Delta \cos 2\theta)^2 + (\Delta \sin 2\theta)^2]}}.
\end{aligned}
\tag{1.21}
$$

Again if one can average out the oscillating term, we get

$$P_{e\mu} = \frac{1}{2} \sin^2 2\theta_m \tag{1.22}$$

and

$$P_{ee} = 1 - \frac{1}{2} \sin^2 2\theta_m. \tag{1.23}$$

Case (2) Medium with varying density

Suppose the neutrino propagates in a medium with varying density. For example the neutrino may be produced in matter and then detected in vacuum, which is what happens in the case of solar neutrinos. Or they may be produced in vacuum and then detected in matter, as in the case of neutrinos from the atmosphere.

Since the mass eigenvalues and mass eigenstates are functions of the density in the medium, the mass eigenstates obtained earlier are no longer eigenstates of the Hamiltonian. Let us start with the evolution equation of the neutrinos in the flavor

basis derived earlier

$$
i\frac{d}{dx}\begin{bmatrix} |\nu_e\rangle \\ |\nu_\mu\rangle \end{bmatrix} = \frac{1}{4p}\begin{bmatrix} A - \Delta\cos 2\theta & \Delta\sin 2\theta \\ \Delta\sin 2\theta & -A + \Delta\cos 2\theta \end{bmatrix}\begin{bmatrix} |\nu_e\rangle \\ |\nu_\mu\rangle \end{bmatrix}
$$

$$
= \frac{1}{2E}U^m\begin{bmatrix} M_1^2 & 0 \\ 0 & M_2^2 \end{bmatrix}\begin{bmatrix} |\nu_1^m\rangle \\ |\nu_2^m\rangle \end{bmatrix}.
$$

(from now on we suppress t and 0 in front of the states) We have also substituted x for t. Now using the fact

$$
\begin{bmatrix} |\nu_e\rangle \\ |\nu_\mu\rangle \end{bmatrix} = U^m\begin{bmatrix} |\nu_1^m\rangle \\ |\nu_2^m\rangle \end{bmatrix}
$$

and keeping in mind that U^m is x dependent, we get

$$
i\frac{d}{dx}\begin{bmatrix} |\nu_1^m\rangle \\ |\nu_2^m\rangle \end{bmatrix} = \frac{1}{2E}\left[\begin{bmatrix} M_1^2 & 0 \\ 0 & M_2^2 \end{bmatrix} - (U^m)^\dagger i\frac{d}{dx}U^m\right]\begin{bmatrix} |\nu_1^m\rangle \\ |\nu_2^m\rangle \end{bmatrix}
$$

$$
= \begin{bmatrix} \frac{M_1^2}{2E} & -i\frac{d\theta_m}{dx} \\ i\frac{d\theta_m}{dx} & \frac{M_2^2}{2E} \end{bmatrix}\begin{bmatrix} |\nu_1^m\rangle \\ |\nu_2^m\rangle \end{bmatrix}. \tag{1.24}
$$

To get the last equation we have used the explicit form of U^m. It is easy to show that

$$
\frac{d\theta_m}{dx} = \frac{1}{2}\frac{\Delta\sin 2\theta}{(A - \Delta\cos 2\theta)^2 + (\Delta\sin 2\theta)^2}\frac{dA}{dx}. \tag{1.25}
$$

and

$$
M_2^2 - M_1^2 = \sqrt{(A - \Delta\cos 2\theta)^2 + (\Delta\sin 2\theta)^2}. \tag{1.26}
$$

The offdiagonal term in (1.24) causes the mixing of the states ν_1^m and ν_2^m. Let us study this term in some detail.

Let us consider the case in which $\rho(x)$ is a slowly varying function, so that $\frac{d\theta_m}{dx}$ is small. The condition for the offdiagonal term to be small can be written as

$$
|\frac{d\theta_m}{dx}| << \frac{|M_2^2 - M_1^2|}{4E} = \frac{\pi}{L_m}.
$$

This can be cast in terms of the electron density as

$$
|\frac{1}{N_e}\frac{dN_e}{dx}| << \frac{1}{\sin 2\theta}\frac{2\pi}{L_m}(\frac{LL_0}{L_m^2}), \tag{1.27}
$$

where

$$
L_0 = \frac{4\pi E}{A}. \tag{1.28}
$$

Equation (1.27) is called the adiabatic condition. If the density variation is very small, the two mass eigenstates evolve independently. There are no transitions between them and the heavier mass eigenstate remains heavier for all time and the lighter mass eigenstate lighter.

Adiabatic evolution in matter can have very interesting consequences. Suppose an electron neutrino is born in matter at a very high density, such that $\theta_m \approx \frac{\pi}{2}$. Then since

$$|\nu_e\rangle = \cos\theta_m |\nu_1^m\rangle + \sin\theta_m |\nu_2^m\rangle$$

we get $|\nu_e\rangle \approx |\nu_2^m\rangle$. That is the electron neutrino is dominantly born in the heavier mass eigenstate. As the neutrino moves from high to low density, the mixing angle will decrease, and at the resonance point where $A = \Delta\cos 2\theta$ it will become $\frac{\pi}{4}$. Then the neutrino proceeds out into the vacuum. Since the evolution in adiabatic, the neutrino state will remain the same mass eigenstate. In vacuum we have

$$|\nu_\mu\rangle = \cos\theta|\nu_2\rangle - \sin\theta|\nu_1\rangle.$$

Since the vacuum mixing angle is expected to be small, we get $|\nu_2\rangle \approx |\nu_\mu\rangle$, i.e the second mass eigenstate is essentially populated by the muon neutrino. Therefore in evolving adiabatically from high densities to vacuum, the flavor content of a mass eigenstate changes almost completely. This is called the Mikheyev, Smirnov and Wolfenstein (MSW) effect [11]. This has tremendous repercussions for what is called the "Solar neutrino problem" which we shall address later. It can be shown easily [12], that if an electron neutrino propagates adiabatically from matter where the mixing angle is θ_m, to vacuum where the mixing angle is θ, then

$$P_{ee} = \frac{1}{2}(1 + \cos 2\theta \cos 2\theta_m). \tag{1.29}$$

One sees from the above equation that if $\theta_m \approx \frac{\pi}{2}$ and for small vacuum mixing angles, $P_{ee} \approx 0$. That is when θ is very small there is almost complete flavor conversion.

Now there may be situations, where the adiabatic approximation does not hold. In such a case there will be corrections to the formula stated above. The adiabatic condition breaks down when eq. (1.27) approaches an equality. That is

$$\left|\frac{d\theta_m}{dx}\right| \approx \frac{M_2^2 - M_1^2}{4E}.$$

Using eq. (1.25), $|\frac{d\theta_m}{dx}|$ has a maximum at the resonance, and eq. (1.26) implies that $|M_2^2 - M_1^2|$ has a minimum at resonance. Therefore the condition for adiabaticity becomes most stringent at resonance. Since at resonance

$$L_m = \frac{L}{\sin 2\theta},$$

we can write the adiabaticity condition as

$$\gamma \equiv \frac{\Delta_{21}}{E|\frac{1}{A}\frac{dA}{dr}|_{res}} \frac{\sin^2 2\theta}{\cos 2\theta} \gg 1. \tag{1.30}$$

If $\gamma \approx 1$, then there will be considerable corrections to the formula for P_{ee} derived earlier. But such corrections will typically be appreciable only in a small region around the resonance. As the resonance region is very narrow, propagation outside this narrow region will be adiabatic. At resonance corrections to adiabaticity take the form of level crossings, where the state ν_1^m can cross over to ν_2^m and vice versa. Let P_c denote the level crossing probability from ν_1^m to ν_2^m (which is also the probability for crossing from ν_2^m to ν_1^m. Then we can write

$$P_c = |\langle \nu_2^m(x_+)|\nu_1^m(x_-)\rangle|^2, \tag{1.31}$$

where $x_{\pm}$ refer to two faraway points on either side of the resonance point. $(1 - P_c)$ is obviously the probability for ν_1^m to remain in ν_1^m. It has been shown [13] that the electron neutrino survival probability now becomes

$$P_{ee} = \frac{1}{2} + (\frac{1}{2} - P_c) \cos 2\theta \cos 2\theta_m. \tag{1.32}$$

P_c can be generically parametrized as

$$P_c = exp(-\frac{\pi}{2}\gamma F), \tag{1.33}$$

where γ is the adiabaticity parameter defined earlier in eq. (2.26). The function F depends on the density profile in which the neutrino propagates, and is tabulated in [12] for various density profiles.

1.5   Three flavor oscillations

Let us now consider the realistic case where all the three neutrino flavors mix with other. As stated previously this can be parametrized in the following way (analogous

to the two flavor case)

$$\begin{bmatrix} \nu_e \\ \nu_\mu \\ \nu_\tau \end{bmatrix} = U^v \begin{bmatrix} \nu_1^v \\ \nu_2^v \\ \nu_3^v \end{bmatrix},$$

where the superscript v on r.h.s. stands for vacuum. The 3×3 unitary matrix U^v can be parametrized by three Euler angles (ω, ϕ, ψ) and a phase. The form of the unitary matrix can therefore be written in general as,

$$U^v = U_{23}(\psi) \times U_{phase} \times U_{13}(\phi) \times U_{12}(\omega),$$

where $U_{ij}(\theta_{ij})$ is the mixing matrix between ith and jth mass eigenstates with the mixing angle θ_{ij} [12]. The explicit form of U is

$$U^v = \begin{pmatrix} c_\phi c_\omega & c_\phi s_\omega & s_\phi \\ -c_\psi s_\omega e^{i\delta} - s_\psi s_\phi c_\omega e^{-i\delta} & c_\psi c_\omega e^{i\delta} - s_\psi s_\phi s_\omega e^{-i\delta} & s_\psi c_\phi e^{-i\delta} \\ s_\psi s_\omega e^{i\delta} - c_\psi s_\phi c_\omega e^{-i\delta} & -s_\psi c_\omega e^{i\delta} - c_\psi s_\phi s_\omega e^{-i\delta} & c_\psi c_\phi e^{-i\delta} \end{pmatrix}, \quad (1.34)$$

where $s_\phi = \sin\phi$ and $c_\phi = \cos\phi$ etc. All the angles can take values between 0 and $\pi/2$. The above equation can also be written as

$$|\nu_a\rangle = U|\nu_i\rangle,$$

where $|\nu_a\rangle$ is the column vector, comprising of the three flavor states, and $|\nu_i\rangle$ is made up of the three mass eigenstates. The matrix U defined earlier can be written as

$$U^v = \begin{pmatrix} U_{e1} & U_{e2} & U_{e3} \\ U_{\mu1} & U_{\mu2} & U_{\mu3} \\ U_{\tau1} & U_{\tau2} & U_{\tau3} \end{pmatrix}. \quad (1.35)$$

In a way, exactly analogous to the two flavor case, we can compute the electron neutrino survival probability in vacuum, after the neutrino has travelled a distance x. We get

$$P_{ee} = 1 - 4U_{e1}^2 U_{e2}^2 \sin^2(\frac{\pi x}{L_{12}}) - 4U_{e2}^2 U_{e3}^2 \sin^2(\frac{\pi x}{L_{23}}) - 4U_{e3}^2 U_{e1}^2 \sin^2(\frac{\pi x}{L_{13}}), \quad (1.36)$$

where

$$L_{12} = \frac{4\pi E}{\delta_{21}}, \quad (1.37)$$

$$L_{23} = \frac{4\pi E}{\delta_{32}}, \quad (1.38)$$

and

$$L_{13} = \frac{4\pi E}{\delta_{31}}. \tag{1.39}$$

In the above equations, $\delta_{21} = m_2^2 - m_1^2$, $\delta_{32} = m_3^2 - m_2^2$ and $\delta_{31} = m_3^2 - m_1^2$. If one neglects CP violation, i.e., put the phase $\delta = 0$, then the mixing matrix contains three angles. Also with three masses, m_1, m_2 and m_3 one can construct two independent mass squared differences. This can be taken as δ_{21} and δ_{31}. Therefore three flavor neutrino oscillations involve five parameters, as compared to two flavor oscillations which involve only two independent parameters. All these five parameters can be modified in matter, and we shall study these in detail when we address the solar neutrino problem.

From eq. (1.36), we see that in the case, where the oscillating term can be averaged out, we get

$$P_{ee} = 1 - 2U_{e1}^2 U_{e2}^2 - 2U_{e2}^2 U_{e3}^2 - 2U_{e3}^2 U_{e1}^2. \tag{1.40}$$

Consider the case where the three neutrinos are maximally mixed with each other, this corresponds to the case $U_{e1} = U_{e2} = U_{e3} = \frac{1}{3}$. Substituting in eq. (1.40), we get $P_{ee} = \frac{1}{3}$. Therefore three flavor vacuum oscillations can give a maximum suppression of $\frac{1}{3}$.

In the next chapter we discuss the implications of neutrino oscillations for the solar neutrino problem, and show that neutrino oscillations can provide an elegant solution to the solar neutrino problem.

Chapter 2

The solar neutrino problem

2.1 Introduction

In order to explain the solar neutrino problem, we first need to know how the neutrinos originate in the sun. Our present understanding of the production of neutrinos in the sun is based on what is usually referred to as the Standard solar model of the sun or simply SSM. The Standard Solar Model is an astrophysical model of the sun. This model attempts to describe the main features of the sun, like surface luminosity, opacity, elemental abundance etc [14]. This model of the sun is based on the following observed parameters:

- Surface luminosity $L_\odot = 3.86 \times 10^{33}$ erg/sec .

- Surface Temperature $T_{s\odot} = 5.78 \times 10^3$ K .

- Solar Mass $M_\odot = 1.99 \times 10^3 3$ g .

- Solar Radius $R_\odot = 6.96 \times 10^1 0$ cm .

- Age of Sun $\approx 4.55 \times 10^9$ yr.

It is also assumed that the sun is spherically symmetric, in hydrostatic and thermal equilibrium, and is described by the ideal gas equation of state.

According to this model the mechanism responsible for energy production in the sun is nuclear fusion. The main set of processes which power the sun is called the proton-proton, or the *pp* chain. The net effect of this chain is the conversion of four protons into a helium nucleus, positrons, electron neutrinos and energy. This set of reactions may be summarized as

$$4p \rightarrow {}^4He + 2e^+ + 2\nu_e.$$

This reaction releases $27.6MeV$ of energy, where the neutrinos on an average carry away $0.59MeV$ of energy. About 99 percent of the sun's energy is produced by the *pp* chain. The remaining comes from what is called the CNO cycle. These nuclear reactions are concentrated in a small region within the core of the sun.

As far as neutrino production is concerned, there are four important reactions in the *pp* chain. They are as follows. The first of these reactions is

$$p + p \rightarrow {}^2H + e^+ + \nu_e.$$
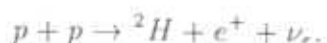
The neutrinos from this reaction are called *pp* neutrinos, and they from a continuous spectrum from 0 to 0.42 MeV. In a sense these neutrinos are the most fundamental, since this reaction initiates the *pp* chain.

The second reaction is

$$p + e^- + p \rightarrow {}^2H + \nu_e.$$
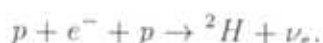
The neutrinos from this reaction are known as the *pep* neutrinos, and it is a line spectrum at $1.442MeV$.

The third reaction is

$$e^- + {}^7Be \rightarrow {}^7Li + \nu_e.$$

The neutrinos from this reaction is known as the Beryllium neutrinos, and it is a line spectrum at 0.861 MeV.

The last of the reactions is

$$^8B \rightarrow {}^8Be + e^+ + \nu_e.$$

These neutrinos form a continuos spectrum from 0 to 15 MeV. Neutrinos are also emitted in several other reactions as well as through CNO cycle. But the only relevant ones are the four reactions given above.

Neutrino type.	Flux ($\times 10^{10}$)
pp	5.91
pep	0.014
^7Be	0.515
^8B	6.62×10^{-4}

Table 2.1: Neutrino fluxes from BP (95) Solar model.

At present the standard solar model of Bahcall and Pinsonneault (BP) [15] is the widely accepted model of the sun. This model has specific predictions for the neutrino fluxes which come from the above reactions. The BP model predictions of the neutrino fluxes from the four reactions listed in table 1.1. The line spectra are given in $cm^{-2}s^{-1}$, while the continuous ones are given in $cm^{-2}s^{-1}MeV^{-1}$.

So the low energy neutrinos are the most copious, while the high energy neutrinos are the least. The Standard solar model also gives the neutrino spectrum as a function of energy, for the pp and the Boron neutrinos.

Today there are four detectors on earth which measure the flux of these solar neutrinos. The oldest of the solar neutrino experiments is the ^{37}Cl experiment at Homestake. Its energy threshold is 0.814 MeV and it can detect the neutrinos from ^7Be ($E_\nu = 0.861$ MeV) and ^8B ($E_\nu \leq 14.02$ MeV) reactions. The detection is via inverse beta decay. The reaction is:

$$\nu_e + {}^{37}Cl \rightarrow e^- + {}^{37}Ar.$$

In the standard solar model (SSM) of Bahcall-Pinnsonneault [15]. the capture rate in the ^{37}Cl experiment is predicted to be $9.3^{+1.2}_{-1.4}$ SNU. However, the measured rate is only [16]

$$R_{Cl} = 2.54 \pm 0.16 \pm 0.14 \text{ SNU.} \tag{2.1}$$

The water Cerenkov detector at Kamioka, with a threshold of 7.5 MeV, can detect only the neutrinos from the upper end of ^8B spectrum. The detection is via elastic neutrino electron scattering:

$$\nu_e + e^- \rightarrow \nu_e + e^-.$$

The Kamioka result [17] is given by the ratio,

$$y_{Kam} = \frac{R_{Kam}}{R_{Kam:SSM}} = 0.423 \pm 0.058, \tag{2.2}$$

which is the ratio of the observed neutrino flux to that predicted by the SSM. The gallium experiments SAGE and GALLEX, with energy threshold of 0.233 MeV can detect the neutrinos coming from the dominant $p - p$ reaction ($E_\nu \leq 0.42$ MeV) as well as the neutrinos from ^7Be and ^8B reactions. Like the chlorine experiment the detection is again via inverse beta decay, but on a Gallium target. The reaction is:

$$\nu_e + {}^{71}Ga \rightarrow e^- + {}^{71}Ge.$$
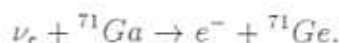
Their measured rates are [18, 19]

$$R_{SAGE} = 73 \pm 8.5^{+5.2}_{-6.9} \text{ SNU},$$
$$R_{GALLEX} = 76.2 \pm 6.5 \pm 5 \text{ SNU},$$

and the average is

$$R_{Ga;avg} = 74.6 \pm 9.33 \text{ SNU} \tag{2.3}$$

as opposed to the SSM prediction of 137^{+8}_{-7} SNU. Recently, Super-Kamioka have announced their first results. This detector is a much larger version of Kamioka, with a threshold of 6.5 MeV. The Super-Kamioka result [20] is

$$y_{SKam} = \frac{R_{SKam}}{R_{SKam:SSM}} = 0.379 \pm 0.034. \tag{2.4}$$

This discrepancy between the solar model predictions and experiment is known as the "Solar Neutrino problem". A rough model independent analysis of these results indicates that the low energy neutrinos from the $p - p$ reaction suffer little suppression whereas the high energy neutrinos are suppressed to a large extent. That is one has an *energy dependent suppression* of the solar neutrino flux. Also The Kamioka result, combined with either ^{37}Cl experiment result or the results of ^{71}Ga experiments, rules out astrophysics or nuclear physics based solutions [21] to the solar neutrino problem. On the other hand nonstandard neutrino physics with neutrino oscillations, with the MSW effect [10, 11] included, provide the best solution to SNP. If one assumes that the electron neutrino ν_e mixes with only one

other active flavor, then the corresponding solution has two disjoint viable regions in the parameter space of mass-squared difference (δ_{21}) and the mixing angle ω. These are the so called small angle and large angle solutions [21]. However, since there are three active neutrinos, one must consider mixing and oscillations between all the three flavors. With this point in view, we analyze the solar neutrino problem in a three flavor framework. Note that since both Kamioka and Super-Kamioka are real time detectors, they give us event rates as a function of time of arrival of the neutrino (or equivalently of the distance travelled by the neutrino). Hence it is possible for these real time detectors to study if there is a difference between the day time and the night time counting rate. The night time counting rate could in principle be different from the day time counting rate, because during night the neutrinos have to travel through the earth, and the earth matter could affect the flavor composition of the neutrino beam. This possible asymmetry between day time and night time counting rates is called "day - night" effect. In this chapter we shall ignore day-night effect, and assume that the day time counting rate is the same as the night time counting rate. The analysis presented in this chapter is similar to ref.[22]. The flux and cross sections have been updated, and the latest experimental data have been used to make the analysis up-to-date. Constraints coming from day-night effect will be presented in detail in a later chapter.

2.2 Three neutrino oscillations in matter

We briefly discuss the mixing between three flavors of neutrinos and then obtain the probability for a ν_e produced in the sun to be detected as a ν_e on earth. The three flavor eigenstates are related to the three mass eigenstates in vacuum through a unitary transformation,

$$\begin{bmatrix} \nu_e \\ \nu_\mu \\ \nu_\tau \end{bmatrix} = U^v \begin{bmatrix} \nu_1^v \\ \nu_2^v \\ \nu_3^v \end{bmatrix},\qquad(2.5)$$

where the superscript v on r.h.s. stands for vacuum. The 3×3 unitary matrix U^v can be parametrized by three Euler angles (ω, ϕ, ψ) and a phase. The form of the

unitary matrix can therefore be written in general as,

$$U^v = U_{phase} \times U_{23}(\psi) \times U_{13}(\phi) \times U_{12}(\omega),$$

where $U_{ij}(\theta_{ij})$ is the mixing matrix between ith and jth mass eigenstates with the mixing angle θ_{ij} [12]. The explicit form of U is

$$U^v = \begin{pmatrix} c_\phi c_\omega & c_\phi s_\omega & s_\phi \\ -c_\psi s_\omega e^{i\delta} - s_\psi s_\phi c_\omega e^{-i\delta} & c_\psi c_\omega e^{i\delta} - s_\psi s_\phi s_\omega e^{-i\delta} & s_\psi c_\phi e^{-i\delta} \\ s_\psi s_\omega e^{i\delta} - c_\psi s_\phi c_\omega e^{-i\delta} & -s_\psi c_\omega e^{i\delta} - c_\psi s_\phi s_\omega e^{-i\delta} & c_\psi c_\phi e^{-i\delta} \end{pmatrix}, \quad (2.6)$$

where $s_\phi = \sin\phi$ and $c_\phi = \cos\phi$ etc. All the angles can take values between 0 and $\pi/2$. It has been shown that the expression for electron neutrino survival probability, integrated over the time of emission and of absorption, is independent of the phase and the third Euler angle ψ [23, 24]. They can be set to zero without loss of generality and we have the following form for U^v

$$U^v = \begin{pmatrix} c_\phi c_\omega & c_\phi s_\omega & s_\phi \\ -s_\omega & c_\omega & 0 \\ -s_\phi c_\omega & -s_\phi s_\omega & c_\phi \end{pmatrix}, \quad (2.7)$$

where $s_\phi = \sin\phi$ and $c_\phi = \cos\phi$ etc. The angles ω and ϕ can take values between 0 and $\pi/2$. Note that one of the flavors decouples if either ω or ϕ is zero and we have a two flavor scenario.

The masses of the vacuum eigenstates are taken to be μ_1, μ_2 and μ_3. In the mass eigenbasis, the (mass)^2 matrix is diagonal,

$$M_0^2 = \begin{pmatrix} \mu_1^2 & 0 & 0 \\ 0 & \mu_2^2 & 0 \\ 0 & 0 & \mu_3^2 \end{pmatrix}$$

$$= \mu_1^2 I + \begin{pmatrix} 0 & 0 & 0 \\ 0 & \delta_{21} & 0 \\ 0 & 0 & \delta_{31} \end{pmatrix}, \quad (2.8)$$

where $\delta_{21} = \mu_2^2 - \mu_1^2$ and $\delta_{31} = \mu_3^2 - \mu_1^2$. Without loss of generality, we can take δ_{21} and δ_{31} to be greater than zero. Neutrino oscillation amplitudes are independent of

the first term so we drop it from further calculation. In the flavor basis the (mass)^2 matrix has the form

$$
\begin{aligned}
M_v^2 &= U^v M_0^2 U^{v\dagger} \\
&= \delta_{31} M_{31} + \delta_{21} M_{21},
\end{aligned}
\tag{2.9}
$$

where

$$
M_{31} = \begin{pmatrix} s_\phi^2 & 0 & s_\phi c_\phi \\ 0 & 0 & 0 \\ s_\phi c_\phi & 0 & c_\phi^2 \end{pmatrix}
$$

$$
M_{21} = \begin{pmatrix} c_\phi^2 s_\omega^2 & c_\phi s_\omega c_\omega & -c_\phi s_\phi s_\omega^2 \\ c_\phi s_\omega c_\omega & c_\omega^2 & -s_\phi s_\omega c_\omega \\ -c_\phi s_\phi s_\omega^2 & -s_\phi s_\omega c_\omega & s_\phi^2 s_\omega^2 \end{pmatrix}.
\tag{2.10}
$$

As in the two flavor case, matter effects can be included by adding $A(r)$, to the $e-e$ element of M_v^2 where

$$
A = 2\sqrt{2}(\frac{GY_e}{m_n})\rho E.
\tag{2.11}
$$

In the above equation m_n is the mass of the nucleon, Y_e the number of electrons per nucleon in the matter which is $\approx \frac{1}{2}$, and ρ is the density of matter in gm/cc. In the Sun A can be written as

$$
A = 0.76 \times 10^{-7} \rho E.
$$

A is in eV^2, if E is expressed in MeV. The matter corrected (mass)^2 matrix in the flavor basis is

$$
M_m^2 = \delta_{31} M_{31} + \delta_{21} M_{21} + A M_A,
\tag{2.12}
$$

where

$$
M_A = \begin{pmatrix} 1 & 0 & 0 \\ 0 & 0 & 0 \\ 0 & 0 & 0 \end{pmatrix}.
\tag{2.13}
$$

To calculate the evolution of a neutrino in matter we have to find the matter corrected eigenstates by diagonalizing M_m^2. For arbitrary values of δ_{31} and δ_{21}, it is cumbersome to find the eigenvalues and eigenvectors of M_m^2 algebraically. However, the eigenvalue problem can be solved using perturbation theory, if the mass differences have the following hierarchy $\delta_{31} \gg \delta_{21}$. This assumption is plausible in light of

the observed atmospheric muon neutrino deficit. Kamiokande have analyzed their atmospheric neutrino data, assuming that the deficit is caused by the oscillation of a ν_μ into another flavor. Their analysis assumes mixing between only two flavors ($\nu_\mu \leftrightarrow \nu_e$ or $\nu_\mu \leftrightarrow \nu_\tau$). For both cases their best fit yields a mass square difference of the order of 10^{-2} eV^2 [25, 26]. In our analysis we take δ_{31} to be 10^{-2} eV^2. Thus we have δ_{31} much larger than A_{max} and hence the oscillations involving the third generation are not influenced very much by the matter effects. In order for the matter effects to be significant (as necessitated by the solar neutrino problem), the other mass difference in the problem, δ_{21}, should be such that the resonance condition is satisfied for some values of parameters. This means $\delta_{21} \sim A_{max}$. *Thus we work in an approximation where $\delta_{21}, A_{max} \ll \delta_{31}$.* Hence we now have a two scale problem, with the two scales well seperated from each other. Therefore the analysis becomes simpler.

In this approximation, to the zeroth order, both the matter term and the term proportional to δ_{21} can be neglected in eq. (2.12). Then $M_m^2 = \delta_{31}M_{31}$, whose eigenvalues and eigenvectors are

$$0 \;;\; \begin{pmatrix} c_\phi \\ 0 \\ -s_\phi \end{pmatrix},$$

$$0 \;;\; \begin{pmatrix} 0 \\ 1 \\ 0 \end{pmatrix},$$

$$\delta_{31} \;;\; \begin{pmatrix} s_\phi \\ 0 \\ c_\phi \end{pmatrix}. \tag{2.14}$$

Treating $AM_A + \delta_{21}M_{21}$ as perturbation to the dominant term in M_m^2 and carrying out degenerate perturbation theory, we get the matter dependent eigenvalues and eigenvectors,

$$m_1^2 \;;\; \begin{pmatrix} c_{\phi m}c_{\omega m} \\ -s_{\omega m} \\ -s_{\phi m}c_{\omega m} \end{pmatrix},$$

$$m_2^2 \quad ; \quad \begin{pmatrix} c_{\phi_m} s_{\omega_m} \\ c_{\omega_m} \\ -s_{\phi_m} s_{\omega_m} \end{pmatrix},$$

$$m_3^2 \quad ; \quad \begin{pmatrix} s_{\phi_m} \\ 0 \\ c_{\phi_m} \end{pmatrix}. \tag{2.15}$$

The above eigenvectors are the columns of the unitary matrix U^m which relates the flavor eigenstates to matter dependent mass eigenstates ν_i^m through the relation

$$\begin{bmatrix} \nu_e \\ \nu_\mu \\ \nu_\tau \end{bmatrix} = U^m \begin{bmatrix} \nu_1^m \\ \nu_2^m \\ \nu_3^m \end{bmatrix}. \tag{2.16}$$

The matter dependent mixing angles can be expressed in terms of the vacuum parameters and A as

$$\tan 2\omega_m = \frac{\delta_{21} \sin 2\omega}{\delta_{21} \cos 2\omega - A \cos^2 \phi}, \tag{2.17}$$

$$\sin \phi_m = \sin \phi \left[1 + \frac{A}{\delta_{31}} \cos^2 \phi \right] \quad ; \quad \cos \phi_m = \cos \phi \left[1 - \frac{A}{\delta_{31}} \sin^2 \phi \right]. \tag{2.18}$$

The matter dependent eigenvalues m_i^2 are given by

$$\begin{aligned} m_1^2 &= A \cos^2 \phi \cos^2 \omega_m + \delta_{21} \sin^2 (\omega - \omega_m), \\ m_2^2 &= A \cos^2 \phi \sin^2 \omega_m + \delta_{21} \cos^2 (\omega - \omega_m), \\ m_3^2 &= \delta_{31} + A \sin^2 \phi \simeq \delta_{31}. \end{aligned} \tag{2.19}$$

ω_m can undergo a resonance if the values of δ_{21}, ϕ and ω are such that the resonance condition

$$A(r) \cos^2 \phi = \delta_{21} \cos 2\omega \tag{2.20}$$

is satisfied for some r [12]. Note that this condition is very similar to the resonance condition in the two flavor case

$$A(r) = \delta_{21} \cos 2\omega.$$

The new feature here, which occurs due to the mixing among the three neutrino flavors, is the presence of the second mixing angle ϕ in the resonance condition.

This dependence on ϕ leads to a larger region of allowed parameter space in the three flavor oscillation scenario as will be shown in the next section. Since δ_{21}, $A(r)$ and $\cos^2 \phi$ are all positive, a resonance can occur only if $\cos 2\omega$ is also positive, or if $\omega < \pi/4$.

In the three flavor case, the electron neutrino survival probability is given by

$$\langle P_{ee} \rangle = \sum_{i,j=1}^{3} |U_{ei}^v|^2 \, |U_{ej}^m|^2 \, |\langle \nu_i^v \mid \nu_j^m \rangle|^2. \tag{2.21}$$

$|\langle \nu_i^v \mid \nu_j^m \rangle|^2$ is the probability that the jth matter dependent eigenstate evolves into ith vacuum eigenstate. As in the two flavor case, if the adiabatic approximation holds, then

$$|\langle \nu_i^v \mid \nu_j^m \rangle|^2 = \delta_{ij}. \tag{2.22}$$

We introduce the jump probabilities

$$x_{ij} = |\langle \nu_i^v \mid \nu_j^m \rangle|^2 \text{ for } i \neq j \tag{2.23}$$

to take into account the non-adiabatic transitions, if the adiabatic condition doesn't hold.

Because $\delta_{31} \gg A_{max}, \delta_{21}$, the third eigenvalue, both in vacuum and in matter, is much larger than the other two eigenvalues. Non-adiabatic effects are significant only if the eigenvalues of two states come close together [27]. Therefore the jump probabilities involving the third state, x_{13} and x_{23} are expected to be negligibly small. Thus we have the expression for electron neutrino survival probability to be

$$\begin{aligned} \langle P_{ee} \rangle &= \cos^2 \phi \cos^2 \phi_m \left(\cos^2 \omega \cos^2 \omega_m + \sin^2 \omega \sin^2 \omega_m \right) + \sin^2 \phi \sin^2 \phi_m \\ &\quad - x_{12} \cos^2 \phi \cos^2 \phi_m \cos 2\omega \cos 2\omega_m. \end{aligned} \tag{2.24}$$

For x_{12} we use the formula,

$$x_{12} = \frac{\exp[-\frac{\pi \gamma F}{2}] - \exp[-\frac{\pi \gamma F}{2 \sin^2 \omega}]}{1 - \exp[-\frac{\pi \gamma F}{2 \sin^2 \omega}]}, \tag{2.25}$$

where γ is defined as

$$\gamma \equiv \frac{\delta_{21}}{E |\frac{1}{A} \frac{dA}{dr}|_{res}} \frac{\sin^2 2\omega}{\cos 2\omega}. \tag{2.26}$$

γ is known as the adiabaticity parameter, and it gives us a criterion for estimating the nonadiabatic effects during the propagation of the neutrino. If $\gamma \gg 1$, then nonadiabatic effects are negligible and the propagation is essentially adiabatic. On the other hand $\gamma \approx 1$ means there can be substantial corrections to the adiabatic approximation. Note that γ is evaluated at the resonance point, that is because nonadiabatic effects are important only in the vicinity of the resonance. The function F depends upon the density profile in which the neutrino propagates, and

$$F = 1 - \tan^2 \omega \qquad (2.27)$$

for an exponentially varying solar density[12] as in the case of the sun. We use eq. (2.25) for the jump probability since it is valid both for large and small mixing angles. In the extreme non-adiabatic limit $x_{12} \to \cos^2 \omega$ and when $\gamma F >> 1$, we have the usual Landau-Zener jump probability given by $x_{12} \to \exp[-\frac{\pi\gamma F}{2}]$ [12] as expected.

2.3   Results

We use the expression for $\langle P_{ee} \rangle$ in (2.24) and find the ranges of δ_{21}, ω and ϕ allowed by the three solar neutrino experiments. Since $\delta_{31} \gg A_{max}$, we see from the expression for ϕ_m in (2.18) that the angle ϕ is almost unaffected by the matter effects. However, ω_m can be significantly different from ω and can undergo resonance if the resonance condition in (2.20) is satisfied. Since this resonance condition depends on ϕ, in addition to δ_{21} and ω, a larger region of parameter space satisfies the three constraints from the experiments.

To search for the regions allowed in the three parameter space δ_{21}, ω and ϕ, we define the suppression factors observed by the four types of experiments

$$y_{Ga} = \frac{R_{Ga;avg}}{R_{Ga;SSM}} = 0.544 \pm 0.074,$$

$$y_{Cl} = \frac{R_{Cl}}{R_{Cl;SSM}} = 0.2731 \pm 0.044,$$

$$y_{Kam} = \frac{R_{Kam}}{R_{Kam;SSM}} = 0.423 \pm 0.058, \qquad (2.28)$$

$$y_{SKam} = \frac{R_{SKam}}{R_{SKam;SSM}} = 0.379 \pm 0.034, \tag{2.29}$$

where the first number refers to the average of the data given by two experiments-namely GALLEX and SAGE. The predicted SSM rates for various experiments were taken from Bahcall-Pinsonneault SSM calculations [15]. The uncertainties in y_i are the sum of the experimental uncertainty in the numerator and the theoretical uncertainty in the denominator, added in quadrature. Because of its different threshold, we treat Super-Kamioka as a different experiment.

The predictions for y_i for the three flavor oscillation scenario are obtained by convoluting the SSM fluxes and the detector cross sections with $\langle P_{ee} \rangle$ from (2.24). The expression we use is

$$y = \frac{\sum_K \int_{E_{min}}^{E_{max}} dE \Phi_K(E) \sigma(E) < P_{ee} > (E)}{\sum_K \int_{E_{min}}^{E_{max}} dE \Phi_K(E) \sigma(E)}, \tag{2.30}$$

where the sum over K refers to the neutrino fluxes from various sources contributing to the process. We also include the contributions from the CNO cycle apart from the dominant contributions from the $p - p$ cycle. In the case of Kamioka, and Super-Kamioka only the ^8B flux contributes and one must also take into account the neutral current contribution arising from the muon and tau neutrinos interacting with the detector material. The parameter ranges are then calculated by putting vetos on y at 1.6σ levels. The energy dependent fluxes were taken from Ref. [15] and the cross sections were taken from Ref. [14].

We show the results in Fig.(2.1) as regions allowed at 90 percent C.L in the $\omega - \delta_{21}$ plane, for various values of ϕ. The following features emerge from the graphs.

1. The panel labelled (a) shows the region allowed for $\phi = 0°$. There are two distinct regions in the parameter space. The first region has $\delta_{21} < 10^{-5} eV^2$, and ω about $3°$. This is called the small angle region. The other region has $\delta_{21} > 10^{-5} eV^2$, and $\omega > 25°$. This is called the large angle region. Notice the clear seperation between the two regions.

2. Panel (b) shows the region allowed for $\phi = 10°$. One sees that there is no perceptible difference, when compared to the $\phi = 0°$ case.

3. Panel (c) shows the region allowed for $\phi = 20°$. Now the value of ϕ starts influencing the parameter space. The small angle region almost the same, while the large angle region broadens a bit to include slightly smaller values of ω.

4. Panel (d) shows the region allowed for $\phi = 30°$. Now both the small angle as well as the large angle regions broaden, and they almost merge at a point. Each region has the appearance of two limbs.

5. Panel (e) shows the region allowed for $\phi = 40°$. The two limbs merge with each other at one end of each limb. But one can still discern the two different limbs.

6. Panel (f) shows the region allowed for $\phi = 45°$. Now two limbs completely merge with each other, and there is one single patch in the parameter space. Hence the effect of increasing ϕ is finally to merge the two disjoint regions into one single region.

Note that the parameter space obtained in the present analysis, is more or less the same parameter space which was obtained in previous analyses of solar neutrino problem in three flavors using older data [22, 28].

The various regions of the allowed parameter space may be classified as follows:

1. small δ_{21}, small ω, small ϕ,

2. large δ_{21}, large ω, small ϕ,

3. small δ_{21}, small ω, large ϕ,

4. large δ_{21}, small ω, large ϕ,

5. large δ_{21}, large ω, large ϕ,

where the small or large δ_{21} means either $\delta_{21} < 10^{-5} eV^2$ or $\delta_{21} > 10^{-5} eV^2$. The first two regions corresponding to small ϕ in the above classification belong to an approximate two generation situation since the angle ϕ is small. The one corresponding

to small ω is the usual non-adiabatic solution, whereas the one corresponding to large ω is the usual adiabatic solution. The rest invoke the genuine three generation oscillation mechanism. In the two flavor scenario, the small angle solution (corresponding to ω small as in case 1 above) gives the best fit [21]. There the parameter space allowed is small because the resonance condition and the non-adiabatic jump factor fix δ_{21} and ω almost uniquely. These values of parameters indicate that the neutrinos from the $p - p$ cycle suffer very little suppression and those from ^7Be suffer almost complete suppression as will be illustrated soon in the analysis of the survival probability. In the three flavor scenario, the resonance condition (eq. 2.20) and the survival probability (eq. 2.24) are dependent on the second angle ϕ also. The suppression of the $p-p$ neutrinos depends on the value of ϕ and if this suppression is significant, then the complete suppression for ^7Be neutrinos can be relaxed. This is one of the important differences between the three flavor and the two flavor oscillations.

Fig.(2.2) shows the energy dependence of $\langle P_{ee}\rangle$ for some representative values of ω, ϕ and δ_{21}. The curve labelled (a) corresponds to $\phi = 2°$. As there is very little mixing between the first and the third generation of neutrinos, this is infact an almost two generation case. In agreement with the two generation analysis, there is almost no suppression of the $p - p$ neutrinos and the ^7Be neutrinos are almost completely suppressed. The survival probability at high energies relevant to Kamioka is almost a linear function with an average around 0.5 as one would expect. Also here the values of ω and δ_{21} are small (they are almost equal to the values obtained in the two flavor case) and the non-adiabatic effects become important beyond 2 MeV. Keeping ω small if we increase ϕ in the allowed region there is a perceptible reduction in the probability in the $p - p$ energy range and an increase in the survival probability of the ^7Be neutrinos (curves (b) and (c)). When δ_{21} is increased, however, there is a qualitative change in the survival probability profile. In this range both ω and ϕ are allowed to be large. Here also there is a qualitative change when ω is small or large. For large ω the survival probability is a smooth function resembling the adiabatic case of the two generation analysis (curves (d) and (f)) whereas for small ω it is almost a step function (curve (e)) which is like the classic adiabatic case discussed by Bethe in the two generation case [9]. One

common feature of the large δ_{21} case is that the $p-p$ neutrinos undergo substantial suppression varying between 0.6 -0.5. The resonance also occurs at a much higher energy than in the small δ_{21} case. Curve (f) has ω, ϕ and δ_{21} all large and in some sense it can be called 'most representative' of the three flavor oscillation scenario because both the mixing angles in this case are large. In all the above cases, except (e), the average survival probability above 7 MeV is in the neighbourhood of 0.4 which is what is required by Kamioka and Super-Kamioka data, and there is no dramatic change from one to the other. This is not so at low energies where the curves differ dramatically.

One way of experimentally measuring the energy dependence of $\langle P_{ee} \rangle$ is to look at the recoil electron spectrum in those detectors that use $\nu_e - e$ scattering. In Fig.(2.3) we have shown the recoil electron spectrum for the six cases plotted in Fig.(2.3). Except case (f), they cannot be distinguished beyond 10 MeV, whereas there are substantial differences at low energies. It is interesting to note that it may be possible to see this difference in the experimental recoil electron spectrum in the SNO[29] and Borexino[30] detectors. Note that in computing the recoil electron spectrum, we have used the spectrum of ^8B neutrinos as input. This is because the threshold in experiments which can measure the recoil electron spectrum (like SNO and Kamioka) is more than a few MeVs where only this flux matters. The only exception is Borexino where the threshold is much lower and there are other contributions below 1.5MeV. In particular the recoil spectrum induced by the ^7Be neutrinos, can give a clear pointer to the vacuum parameters. We will analyse Borexino in detail at a later stage. We mention in passing that a recent analysis of the Kamioka recoil spectrum [21] rules out large values of $\delta_{21} \approx 10^{-4}eV^2$.

In conclusion the solar neutrino problem enables us to put bounds on three of the five parameters, which occur in three flavor neutrino mixing. In the next chapter we shall analyze the atmospheric neutrino problem, and show that one can obtain bounds on the other two parameters also. Hence together with the solar neutrino problem, one can obtain bounds on all the five parameters which occur in three flavor neutrino oscillations.
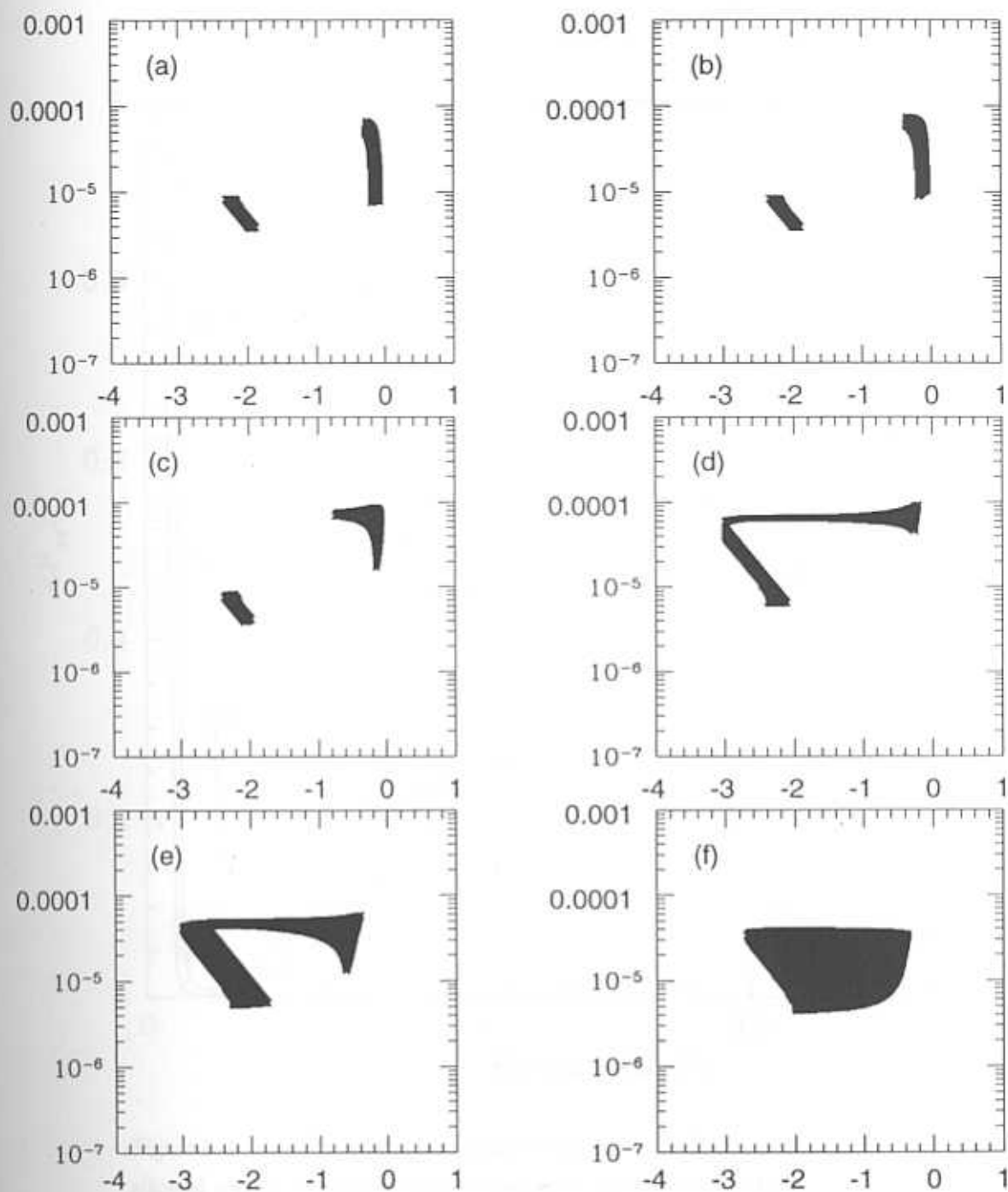
Figure 2.1: Allowed regions in the $\omega - \delta_{21}$ plane for various values of ϕ. The x axis shows $\log(\sin^2 2\omega)$ and the y axis δ_{21} in eV^2
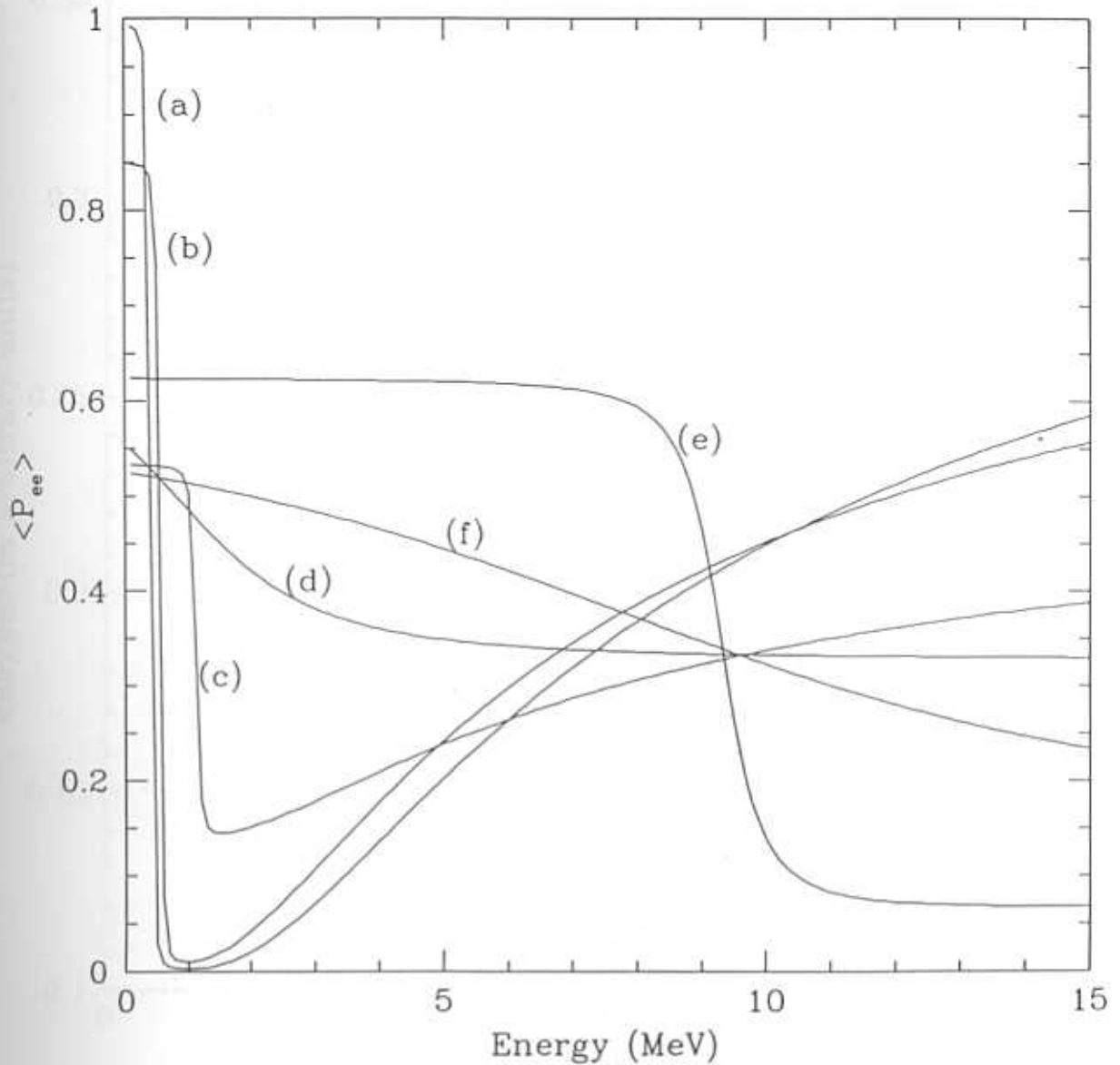
Figure 2.2: Survival probability (P_{ee}) vs E_{ν} for typical values of ϕ, ω and δ_{21} in the allowed region. The parameters chosen are: (a) $\delta_{21} = 4.0 \times 10^{-6}, \omega = 3.0°, \phi = 2.0°$; (b) $\delta_{21} = 4.0 \times 10^{-6}, \omega = 3.0°, \phi = 16.0°$; (c) $\delta_{21} = 7.0 \times 10^{-6}, \omega = 2.0°, \phi = 38.0°$; (d) $\delta_{21} = 2.5 \times 10^{-5}, \omega = 33.0°, \phi = 3.0°$; (e) $\delta_{21} = 3.0 \times 10^{-5}, \omega = 1.0°, \phi = 30.0°$; (f) $\delta_{21} = 9.0 \times 10^{-5}, \omega = 24.5°, \phi = 24.0°$; δ_{21} is given in terms of eV^2.
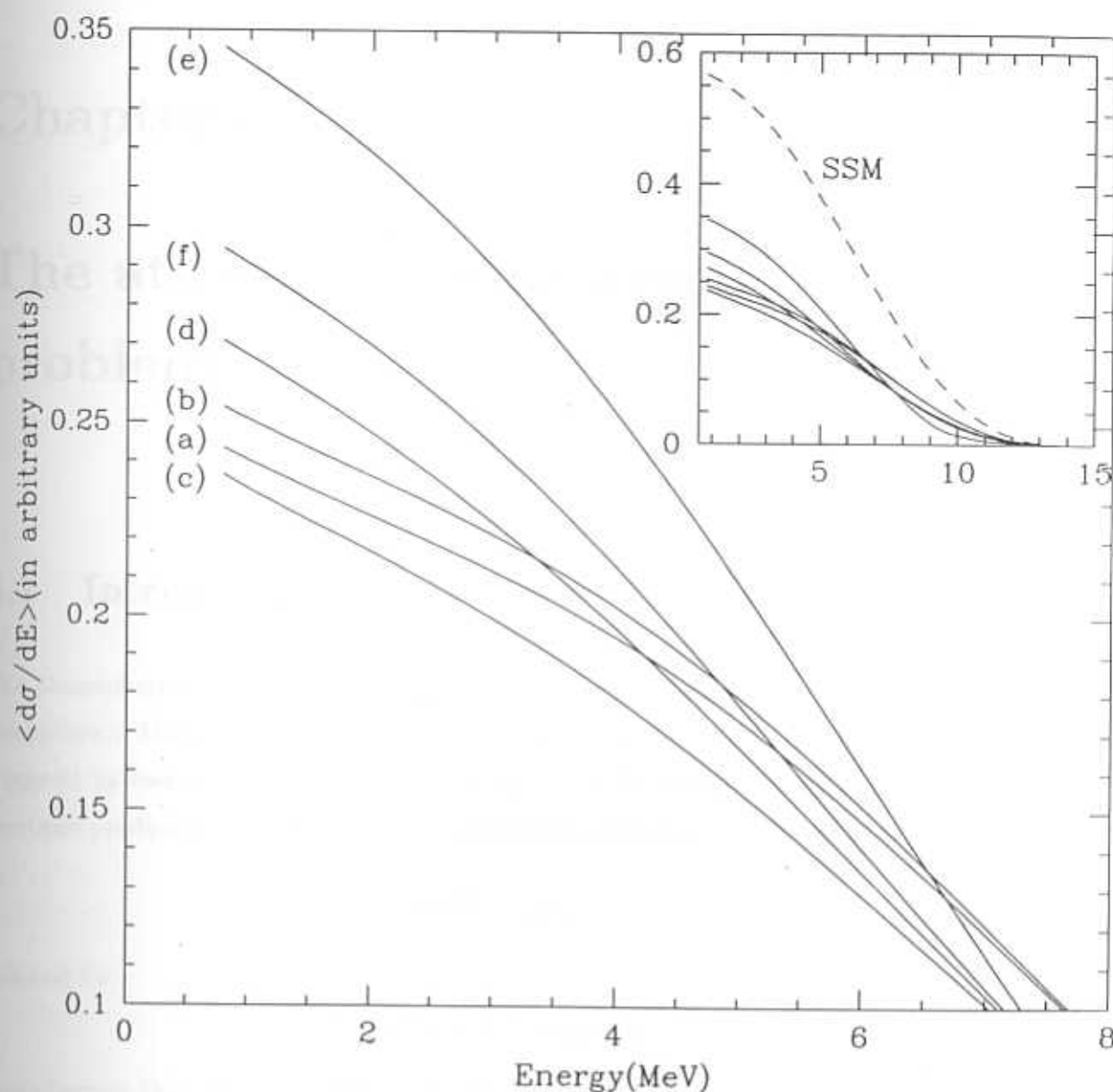
Figure 2.3: Recoil electron spectrum for different representative points of the allowed parameter region. The parameters for the difference curves labelled (a)-(f) are the same as in Fig.2.2 The inset shows a comparison of all six cases with the SSM spectrum(dashed line).

Chapter 3

The atmospheric neutrino problem

3.1 Introduction

The atmosphere is a source of electron as well as muon type of neutrinos and antineutrinos. These neutrinos are the end product of a cascade process which is triggered by cosmic rays interacting with nuclei in the earth's atmosphere. These reactions produce pions which, in turn undergo the following decay.

$$\pi^{\pm} \to \mu^{\pm} + \nu_{\mu}(\bar{\nu}_{\mu}),$$

followed by

$$\mu^{\pm} \to e^{\pm} + \nu_{e}(\bar{\nu}_{e}) + \bar{\nu}_{\mu}(\nu_{\mu}).$$

One observes that there are twice as many muon type of neutrinos as that of the electron type. (Unless explicitly stated, in this chapter we call neutrinos and antineutrinos collectively as neutrinos). The atmospheric neutrino spectrum extends upto about $100~GeV$. The flux has a strong energy dependence, which goes roughly as E^{-3}, and also has an angular dependence, which is different at each location on the earth. This is primarily due to the effect of the earth's magnetic field. The calculation of these fluxes is hence quite involved. There are detailed Monte Carlo

predictions for these fluxes, and they confirm that the ratio of the flux of muon neutrinos Φ_{ν_μ} to the flux of electron neutrinos Φ_{ν_e} is about 2 [31, 32]. The absolute neutrino fluxes predicted from different calculations however differ significantly from each other (by as much as 30%), but the predictions for the ratio of the fluxes $\Phi_{\nu_\mu}/\Phi_{\nu_e}$ are in good agreement with each other (to within 5%). This is because though the individual fluxes have large uncertainties, this cancels out in the prediction of the ratio.

In recent years, deep underground detectors have been measuring the flux of these neutrinos. The large water Cerenkov detectors Kamiokande and IMB [33] have measured this ratio and have found it to be about half of what is predicted [34]. This anomalous value of the ratio is called "The Atmospheric neutrino problem". The experimental results are presented in the form of a double ratio

$$R = \frac{\left(\frac{N_{\nu_\mu}}{N_{\nu_e}}\right)_{obs}}{\left(\frac{N_{\nu_\mu}}{N_{\nu_e}}\right)_{MC}} = \frac{r_{obs}}{r_{MC}}. \tag{3.1}$$

N_{ν_μ} is the number of events which are induced by muon type of neutrinos, while N_{ν_e} is the number of events induced by electron type of neutrinos. The suffix "obs" stands for the observed number of events, while "MC" stands for the Monte Carlo prediction. Kamiokande collaboration have presented their results for neutrinos with energy less than 1.33 GeV (sub-GeV data) [54] and for neutrinos with energy greater then 1.33 GeV (multi-GeV data) [55]. For the sub-GeV data, $R = 0.60^{+0.07}_{-0.06} \pm 0.05$ and for the multi-GeV data, $R = 0.57^{+0.08}_{-0.07} \pm 0.07$ after averaging over the zenith angle. Here the zenith angle denoted by θ is the angle between the direction of the incident neutrino, and the vertical axis passing through the detector. As the detector is located about a few Km below the surface of the earth, $\theta = 0°$, means the neutrinos are coming straight from above, and $\theta = 180°$ means the neutrinos are coming from below, i.e., neutrinos which travel the whole diameter of the earth to reach the detector (Note the downward direction is taken as the positive zenith axis). The value of R has no significant zenith angle dependence for the sub-GeV data. However, for the multi-GeV data, R is small for large values of zenith angle (upward going neutrinos) and is large for small values of zenith angle (downward going neutrinos). Also the number of electron neutrino events alone are in reasonable agreement with data, while there is an appreciable deficit of the muon neutrino

events. Similar to the solar neutrino problem it is quite natural to assume that neutrino oscillations are the cause of this departure of the ratio R from unity (i.e., the Monte Carlo expectation).

Kamiokande have analyzed their data assuming that the smaller observed value of R is caused by neutrino oscillations. Since the upward going neutrinos travel large distances inside the earth before entering the detector, matter effects may be important for these, especially at higher energies [35, 36]. Therefore one must take matter effects into consideration while analyzing $\nu_\mu \leftrightarrow \nu_e$ oscillations. The Kamikande collaboration [54, 55] have in fact taken matter effects into consideration in their analysis. They have done two independent analyses, one assuming two flavor oscillations between $\nu_\mu \leftrightarrow \nu_e$ and the other assuming two flavor oscillations between $\nu_\mu \leftrightarrow \nu_\tau$. For both the cases, they obtain a mass-squared difference $\delta m^2 \sim 10^{-2} eV^2$ and a mixing angle nearly 45^0. However since there are three flavors of neutrinos, a proper analysis of the atmospheric neutrino problem must take mixing and oscillations between all the three flavors into account. Atmospheric neutrino problem was analyzed in the three flavor neutrino oscillation framework previously. In Ref. [37] the sub-GeV data were analyzed under the assumption that one of the mass differences is much smaller than the other. The matter effects due to the passage of neutrinos through the earth were included and the allowed values of neutrino parameters were obtained. Various other authors have analyzed, in the context of three flavor oscillations, accelerator and reactor data in conjunction with the sub-GeV atmospheric data [38] or the multi-GeV data with zenith angle dependence included [39]. However, in both these cases the earth matter effects were not taken into account. Several authors have attempted a simultaneous solution of the solar and atmospheric neutrino problems in three flavor oscillation scenarios. The solution in Ref. [40] assumes maximal mixing between all the three flavors and derives the constraints on the mass differences. The solution thus obtained restricts the mass difference to be very small ($\sim 10^{-10} eV^2$) and is somewhat fine-tuned. Other solutions have assumed the mass hierarchy that was considered in Ref. [37] and obtained the allowed regions in the neutrino parameter space [41, 28, 43, 22]. However, all these analyses were based on the sub-GeV atmospheric neutrino data. The multi-GeV data and its zenith angle dependence were not included. In a recent

analysis of the multi-GeV data, earth matter effects and the zenith angle dependence were taken into account [44]. However, this analysis considered the atmospheric neutrino problem only.

In this chapter, we analyze the Kamiokande atmospheric neutrino data in the framework of three flavor neutrino oscillations. We only assume that, of the two mass differences in a three flavor analysis, the smaller one is chosen to solve the solar neutrino problem and the larger one will be relevant for the atmospheric neutrino problem. This was the same assumption we made in analyzing the solar neutrino problem in chapter 1. We do not, apriori, make any assumption about the form of the mixing matrix. Our starting point is the same as that in Ref. [37]. We include the matter effects due to the passage of neutrinos through the earth. We also take the allowed values of neutrino parameters from our earlier analysis of the solar neutrino problem as inputs to our present analysis.

3.2   Oscillation probabilities

In this section we describe the three flavor neutrino mixing and calculate the probability for a neutrino produced as ν_α in the atmosphere to be detected as ν_β in the earth, where α and β are flavor indices.

In vacuum the flavor eigenstates are related to the mass eigenstates by

$$\begin{bmatrix} \nu_e \\ \nu_\mu \\ \nu_\tau \end{bmatrix} = U^v \begin{bmatrix} \nu_1^v \\ \nu_2^v \\ \nu_3^v \end{bmatrix}, \tag{3.2}$$

where the superscript 'v' denotes vacuum. The unitary matrix U^v can be parametrized as

$$U^v = U^{23}(\psi) \times U^{phase} \times U^{13}(\phi) \times U^{12}(\omega), \tag{3.3}$$

where $U^{ij}(\theta_{ij})$ is the two flavor mixing matrix between the ith and jth mass eignestates with the mixing angle θ_{ij}. For simplicity, we neglect the CP violation and set $U^{phase} = I$.

In the mass basis the mass-squared matrix is diagonal and can be taken to be

$$M_0^2 = \begin{bmatrix} \mu_1^2 & 0 & 0 \\ 0 & \mu_2^2 & 0 \\ 0 & 0 & \mu_3^2 \end{bmatrix} = \mu_1^2 I + \begin{bmatrix} 0 & 0 & 0 \\ 0 & \delta_{21} & 0 \\ 0 & 0 & \delta_{31} \end{bmatrix}, \tag{3.4}$$

where $\delta_{21} = \mu_2^2 - \mu_1^2$ and $\delta_{31} = \mu_3^2 - \mu_1^2$. μ_i^2, $i = 1,3$ are the squares of the vacuum mass eigenvalues. Without loss of generality we can take $\mu_3 > \mu_2 > \mu_1$ so that both δ_{21} and δ_{31} are positive. For extreme relativistic neutrinos, the oscillation probability depends only on the mass-squared differences so we ignore the first term $\mu_1^2 I$. In the flavor basis, the mass-squared matrix is non-diagonal and is given by

$$M_v^2 = U^v M_0^2 (U^v)^\dagger. \tag{3.5}$$

For the propagation of neutrinos through the earth, we need to take the matter effects into account. The charged current scattering between electrons and ν_e induces an effective mass-squared term for ν_e which is of the form $A = 2\sqrt{2} G_F N_e E$, where N_e is the number density of electrons and E is the neutrino energy [10]. In this chapter A is the Wolfenstein term induced by passage of the neutrinos through the earth. This term is present only for the $e - e$ element in the flavor basis so the mass-squared matrix including the matter effects is

$$M_m^2 = M_v^2 + \begin{bmatrix} A & 0 & 0 \\ 0 & 0 & 0 \\ 0 & 0 & 0 \end{bmatrix}. \tag{3.6}$$

M_m^2 is a hermitian matirx and can be diagonalized by unitary matrix U^m, which relates the flavor eigenstates to matter dependent mass eigenstates

$$\begin{bmatrix} \nu_e \\ \nu_\mu \\ \nu_\tau \end{bmatrix} = U^m \begin{bmatrix} \nu_1^m \\ \nu_2^m \\ \nu_3^m \end{bmatrix}, \tag{3.7}$$

where the superscript 'm' stands for matter. We denote the matter dependent mass eigenvalues as m_1, m_2 and m_3. The matter dependent mixing matrix U^m can be parametrized in terms of three mixing angles in a manner similar to that of U^v as given in eq.(3.8). The matter dependent mass eigenvalues and mixing angles can

be obtained, in terms of the vacuum parameters and A, by solving the eigenvalue problem of M_m^2 in eq. (3.6).

The distance scales and the energy scales in the solar neutrino problem and the atmospheric neutrino problem are very different. Therefore, one needs two distinct mass scales to solve the solar and the atmospheric neutrino problems simultaneously. As we saw in the previous chapter to simultaneously satisfy the constraints from all the solar neutrino experiments, one must choose $\delta_{21} \sim 10^{-5}$ eV^2, which is roughly the matter term A for the solar neutrinos due to their passage through the sun. The analysis of the atmospheric neutrino problem by Kamioka [55], requires that the mass scale relevant for atmospheric neutrino oscillations is $\sim 10^{-2}$ eV^2. We take δ_{31} to be the scale relevant to the atmospheric neutrino problem. Hence we have $\delta_{31} \gg \delta_{21}$. If $\delta_{21} \sim 10^{-5}$ eV^2, the oscillation length corresponding to it, even for the minimum of the atmospheric neutrino energies, is of the order of the diameter of the earth. In the expression for the oscillation probability, δ_{21} can be set to zero. Therefore the oscillations are dependent on only one mass difference δ_{31} in the atmospheric neutrino problem.

In the approximation of neglecting δ_{21}, it is straightforward to show that the oscillation probability is independent of the mixing angle ω. The argument is as follows. The explicit form of the vacuum mixing matrix is

$$U^v = \begin{pmatrix} c_\phi c_\omega & c_\phi s_\omega & s_\phi \\ -c_\psi s_\omega - s_\psi s_\phi c_\omega & c_\psi c_\omega - s_\psi s_\phi s_\omega & s_\psi c_\phi \\ s_\psi s_\omega - c_\psi s_\phi c_\omega & -s_\psi c_\omega - c_\psi s_\phi s_\omega & c_\psi c_\phi \end{pmatrix}, \tag{3.8}$$

where $s_\phi = \sin\phi$ and $c_\phi = \cos\phi$ etc. All the angles can take values between 0 and $\pi/2$. U^v can also be written as

$$U^v = \begin{pmatrix} U_{e1} & U_{e2} & U_{e3} \\ U_{\mu 1} & U_{\mu 2} & U_{\mu 3} \\ U_{\tau 1} & U_{\tau 2} & U_{\tau 3} \end{pmatrix}. \tag{3.9}$$

Neglecting δ_{21}, the mass-squared matrix in vacuum mass eigenbasis becomes

$$M_0^2 = \begin{bmatrix} 0 & 0 & 0 \\ 0 & 0 & 0 \\ 0 & 0 & \delta_{31} \end{bmatrix}$$

$$= \delta_{31} \begin{bmatrix} 0 & 0 & 0 \\ 0 & 0 & 0 \\ 0 & 0 & 1 \end{bmatrix} \tag{3.10}$$

Transforming to flavor basis we get

$$
\begin{aligned}
M_\nu^2 &= U^\nu M_0^2 \left(U^\nu\right)^\dagger \\
&= \delta_{31} \begin{pmatrix} U_{e3}^2 & U_{e3}U_{\mu3} & U_{e3}U_{\tau3} \\ U_{\mu3}U_{e3} & U_{\mu3}^2 & U_{\mu3}U_{\tau3} \\ U_{\tau3}U_{e3} & U_{\tau3}U_{\mu3} & U_{\tau3}^2 \end{pmatrix}.
\end{aligned}
\tag{3.11}
$$

Note that the mass squared matrix is a function of only three elements of the mixing matrix, viz $U_{e3}, U_{\mu3}$ and $U_{\tau3}$. From eq. (3.8), we see that these three elements of the mixing matrix do not involve ω. Therefore the eigenvalues and eigenvectors of M_ν^2 will also be independent of ω. So the oscillation probabilities which are built from the elements of the eigenvectors will also be independent of ω. It is obvious that adding matter effects does not change the above conclusion. Note, however, that neglecting δ_{21} does not reduce the problem to an effective two flavor mixing. The three flavor nature of the problem is reflected by the fact that the oscillation probability is a function of the mass difference δ_{31} and *two* mixing angles ϕ and ψ. In the case of an effective two flavor mixing, the oscillation probability is dependent on one mixing angle only. Including matter effects and diagonalizing the mass squared matrix defined in eq. (3.11), we get the mixing angles and mass eigenvalues in matter. The mixing angle ψ remains unaffected but the angle ϕ becomes matter dependent. We obtain

$$\tan 2\phi_m = \frac{\delta_{31}\sin 2\phi}{\delta_{31}\cos 2\phi - A}, \tag{3.12}$$

and

$$\psi_m = \psi. \tag{3.13}$$

The mass eigenvalue of ν_1^m remains 0 (actually it is of the order of δ_{21} which we are neglecting here). The other two matter dependent mass eigenvalues are given by

$$m_2^2 = \frac{1}{2}\left[(\delta_{31} + A) - \sqrt{(\delta_{31}\cos 2\phi - A)^2 + (\delta_{31}\sin 2\phi)^2}\right], \tag{3.14}$$

$$m_3^2 = \frac{1}{2}\left[(\delta_{31} + A) + \sqrt{(\delta_{31}\cos 2\phi - A)^2 + (\delta_{31}\sin 2\phi)^2}\right]. \tag{3.15}$$

Equations (3.12), (3.14) and (3.15) are valid for neutrinos. For anti-neutrinos, we get a similar set of formulae with A replaced by $-A$.

The neutrinos produced in the atmosphere enter the earth after travelling through the atmosphere for about 20 Km and finally reach the detector after travelling through the earth. The distance travelled through the earth is a function of the zenith angle. For the five bins considered by Kamiokande [55], the average values of the cosine of the zenith angle are $-0.8, -0.4, 0.0, 0.4, 0.8$ and the average distances travelled through the earth are 10210, 5137, 832, 34, 6 Km respectively [40].

A neutrino of flavor α, produced in the atmosphere at time $t = 0$, propagates through the atmosphere as a linear combination of the vacuum mass eigenstates. If the neutrino enters earth at time $t = t_1$, its state vector at that time can be written as

$$|\Psi_\alpha(t_1)\rangle = \sum_i U^v_{\alpha i} exp\left(-i\frac{\mu_i^2 t_1}{2E}\right) |\nu_i^v\rangle. \tag{3.16}$$

Reexpressing the vacuum mass eigenstates in terms of flavor states, we have

$$|\Psi_\alpha(t_1)\rangle = \sum_i U^v_{\alpha i} exp\left(-i\frac{\mu_i^2 t_1}{2E}\right) \sum_\lambda U^{v*}_{\lambda i}|\nu_\lambda\rangle. \tag{3.17}$$

After entering the earth, the neutrino propagates as a linear combination of the matter dependent mass eigenstates. We take the earth to be a slab of constant density. At the time of detection $t = t_d$, the state vector takes the form

$$|\Psi_\alpha(t_d)\rangle = \sum_i U^v_{\alpha i} exp\left(-i\frac{\mu_i^2 t_1}{2E}\right) \sum_\lambda U^{v*}_{\lambda i} \sum_j U^m_{\lambda j} exp\left(-i\frac{m_j^2(t_d - t_1)}{2E}\right) |\nu_j^m\rangle. \tag{3.18}$$

Hence the amplitude for the neutrino produced as flavor α at t = 0 to be detected as a neutrino of flavor β at time t_d is given by

$$\langle\nu_\beta|\Psi_\alpha(t_d)\rangle = \sum_i \sum_\lambda \sum_j U^v_{\alpha i} U^{v*}_{\lambda i} U^m_{\lambda j} U^{m*}_{\beta j} exp\left(-i\frac{\mu_i^2 t_1}{2E}\right) exp\left(-i\frac{m_j^2(t_d - t_1)}{2E}\right). \tag{3.19}$$

The probability of oscillation $P_{\alpha\beta}$ is given by the modulus square of the above amplitude. If $t_d - t_1$ is set equal to zero (that is if the total time of travel is equal to the time of travel through the atmosphere) then the expression in eq.(3.19) reduces to the simple vacuum oscillation amplitude. The same is true if the matter effects are ignored, i.e., if $U^m = U^v$ and $m_i = \mu_i$.

For bins 1, 2 and 3, the distance travelled in earth is much larger than the distance travelled in the atmosphere. Therefore t_1 is much smaller than t_d for these bins and can be neglected. Neglecting t_1, simplifies the expressions for oscillation probability and we obtain the expressions derived earlier in Ref. [37]. However, for bins 4 and 5, the distance of travel in atmosphere is comparable to that in earth. Therefore t_1 is of the same of order of magnitude as t_d and can not be neglected. Keeping $t_1 \neq 0$ in eq.(3.19) properly takes into account the non-adiabaticity in the abrupt change in density when the neutrino enters earth.

3.3   Calculation and results

3.3.1   Sub-GeV Data

First we describe our analysis of the sub-GeV data. Matter effects are unimportant for the sub-GeV data. If the earth is taken to be a slab of density 5.5 gm/cm^3, the matter term A for the sub-GeV neutrinos is less than 3.8×10^{-4} eV^2. As we will shortly see, the sub-GeV data sets a lower limit on $\delta_{31} > 10^{-3}$ eV^2. Hence the matter effects can be neglected and the expressions for $P_{\alpha\beta}$ in the sub-GeV analysis are simply the vacuum oscillation probabilities

$$
\begin{aligned}
P_{\alpha\beta}^0 &= \left(U_{\alpha1}^v U_{\beta1}^v\right)^2 + \left(U_{\alpha2}^v U_{\beta2}^v\right)^2 + \left(U_{\alpha3}^v U_{\beta3}^v\right)^2 \\
&+ 2\, U_{\alpha1}^v U_{\alpha2}^v U_{\beta1}^v U_{\beta2}^v \cos\left(2.53 \frac{d\,\delta_{21}}{E}\right) \\
&+ 2\, U_{\alpha1}^v U_{\alpha3}^v U_{\beta1}^v U_{\beta3}^v \cos\left(2.53 \frac{d\,\delta_{31}}{E}\right) \\
&+ 2\, U_{\alpha2}^v U_{\alpha3}^v U_{\beta2}^v U_{\beta3}^v \cos\left(2.53 \frac{d\,\delta_{32}}{E}\right),
\end{aligned}
\tag{3.20}
$$

where d is the distance of travel in meters, δ's are the mass differences in eV^2 and E is the neutrino energy in MeV. Because we have neglected the CP violating phase, the oscillation probability for the anti-neutrinos is the same as that for the neutrinos. Since δ_{21} is very small, the cosine term containing it in eq.(3.20) can be set equal to 1. The other two cosine terms are dependent on δ_{31} (and $\delta_{32} \simeq \delta_{31}$), the neutrino energy and the distance of travel which is related to the zenith angle. As mentioned earlier,

the double ratio R defined in eq.(3.1) does not have any zenith angle dependence for the sub-GeV data. One can account for this if it is possible to replace the distance dependent terms in eq.(3.20) by their average values. This replacement is possible only if the average distance travelled contains many oscillation lengths. The above condition sets a lower limit on the mass difference $\delta_{31} > 10^{-3} \ eV^2$ [22]. Note that this lower limit is consistent with the approximation $\delta_{31} \gg \delta_{21} \sim 10^{-5} \ eV^2$, which was made so that both solar and atmospheric neutrino problems could be solved simultaneously.

In the presence of oscillations, the number of muon type and electron type events can be written as

$$N_\mu = \int \phi_{\nu_\mu} P_{\mu\mu} \sigma_\mu dE + \int \phi_{\bar{\nu}_\mu} P_{\bar{\mu}\bar{\mu}} \sigma_{\bar{\mu}} dE + \int \phi_{\nu_e} P_{e\mu} \sigma_\mu dE \qquad (3.21)$$
$$+ \int \phi_{\bar{\nu}_e} P_{\bar{e}\bar{\mu}} \sigma_{\bar{\mu}} dE$$

$$N_e = \int \phi_{\nu_e} P_{ee} \sigma_e dE + \int \phi_{\bar{\nu}_e} P_{\bar{e}\bar{e}} \sigma_{\bar{e}} dE + \int \phi_{\nu_\mu} P_{\mu e} \sigma_e dE \qquad (3.22)$$
$$+ \int \phi_{\bar{\nu}_\mu} P_{\bar{\mu}\bar{e}} \sigma_{\bar{e}} dE$$

where ϕ's are the atmospheric neutrino fluxes, $P_{\alpha\beta}$'s are the probabilities for neutrino of flavor α to oscillate into flavor β and σ_α's are the charged current cross sections for the neutrinos of flavor α to interact with the material of the detector. We make one further approximation which simplifies the analysis considerably. The charged current cross sections σ_μ and σ_e, in general, have different energy dependence. However, it was shown [45] that $\sigma_\mu \simeq \sigma_e$ and $\sigma_{\bar{\mu}} \simeq \sigma_{\bar{e}}$ for $E_\nu > 200 \ MeV$. Therefore we restrict our attention to the part of the data satisfying the constraint $E > 200 \ MeV$. Using all these above approximations, the expression for R can simply be written as

$$R = \frac{P^0_{\mu\mu} + \frac{1}{r_{MC}} P^0_{e\mu}}{P^0_{ee} + r_{MC} P^0_{\mu e}}, \qquad (3.23)$$

where

$$r_{MC} = \frac{\int \left[\phi_{\nu_\mu} \sigma_\mu + \phi_{\bar{\nu}_\mu} \sigma_{\bar{\mu}} \right] dE}{\int \left[\phi_{\nu_e} \sigma_e + \phi_{\bar{\nu}_e} \sigma_{\bar{e}} \right] dE}. \qquad (3.24)$$

where r_{MC} is the Monte Carlo expectation of the ratio of number μ-like events to the number of e-like events. From the sub-GeV data of Kamiokande, we find $r_{MC} = 1.912$ and $R = 0.60^{+0.07}_{-0.06} \pm 0.05$ [54]. We take the allowed values of ϕ

Bin No.	$\langle cos\theta \rangle$	$\langle distance \rangle$ in Km	r^i_{MC}	r^i_{obs}	R^i_{obs}
1	-0.8	10,210	3.0	$0.87^{+0.36}_{-0.21}$	$0.29^{+0.12}_{-0.07}$
2	-0.4	5,137	2.3	$1.06^{+0.39}_{-0.30}$	$0.46^{+0.17}_{-0.13}$
3	0.0	832	2.1	$1.07^{+0.32}_{-0.23}$	$0.51^{+0.15}_{-0.11}$
4	0.4	34	2.3	$1.45^{+0.51}_{-0.34}$	$0.63^{+0.22}_{-0.16}$
5	0.8	6	3.0	$3.9^{+1.8}_{-1.2}$	$1.3^{+0.6}_{-0.4}$

Table 3.1: Zenith angle dependent data from Kamiokande [6]

the experimental value. The region allowed by the sub-GeV data, where ϕ was restricted by the solar neutrino data and ψ is allowed to vary between 0 to 90^0, is shown in Fig.(3.1). The region between the solid lines is the parameter space which satisfies the experimental constraints at 1σ level whereas the region between dashed lines satisfies the experimental constraints at 1.6σ level. One important point to be noted in this analysis is that the sub-GeV data place only lower bound on δ_{31}. The allowed region in $\phi - \psi$ plane is quite large.

3.3.2 Multi-GeV data

The multi-GeV data of Kamiokande have been presented for five zenith angle bins in Ref. [55]. For each of these bins, the observed numbers of electron-like events and muon-like events and their Monte Carlo expectations (without neutrino oscillations) have been given. From these one can calculate two sets of ratios

$$r^i_{MC} = \left(\frac{N^i_\mu}{N^i_e}\right)_{MC} \tag{3.25}$$

$$r^i_{obs} = \left(\frac{N^i_\mu}{N^i_e}\right)_{obs}, \tag{3.26}$$

and the set of double ratios

$$R^i_{obs} = r^i_{obs}/r^i_{MC} \tag{3.27}$$

for each bin $i = 1, 2, ..., 5$. We summarize the multi-GeV data of Kamiokande [55] in Table 2.1.

The μ-like events are subdivided into fully contained (FC) and partially contained (PC) events whereas all the e-like events are fully contained. The efficiency of detection for each type of event is different and is a function of the neutrino energy. Thus we have three detection efficiencies $\varepsilon_{FC}^{\mu}(E)$, $\varepsilon_{PC}^{\mu}(E)$ and $\varepsilon^{e}(E)$. We obtained these efficiencies from Kamiokande Collaboration [46].

Muons produced in the charged current (CC) interactions of ν_{μ} can either decay in the detector or pass out of the detector. Hence the μ-like events are subdivided into fully contained (FC) and partially contained (PC) events. However, all the e-like events are fully contained. The efficiency of detection for each type of event is different and is a function of the neutrino energy. Thus we have three detection efficiencies $\varepsilon_{FC}^{\mu}(E)$, $\varepsilon_{PC}^{\mu}(E)$ and $\varepsilon^{e}(E)$. We obtained these efficiencies from Kamiokande Collaboration [46]. The detection efficiency for a particular type of event is defined to be the ratio of the number of correctly identified CC events of that type to the number of generated CC ν_{μ} or ν_{e} events. Fully contained events are produced by muons of low energy and hence by neutrinos at the lower end of the spectrum. Almost all of the partially contained events are produced by neutrinos of high energy. The shapes of the efficiency curves are roughly as follows:

- ε_{FC}^{μ}: is non-zero only for smaller neutrino energies. It has its maximum value of 0.2 at $E_{\nu} \simeq 2\ GeV$ and falls sharply to 0 when $E_{\nu} \geq 5\ GeV$.

- ε_{PC}^{μ}: rises sharply from 0.1 to 0.8 in the neutrino energy range $2\ GeV \leq E_{\nu} \leq 20\ GeV$. Then it slowly decreases at higher energies.

- ε^{e}: rises to about 0.6 at about $E_{\nu} \simeq 10\ GeV$ and slowly decreases at higher energies.

The Kamiokande data set of μ-like events is the sum of both fully and partially contained events. Hence we add the efficiencies for fully and partially contained events to obtain the number of muon events.

The expected number of μ-like and e-like events, in the absence of neutrino oscillations, is given by

$$N_{\mu}^{i}|_{M.C.} = \int \left[\phi_{\nu_{\mu}}^{i}(E)\sigma(E) + \phi_{\bar{\nu}_{\mu}}^{i}(E)\bar{\sigma}(E) \right] \left(\varepsilon_{FC}^{\mu}(E) + \varepsilon_{PC}^{\mu}(E) \right) dE \quad (3.28)$$

$$N_e^i|_{M.C.} = \int \left[\phi_{\nu_e}^i(E)\sigma(E) + \phi_{\bar{\nu}_e}^i(E)\bar{\sigma}(E) \right] \varepsilon^e(E) dE, \qquad (3.29)$$

where ϕ's are the fluxes of the atmospheric neutrinos at the location of Kamiokande. These are tabulated in Ref. [31] as functions of the neutrino energy (from $E = 1.6$ GeV to $E = 100$ GeV) and the zenith angle. σ and $\bar{\sigma}$ are the charged current cross sections of neutrinos and anti-neutrinos respectively with nucleons. The cross section is the sum of the quasi-elastic scattering and the deep inelastic scattering (DIS). The values for quasi-elastic scattering are taken from Gaisser and O'Connel [47] and those for the DIS are taken from Gargamelle data [48]. In calculating the DIS cross section, we took the lepton energy distribution to be given by the scaling formula (which is different for neutrinos and anti-neutrinos) and integrated $d\sigma/dE_{lep}$ from the minimum lepton energy $E_{min} = 1.33$ GeV to the maximum lepton energy $E_{max} = E_\nu - m_\pi$. The maximum lepton energy is chosen by defining DIS to contain at least one pion in addition to the charged lepton and the baryon. The differences in the fiducial volumes and exposure times for fully contained and partially contained events have been incorporated into the detection efficiency $\varepsilon_{PC}^\mu(E)$. From equations (3.28) and (3.29) we calculate our estimation of the Monte Carlo expectation of r_{MC}^i, the ratio of the μ-like events to the e-like events. The numbers we obtain are within 10% of the values quoted by Kamiokande collaboration in Ref. [55]. The differences could be due to the different set fluxes used [49] and due to the simple approximation we made for the cross sections.

In the presence of oscillations, the number of μ-like and e-like events are given by

$$N_\mu^i|_{osc} = \int \left[\phi_{\nu_\mu}^i P_{\mu\mu}\sigma + \phi_{\bar{\nu}_\mu}^i P_{\bar{\mu}\bar{\mu}}\bar{\sigma} + \phi_{\nu_e}^i P_{e\mu}\sigma + \phi_{\bar{\nu}_e}^i P_{\bar{e}\bar{\mu}}\bar{\sigma} \right] \left(\varepsilon_{FC}^\mu + \varepsilon_{PC}^\mu \right) dE \qquad (3.30)$$

$$N_e^i|_{osc} = \int \left[\phi_{\nu_e}^i P_{ee}\sigma + \phi_{\bar{\nu}_e}^i P_{\bar{e}\bar{e}}\bar{\sigma} + \phi_{\nu_\mu}^i P_{\mu e}\sigma + \phi_{\bar{\nu}_\mu}^i P_{\bar{\mu}\bar{e}}\bar{\sigma} \right] \varepsilon^e dE, \qquad (3.31)$$

where $P_{\alpha\beta}$s are the probabilities for neutrino of flavor α to oscillate into flavor β, derived in the last section. These oscillation probabilities are functions of the distance of travel d, the mixing angles ϕ and ψ, the mass difference δ_{31} and the matter term A. These are calculated using the formulae in eqs. (3.12), (3.14), (3.15) and (3.19). The probability of oscillation for anti-neutrinos $P_{\bar{\alpha}\bar{\beta}}$, in general, is different from $P_{\alpha\beta}$ because of the different A dependence.

From equations (3.30) and (3.31) we can calculate the ratio of μ-like events to e-like events in the presence of oscillations to be

$$r_{osc}^i = \left(\frac{N_\mu^i}{N_e^i}\right)_{osc} \tag{3.32}$$

and the double ratio

$$R_{osc}^i = \frac{r_{osc}^i}{r_{MC}^i}. \tag{3.33}$$

If the atmospheric neutrino deficit is due to neutrino oscillations, then the double ratios R_{osc}^i given in eq. (3.33) should be within the range of the corresponding observed double ratios R_{obs}^i, which are given in Table I. We searched for the values of the neutrino parameters ϕ, ψ and δ_{31} for which the predicted values of R_{osc}^i satisfy the experimental constraints on the double ratios for all the five bins. The ranges of variation in the three parameters are

1. $0 \le \phi \le 50^0$. This is the range of ϕ allowed by the solar neutrino problem. For this range of ϕ, there exist values of δ_{21} and ω such that all the three solar neutrino experiments can be explained [22, 50].

2. $0 \le \psi \le 90^0$. ψ is varied over its fully allowed range.

3. $10^{-3}\ eV^2 \le \delta_{31} \le 10^{-1}\ eV^2$. The lower limit is given by the sub-GeV data and the upper limit is the largest value allowed by the two flavor analysis of the multi-GeV data by Kamiokande [55].

The results are plotted in Figs. (3.2), (3.3) and (3.4). Fig.(3.2) gives the projection of the allowed region on the $\phi - \psi$ plane, Fig.(3.3) gives the projection on the $\phi - \delta_{31}$ plane and Fig.(3.4) gives the projection on the $\psi - \delta_{31}$ plane. The solid lines enclose the regions of parameter space whose predictions lie within the experimental range given by 1σ uncertainties. The broken lines enclose regions whose predictions fall within range given by 1.6σ uncertainties.

As seen from Table 2.1, the uncertainties in bin 5, which has $\langle \cos\theta \rangle = 0.8$, are quite large compared to the uncertainties in the other four bins. Moreover, r_{obs}^5 is greater than r_{MC}^5 through most of its range. Hence the double ratio $R_{obs}^5 > 1$ for

most of its range. The Monte Carlo expectation of the electron neutrino flux is less than that of the muon neutrino flux and the oscillation probabilities $P_{\alpha\beta}$ are all less than 1. Using these facts, one can show from eqs. (3.25) and (3.32) that, in general, $r^i_{osc} \leq r^i_{MC}$ or $R^i_{osc} \leq 1$. Therefore, the region of overlap between R^5_{obs} and R^5_{osc} is very small. It is $0.9 - 1.0$ for 1σ uncertainties. It is possible that this small overlap is imposing a very strong constraint, leading to a situation where the bin with the largest uncertainty is essentially controlling the allowed values of the parameters. Because of this unsatisfactory situation, we redid the analysis ignoring the constraint from bin 5. We searched for regions of parameter space for which the values of R^i_{osc} are within the ranges of corresponding R^i_{obs} for only the first four bins.

The results of the 4 bin analysis are plotted in Figs. (3.5), (3.6) and (3.7). Fig.(3.5) gives the projection of the allowed region on the $\phi-\psi$ plane, Fig.(3.6) gives the projection on the $\phi-\delta_{31}$ plane and Fig.(3.7) gives the projection on the $\psi-\delta_{31}$ plane. As before, the solid lines enclose the regions satisfying 1σ vetoes and the broken lines enclose regions allowed by 1.6σ vetoes. Comparing the corresponding figures we find that the allowed values of parameters for the 4 bin fit are the almost identical to those from the 5 bin fit at 1.6σ level. The allowed regions at 1σ level are somewhat larger compared to the 5 bin fit. This is not surprising because the bin 5 imposes a very strong constraint at 1σ level. If this constraint is relaxed, then a somewhat larger region is allowed. The 4 bin fit shows that the 5th bin, which has the largest uncertainty, does not exercise undue influence on the selection of the parameter space. Note that we have presented results for $1\ \sigma$ intervals also, this is because zenith angle dependence is only a 1σ effect. Hence one must also look at the 1σ parameter space. The fact that some amount of $\nu_e - \nu_\mu$ oscillations is needed to fit zenith dependence, which in turn demands a non zero value of ϕ, is seen only at 1σ. (These results have been presented in [51]).

3.4 Discussions and conclusions

The parameter space shown in Figs. (3.1) to (3.4), together with the allowed values
for ω and δ_{21} from our earlier work [22] and chapter 1, provides a complete solution
to the solar and the atmospheric neutrino problems in the framework of three flavor
neutrino oscillations. The salient features of the results of the multi-GeV analysis
are:

- Most of the parameter space allowed by the multi-GeV data is a subset of the
  space allowed by the sub-GeV data.

- The range of δ_{31} allowed by 1σ vetoes is extremely narrow. It is very close to
  the best fit value given by the two flavor analysis of Kamiokande.

- The value of ψ is always large ($\psi \geq 40^0$) and $\psi = 90^0$ is allowed.

- In the region allowed by 1σ vetoes ϕ is always non-zero. $\phi = 0$ is allowed only
  at 1.6σ vetoes.

From the parametrization of U^ν, effective two level mixings can be obtained for
the following choices of the angles:

- $\nu_e \leftrightarrow \nu_\mu$ for $\psi = 90^0$,

- $\nu_e \leftrightarrow \nu_\tau$ for $\psi = 0$ and

- $\nu_\mu \leftrightarrow \nu_\tau$ for $\phi = 0$.

Any solution to the atmospheric neutrino problem should suppress the muon neu-
trinos, enhance the electron neutrinos or do both. The $\nu_e \leftrightarrow \nu_\tau$ channel, which
suppresses electron neutrinos but leaves muon neutrinos untouched, cannot account
for the atmospheric neutrino problem. Hence any solution of atmospheric neutrino
problem should be away from the effective two flavor $\nu_e \leftrightarrow \nu_\tau$ oscillations. The large
value of the angle ψ is just a reflection of this fact. The allowed region includes the
value $\psi = 90^0$. Then the atmospheric neutrino problem is explained purely in terms
of the two flavor oscillations between $\nu_e \leftrightarrow \nu_\mu$, with the relevant mass difference

being δ_{31}. In this case, the solar neutrino problem is solved by $\nu_e \to \nu_\tau$ oscillation which is determined by the mass difference δ_{21} (and the mixing angles ω and ϕ).

How important are the matter effects in the analysis of the multi-GeV data ? It can be seen from figures 2(d)-2(f) of Ref. [55] that most of the expected multi-GeV events are caused by neutrinos with energies less than 10 GeV (over 80% for muon-like events and over 90% for electron-like events). The matter term, for a neutrino of energy 5 GeV, is about $2 \times 10^{-3} eV^2$. Since the initial range we considered for δ_{31} varied from 10^{-3} eV^2 to 0.1 eV^2, apriori one must include the matter effects in the expressions for the oscillation probabilities. However, the value of δ_{31} in the allowed region, especially for the 1σ vetoes, where it is about 0.03 eV^2, is much larger than the matter term. Therefore, it is likely that the matter effects may not play an important role in determining the allowed parameter regions in the analysis of the multi-GeV data. To check this we reran our program with the matter term set equal to zero. With this change, the double ratio R^i_{osc}, defined in equation (3.32), changes by about 10% in the first bin and by about 5% in the second bin. There is no discernible change in the other three bins. Since the errors in R^i_{obs} are about 30%, these small changes in R^i_{osc} do not lead to any appreciable change in the allowed regions of the parameter space. However, the effect of matter terms may become discernible when more accurate data from Super Kamiokande become available.

Since the earth matter effects seem to play no role in the determination of the parameter space, can one interpret the observed zenith angle dependence purely in terms of vacuum oscillations? For an energy of 5 GeV, the mass square difference $10^{-2} eV^2$ corresponds to an oscillation length of about 1200 Km. Thus bins 1 and 2 contain many oscillation lengths and the second and the third cosine terms in the vacuum oscillation probability, given in equation (3.20), average out to zero. For bins 4 and 5 the cosine terms are almost 1. In bin 3, these terms take some intermediate value. Therefore we have large suppression in the first two bins, almost no suppression in the last two bins and moderate suppression in the middle bin.

We now make a brief comment on the LSND results on the search for $\bar{\nu}_\mu \to \bar{\nu}_e$ oscillations [52] in the context of our analysis of atmospheric neutrinos. The LSND collaboration is an accelerator based experiment which searches for signals

of oscillations, by looking for signals of $\bar{\nu}_e$ from an initially pure $\bar{\nu}_\mu$ beam. The LSND collaboration gives an oscillation probability $P_{\bar{\mu}\bar{e}} = (3.1^{+1.1}_{-1.0} \pm 0.5) \times 10^{-3}$ for muon anti-neutrinos in the energy range $20 - 60$ MeV. In the framework described in section II, the oscillation probability relevant for the LSND experiment is the vacuum oscillation probability

$$P^0_{\bar{\mu}\bar{e}} = P^0_{\mu e} = \sin^2 2\phi \sin^2 \psi \sin^2 \left(1.27 \frac{d\, \delta_{31}}{E}\right). \tag{3.34}$$

Note that both ϕ and ψ have to be non-zero for $P_{\mu e}$ to be non-zero. In the region allowed by the 1σ vetoes of the multi-GeV atmospheric neutrino data we have

$$\text{Minimum} \left(\sin^2 2\phi \sin^2 \psi\right) \simeq 0.04 \quad \text{for} \quad \phi \simeq 8^0, \psi \simeq 40^0$$
$$\text{Maximum} \left(\sin^2 2\phi \sin^2 \psi\right) \simeq 1 \quad \text{for} \quad \phi \simeq 40^0, \psi \simeq 90^0.$$

Substituting these values and the oscillation probability obtained by LSND in eq. (5.7), we obtain

$$0.001 \leq \sin^2 \left(1.27 \frac{d\, \delta_{31}}{E}\right) \leq 0.1. \tag{3.35}$$

For the LSND experiment the distance $d = 30$ meters. Taking the average energy to be $\langle E \rangle = 40$ MeV, we obtain the range of δ_{31} to be

$$0.03 \; eV^2 \leq \delta_{31} \leq 0.3 \; eV^2. \tag{3.36}$$

From the analysis of multi-GeV atmospheric neutrino data we have the upper limit on $\delta_{31} \leq 0.06 \; eV^2$ (Figs. (3.3) and (3.4)). Hence there is a small region of overlap between the range of neutrino parameters required by the atmospheric neutrino data and the LSND data. This suggests that the standard three flavor analysis can accommodate all the data so far [53] and perhaps a fourth sterile neutrino is not needed.

In conclusion, we have analyzed the atmospheric neutrino data of Kamiokande in the context of three flavor neutrino oscillations. We took into account both the zenith angle dependence of the multi-GeV data and the matter effects due to the propagation of the neutrinos through the earth. We obtained the regions in neutrino parameters which solve both the solar and the atmospheric neutrino problems. We found that the matter effects have negligible influence on atmospheric neutrinos

even in the multi-GeV range. The allowed regions of the parameter space with or without matter effects are almost identical. Finally since matter effects do not seem to effect the atmospheric neutrino problem, it is conceivable that the atmospheric neutrino problem is mainly driven by $\nu_\mu - \nu_\tau$ oscillations. We shall examine this possibility in detail in a later chapter as well as the constraints coming from other accelerator based experiments on the atmospheric neutrino parameter space.

In the next chapter we shall investigate some novel effects of neutrino oscillations.
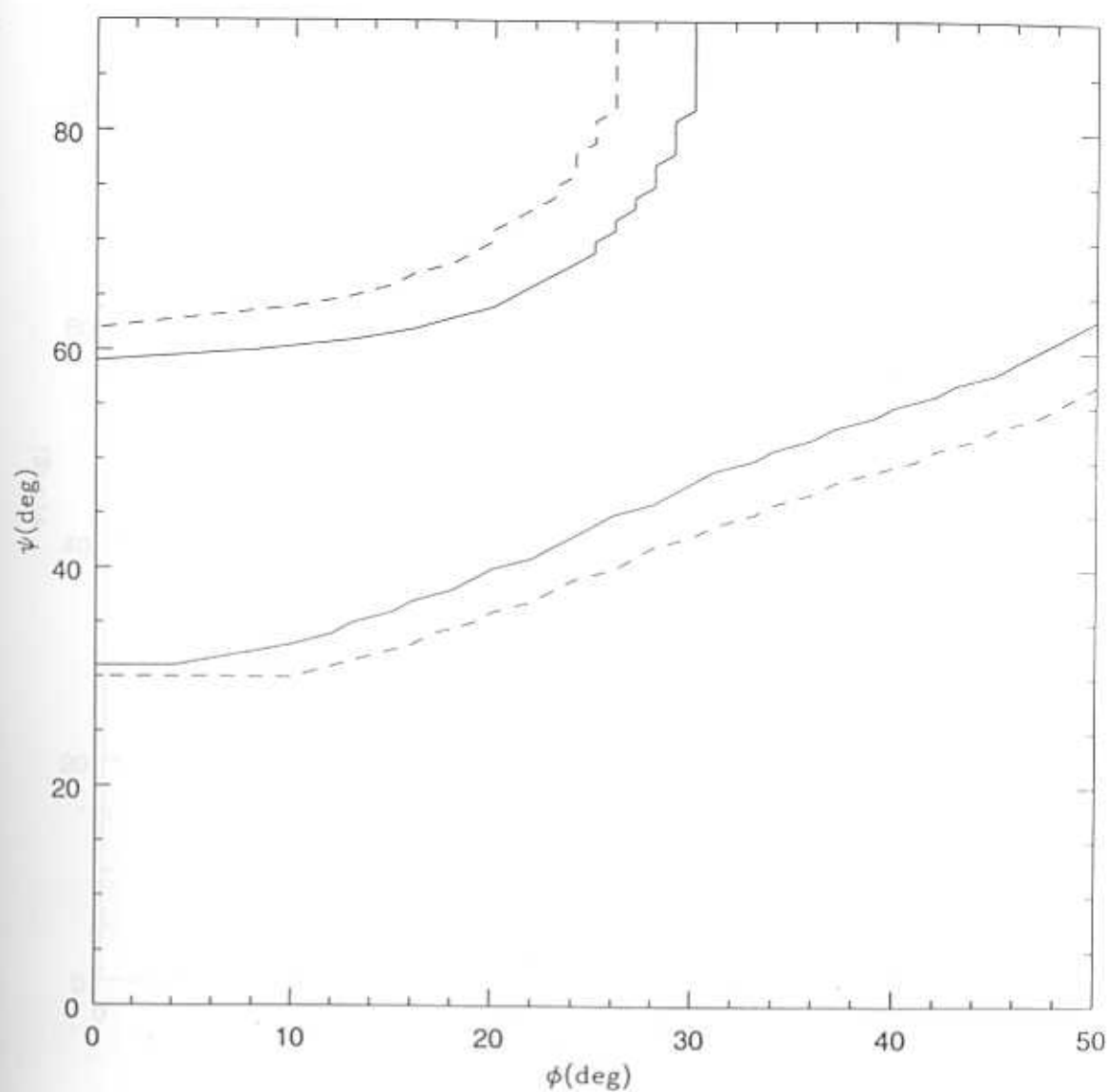
Figure 3.1: Allowed region in $\phi-\psi$ plane by the sub-GeV data (with $\delta_{31} \geq 10^{-3}\ eV^2$) at 1σ (enclosed by solid lines) and at 1.6σ (enclosed by broken lines)
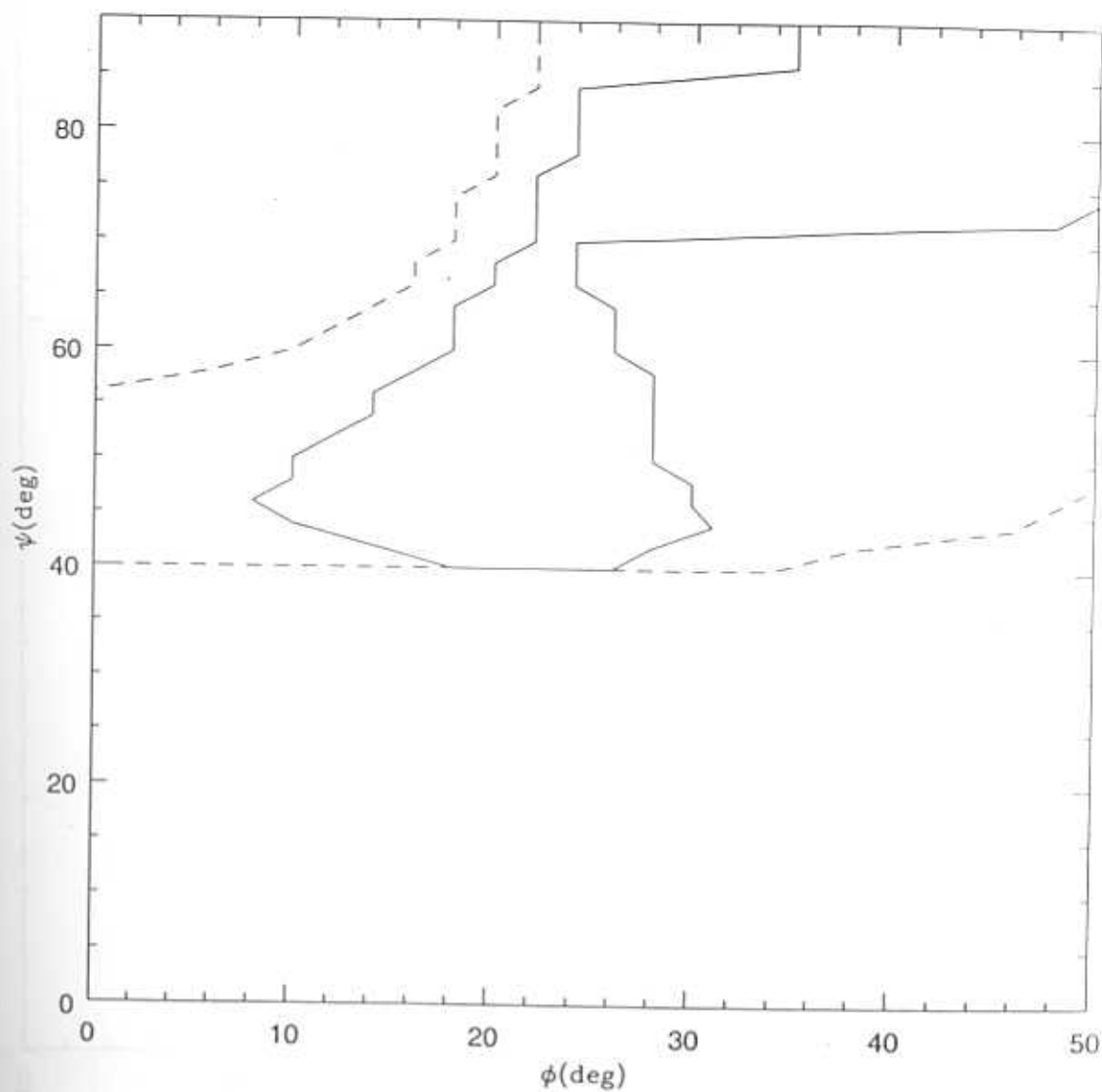
Figure 3.2: Allowed region in $\phi - \psi$ plane by 5 bin analysis of multi-GeV data (with 10^{-3} $eV^2 \leq \delta_{31} \leq 10^{-1}$ eV^2) at 1σ (enclosed by solid lines) and at 1.6σ (enclosed by broken lines)
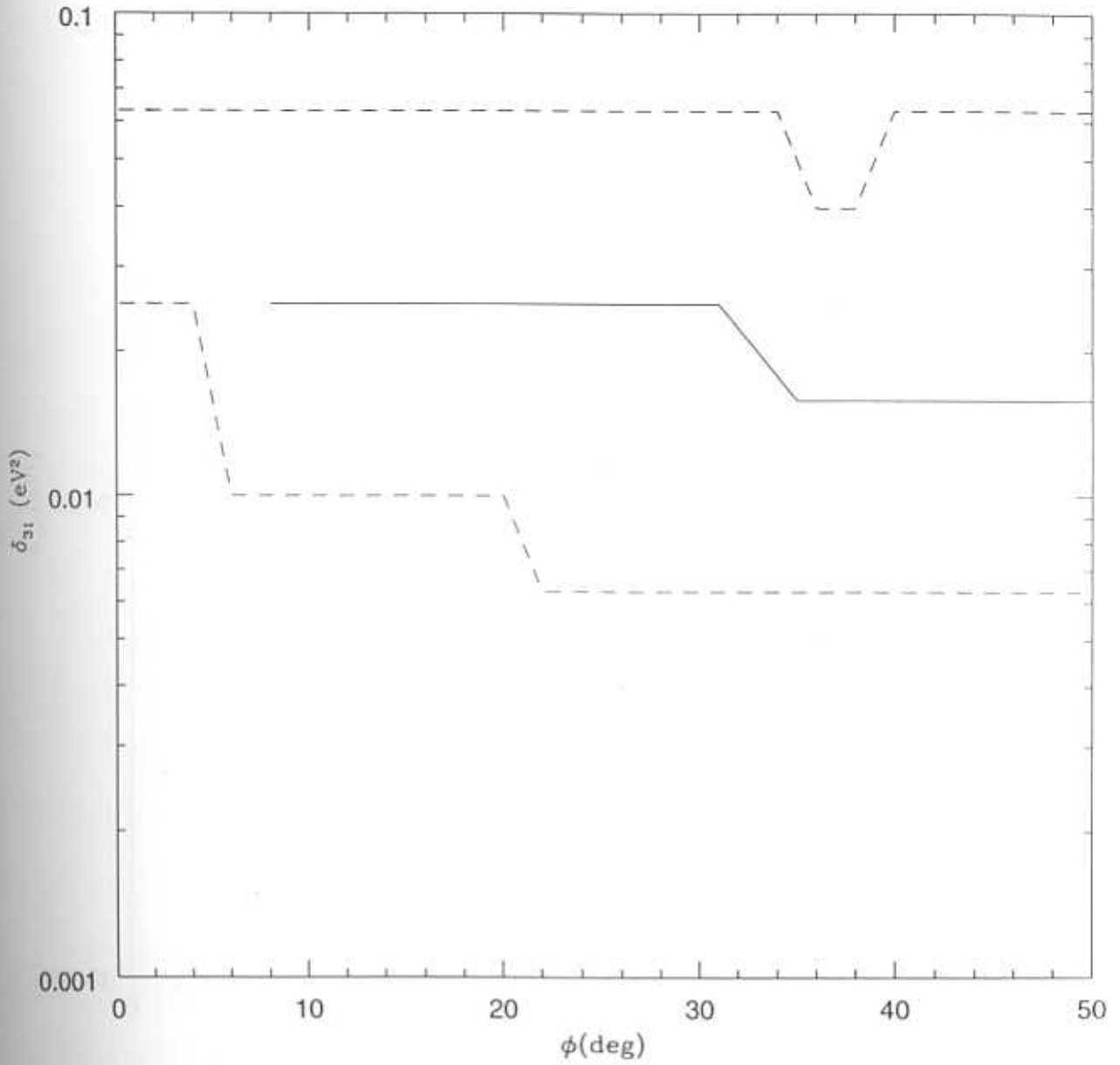
Figure 3.3: Allowed region in $\phi - \delta_{31}$ plane by 5 bin analysis of multi-GeV data (with $0 \leq \psi \leq 90^0$) at 1σ (enclosed by solid lines) and at 1.6σ (enclosed by broken lines)
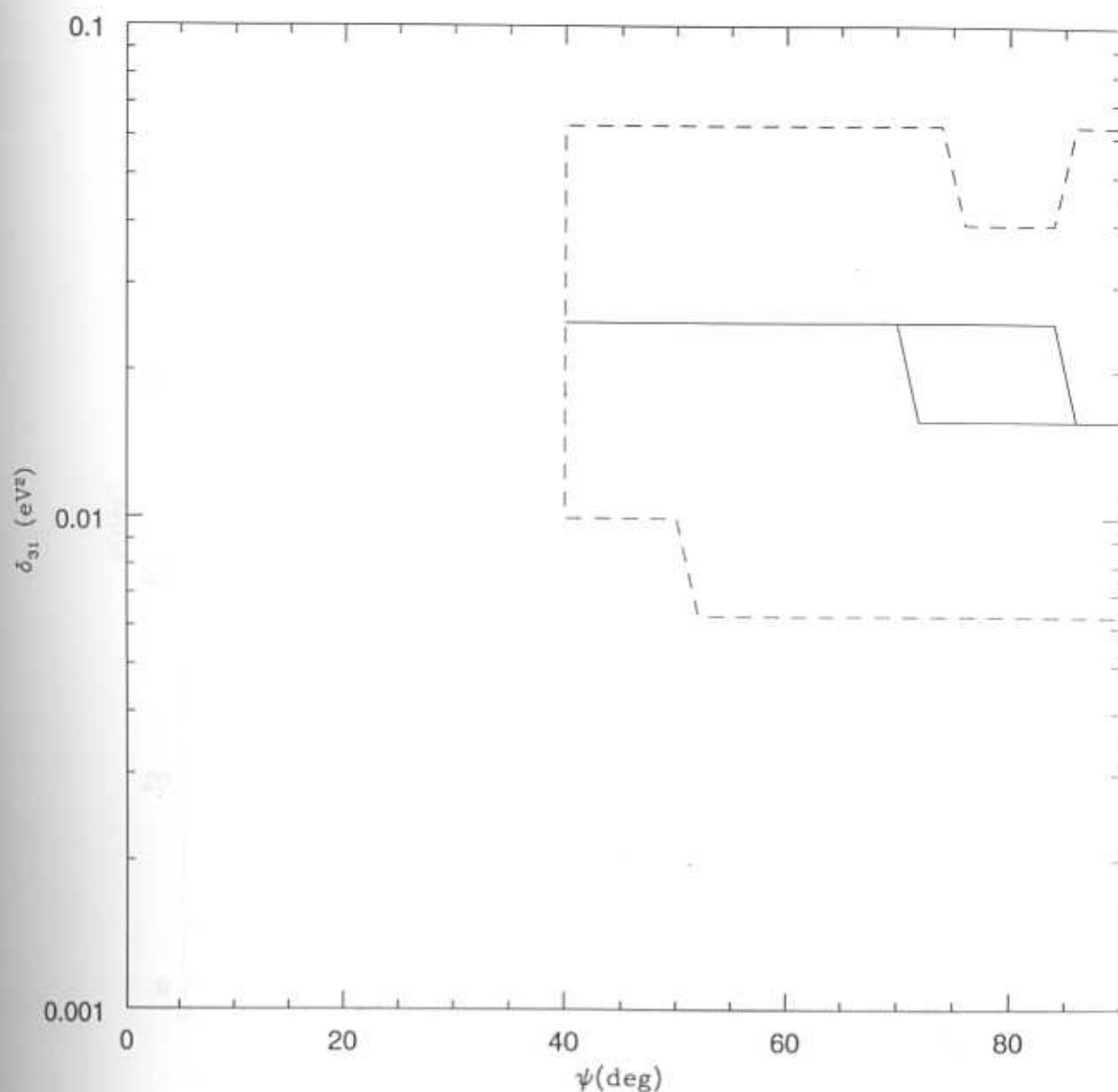
Figure 3.4: Allowed region in $\psi - \delta_{31}$ plane by 5 bin analysis of multi-GeV data (with $0 \leq \phi \leq 50^0$) at 1σ (enclosed by solid lines) and at 1.6σ (enclosed by broken lines)
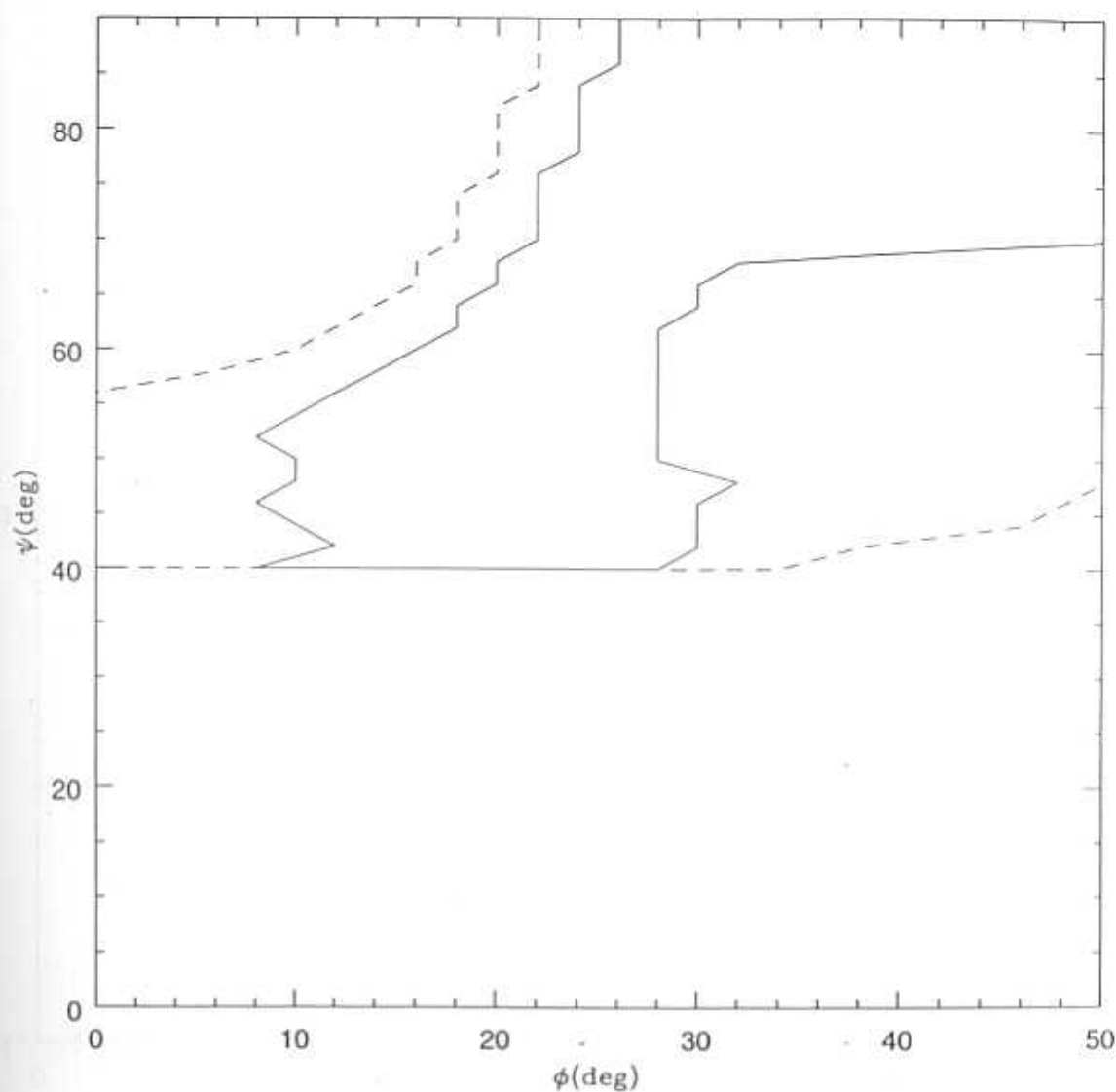
Figure 3.5: Allowed region in $\phi - \psi$ plane by 4 bin analysis of multi-GeV data (with 10^{-3} $eV^2 \leq \delta_{31} \leq 10$ eV^2) at 1σ (enclosed by solid lines) and at 1.6σ (enclosed by broken lines)
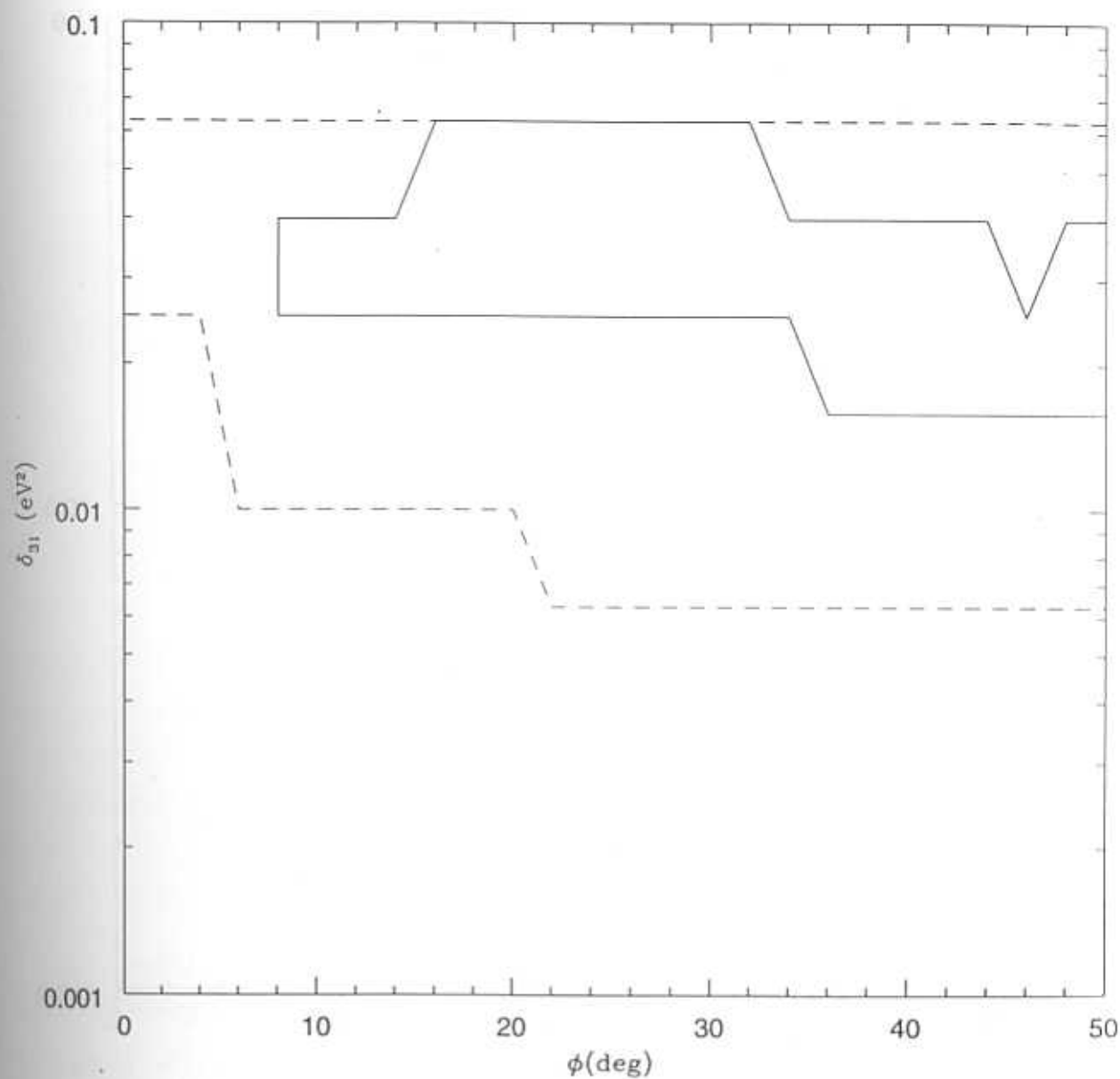
Figure 3.6: Allowed region in $\phi - \delta_{31}$ plane by 4 bin analysis of multi-GeV data (with $0 \leq \psi \leq 90^0$) at 1σ (enclosed by solid lines) and at 1.6σ (enclosed by broken lines)
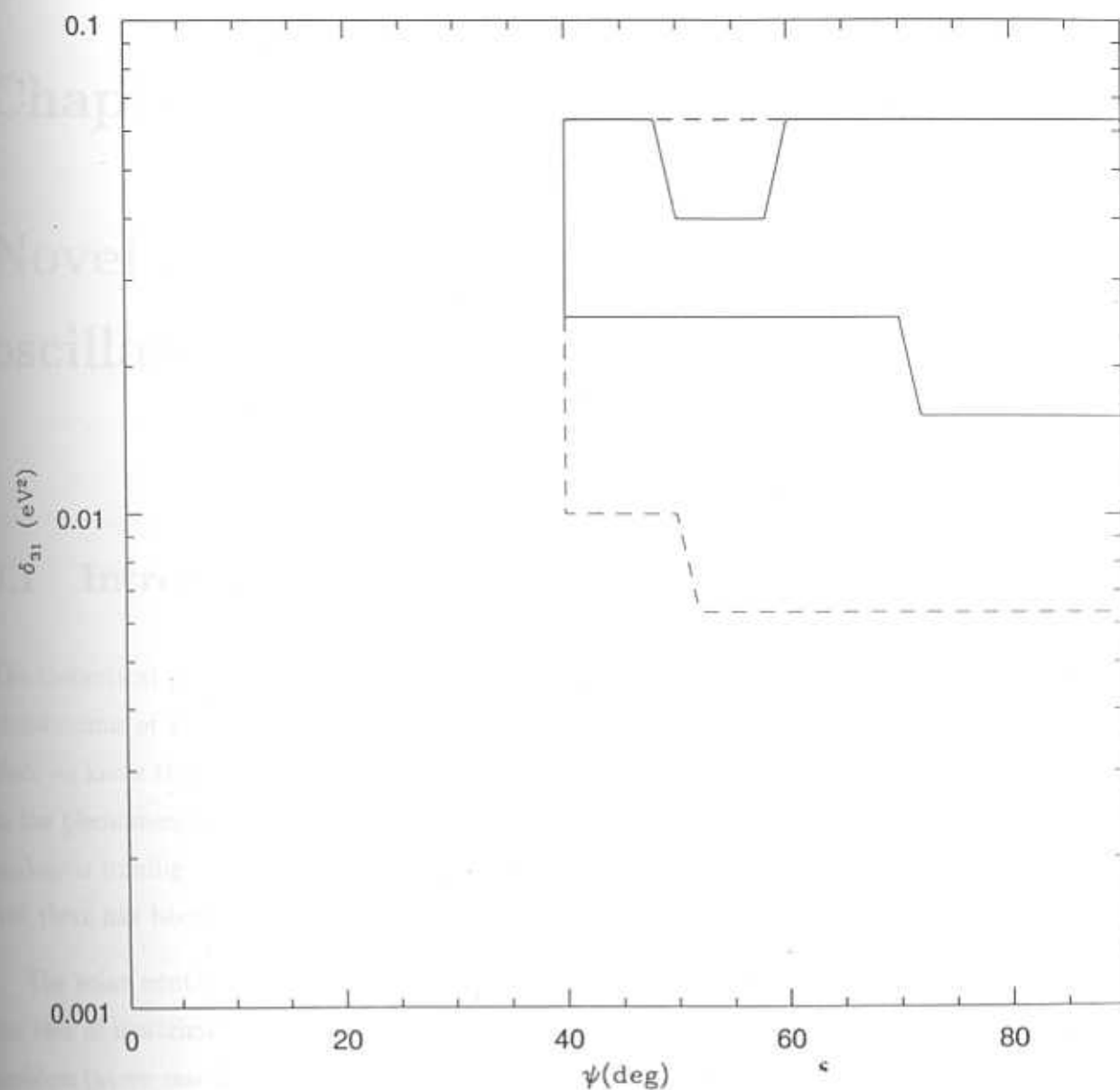
Figure 3.7: Allowed region in $\psi - \delta_{31}$ plane by 4 bin analysis of multi-GeV data (with $0 \leq \psi \leq 90^0$) at 1σ (enclosed by solid lines) and at 1.6σ (enclosed by broken lines)

Chapter 4

Novel effects of neutrino oscillations

4.1 Introduction

The theoretical possibility that neutrinos could be massive, and hence exhibit the phenomenon of mixing and oscillations has been with us for quite some time [8]. Since we know that there is mixing in the quark sector, which for example gives rise to the phenomenon of $K^0 - \bar{K}^0$ oscillations, it is quite likely that there could be analogous mixing in the lepton sector also. However it has to be stated that uptill now there has been no firm evidence of neutrino mass and flavor mixing .

The solar neutrino problem was the first problem to give an strong impetus to the idea of neutrino oscillations, as oscillations provided an elegant solution to the problem (as we saw in chapter 2). There are however a few unsatisfactory aspects of this conclusion. In the solar neutrino problem, the calculated rates for the various detectors is based on the SSM predictions for the neutrino fluxes. These fluxes are in turn dependent on many of the inputs which go into the SSM. So one may question the reliability of the predictions. Even though astrophysical solutions to the solar neutrino problem are highly disfavoured [21], one still cannot escape the fact that the SSM plays a central role in giving a pointer to neutrino oscillations.

In the case of the atmospheric neutrino problem also the event rates for the atmospheric neutrino detectors are dependent upon the Monte Carlo predictions for the atmospheric neutrino fluxes. These predictions have large uncertainities (about $\approx 30\%$) as mentioned previously in the absolute magnitude of the muon and electron type of fluxes, however the ratio of the two types of fluxes is quite robust. So the anomaly in the ratio of the fluxes is a very significant event. So it is the atmospheric neutrino problem which today gives us the strongest evidence in favor of neutrino oscillations.

In spite of the hints given by the solar and the atmospheric neutrino problems in favor of neutrino oscillations, it is natural to ask, are there unambigious signals for neutrino mixing and oscillations, where are reasonably independent of the theoretical flux predictions. One effect which was realised quite some time ago is what is called the "day-night" effect with respect to the solar neutrinos. This effect arises because during the night the neutrinos have to travel through the earth to reach the detector. The passage through the earth could in principle lead to changes in the flavor composition of the neutrino beam which reaches the earth from the sun, if the neutrino parameters (i.e the masses and the mixing angles) are in a suitable range. This change in the flavor composition will reflect itself as a different counting rate during night vis a vis the day counting rate. For real time detectors like Super-Kamioka, Borexino etc it is possible to look for a difference between the day time and night time counting rates. Such an asymmetry in the counting rates if observed will be a model independent signal for neutrino oscillations. Although no day-night asymmetry outside the error-bars was seen at the Kamioka detector [54, 55] the high statistics detectors like Super-Kamioka [56], SNO [29]and Borexino [57] will be much more effective in investigating this effect. All these detectors are however mainly sensitive to neutrino trajectories which go through the mantle of the earth only, as these detectors are quite far from the equator. It was pointed out recently [58] that the small angle solution to the solar neutrino problem could show a dramatic day-night effect, if the neutrino trajectory passes through the core of the earth. Hence a real time solar neutrino detector located around the equator could give a spectacular signal of neutrino oscillations.

Day-night effect has been investigated previously by various authors [59]. All these analyses have however been in a two flavor framework, and have relied on brute force numerical integration of the neutrino trajectory through the earth. In this chapter we analyse in a three flavor framework the day-night and present a completely analytical method of computing the neutrino survival probability at night.

Recently another effect was pointed out, which is similar in spirit to the day-night effect. This is the "eclipse effect" [62]. The basic idea is as follows. If the earth can affect the solar neutrinos on their way to the detector in the night, then it is quite likely that during a solar eclipse, the moon too could affect the neutrinos on their way to the detector. And this effect again could be monitored by the real time detectors, since they continue taking data during the eclipse also, and most importantly they can measure the rate during the specific duration of the eclipse. If a change in the counting rate is seen during an eclipse as compared with the no eclipse rate, it would be a spectacular demonstration of the phenomenon of neutrino mixing and oscillations. The next round of real time detector with high statistics can in fact measure such an effect. In this chapter we analyse in a three flavor framework the eclipse effect.

We also point out that even the absence of such novel effects has significance, because it can exclude some regions in the neutrino parameter space. Therefore even a null effect gives us some information about the neutrino parameters.

4.2 Day - night effect

Since one is interested in computing the counting rate during night, we first obtain the electron neutrino survival probability during night time after the neutrino has travelled some distance through the earth, in addition to the travel through the sun.

Let a neutrino of flavor α be produced at time $t = t_0$ in the core of the sun. Its state vector is

$$|\Psi_\alpha(t_0)\rangle = |\nu_\alpha\rangle = \sum_i U_{\alpha i}^C |\nu_i^C\rangle, \tag{4.1}$$

where $|\nu_i^C\rangle$ are the mass eigenstates with mass eigenvalues μ_i^C and $U_{\alpha i}^C$ are the

elements of the mixing matrix in the core of the sun. We use Greek index α to denote the flavors e, μ, τ and Latin index i to denote the mass eigenstates i = 1,2,3. The neutrino propagates in the sun adiabatically upto t_R (the resonance point), makes non-adiabatic transitions at t_R, propagates adiabatically upto t_1 (the edge of the sun) and propagates as a free particle upto t_2 when it enters the earth. So the state vector at t_2 is

$$
\begin{aligned}
|\Psi_\alpha(t_2)\rangle &= \sum_{j,i} |\nu_j\rangle exp\left(-i\varepsilon_j(t_2 - t_1)\right) exp\left(-i\int_{t_R}^{t_1} \varepsilon_j^S(t)dt\right) M_{ji}^S \\
&\times exp\left(-i\int_{t_0}^{t_R} \varepsilon_i^S(t)dt\right) U_{\alpha i}^C,
\end{aligned}
\tag{4.2}
$$

where $\varepsilon_i^S(t)(\equiv E + (\mu_i^S(t))^2/2E)$ are the matter dependent energy eigenvalues in the sun, ε_i and $|\nu_i\rangle$ are the energy eigenvalues and the corresponding eigenstates in vacuum and M_{ji}^S is the probability amplitude for the non-adiabatic transition $i \to j$. We multiply the right hand side of eq.(4.2) by $\sum_k |\nu_k^E\rangle\langle\nu_k^E|$ (= 1) where $|\nu_k^E\rangle$ (i =1,2,3) is the complete set of matter dependent mass eigenstates inside the earth. The neutrino propagates upto the the other end of the earth adiabatically upto t_3 (we shall soon correct for nonadiabatic jumps during this propagation), and the state vector at t_3 is

$$
\begin{aligned}
|\Psi_\alpha(t_3)\rangle &= \sum_{k,j,i} |\nu_k^E\rangle exp\left(-i\varepsilon_k^E(t_3 - t_2)\right) \langle\nu_k^E|\nu_j\rangle exp\left(-i\varepsilon_j(t_2 - t_1) - i\int_{t_R}^{t_1} \varepsilon_j^S(t)dt\right) \\
&\times M_{ji}^S exp\left(-i\int_{t_0}^{t_R} \varepsilon_i^S(t)dt\right) U_{\alpha i}^C \\
&= \sum_{k,j,i} |\nu_k^E\rangle exp\left(-i\varepsilon_k^E(t_3 - t_2)\right) M_{kj}^E exp\left(-i\varepsilon_j(t_2 - t_1) - i\int_{t_R}^{t_1} \varepsilon_j^S(t)dt\right) \\
&\times M_{ji}^S exp\left(-i\int_{t_0}^{t_R} \varepsilon_i^S(t)dt\right) U_{\alpha i}^C.
\end{aligned}
\tag{4.3}
$$

We have introduced the probability amplitude M_{kj}^E for non-adiabatic transitions $j \to k$ due to the abrupt change in density when the neutrino enters the earth . It is given by

$$
M_{kj}^E = \langle\nu_k^E|\nu_j\rangle = \sum_\gamma \langle\nu_k^E|\nu_\gamma\rangle\langle\nu_\gamma|\nu_j\rangle = \sum_\gamma U_{\gamma k}^E U_{\gamma j}^*
\tag{4.4}
$$

where $U_{\gamma j}$ is the mixing matrix in vacuum . The probability amplitude for detecting a neutrino of flavor β at t_3 is

$$
\langle\nu_\beta|\Psi_\alpha(t_3)\rangle = \sum_{k,j,i} U_{\beta k}^{E*} M_{kj}^E M_{ji}^S U_{\alpha i}^C exp\left\{-i\left(\int_{t_2}^{t_3} \varepsilon_k^E(t)dt\right.\right.
$$

$$+ \, \varepsilon_j(t_2 - t_1) + \int_{t_R}^{t_1} \varepsilon_j^S(t)dt + \int_{t_0}^{t_R} \varepsilon_i^S(t)dt \bigg) \bigg\} . \tag{4.5}$$

Averaging the probability $|\langle \nu_\beta | \Psi_\alpha(t_3) \rangle|^2$ over t_R results in the desired incoherent mixture of mass eigenstates of neutrinos reaching the surface of the earth. Calling this averaged probability as $P_{\alpha\beta}^N$ (the probabilty for a neutrino produced in the sun as ν_α to be detected as ν_β in the earth at night), we can write the result as

$$P_{\alpha\beta}^N = \sum_j P_{\alpha j}^S P_{j\beta}^E, \tag{4.6}$$

$$P_{\alpha j}^S = \sum_i |M_{ji}^S|^2 |U_{\alpha i}^C|^2, \tag{4.7}$$

$$P_{j\beta}^E = \sum_{k,k'} U_{\beta k}^{E*} U_{\beta k'}^E M_{kj}^E M_{k'j}^{E*} exp\left(-2i\Phi_{kk'}\right), \tag{4.8}$$

$$\Phi_{kk'} = \frac{1}{2} \int_{t_2}^{t_3} (\varepsilon_k^E(t) - \varepsilon_{k'}^E(t))dt. \tag{4.9}$$

Here $P_{\alpha j}^S$ is the probability that a flavor state α has oscillated into a mass eigenstate j, at the surface of the sun. $P_{j\beta}^E$ is the probability that a mass eigenstate j is detected as a neutrino of flavor β, after travelling a distance $t_3 - t_2$ through the earth.

For the daytime, put $t_3 = t_2$ so that $P_{j\beta}^E$ becomes $|U_{\beta j}|^2$ and so eq.(4.6) reduces to the usual [13, 22] transition probability in the day:

$$P_{\alpha\beta}^D = \sum_i \sum_j |U_{\beta j}|^2 |M_{ji}^S|^2 |U_{\alpha i}^S|^2. \tag{4.10}$$

Note putting $\alpha = \beta = e$, we get the formula obtained in chapter 1 for P_{ee}. It is important to note that the factorization of probabilities seen in eq.(4.6) is valid only for mass eigenstates in the intermediate state. An equivalent statement of this result is that the density matrix is diagonal only in the mass-eigenstate representation and not in the flavor representation.

We next show how to take into account nonadiabatic jumps during the propagation inside the earth. Consider ν propagation through a series of slabs of matter, density varying inside each slab smoothly but changing abruptly at the junction between adjacent slabs. The state vector of the neutrino at the end of the nth slab $|n\rangle$ is related to that at the end of the $(n-1)^{th}$ slab $|n-1\rangle$ by

$$|n\rangle = F^{(n)} M^{(n)} |n-1\rangle, \tag{4.11}$$

where $M^{(n)}$ describes the nonadiabatic jump occuring at the junction between the $(n-1)^{th}$ and n^{th} slabs while $F^{(n)}$ describes the adiabatic propagation in the nth slab. They are given by

$$M_{ij}^{(n)} = \langle \nu_i^{(n)} | \nu_j^{(n-1)} \rangle = (U^{(n)\dagger} U^{(n-1)})_{ij}^*, \tag{4.12}$$

$$F_{ij}^{(n)} = \delta_{ij} exp \left(-i \int_{t_{n-1}}^{t_n} \varepsilon_i(t)dt \right), \tag{4.13}$$

where the indices (n) and $(n-1)$ occuring on ν and U refer respectively to the nth and $(n-1)^{th}$ slabs at the junction between these slabs. Also note that $M^{(1)}$ is the same as M^E defined in eq(4.4). Defining the density matrix at the end of the nth slab as $\rho^{(n)} = |n\rangle\langle n|$, we have the recursion formula

$$\rho^{(n)} = F^{(n)} M^{(n)} \rho^{(n-1)} M^{(n)\dagger} F^{(n)\dagger}. \tag{4.14}$$

Starting with $\rho^{(0)} = |\nu_j\rangle\langle\nu_j|$ (i.e ν_j entering the earth), we can calculate $\rho^{(N)}$ at the end of the Nth slab using eq.(4.14). The probability of observing ν_β at the end of the Nth slab is

$$P_{j\beta}^E = \langle \nu_\beta | \rho^{(N)} | \nu_\beta \rangle = (U^{(N)} \rho^{(N)*} U^{(N)\dagger})_{\beta\beta}. \tag{4.15}$$

This formula (which reduces to eq(4.8) for $N = 1$) can be used for the earth modelled as consisting of $(N + 1)/2$ concentric shells, with the density varying gradually within each shell. We shall present numerical results for $N = 3$ (mantle and core) [63]. However for $x < 0.84$, neutrinos pass only through the mantle and so $N = 1$. Accuracy achieved with this model is adequate for the present purposes, but the formalism allows one to improve the accuracy to any desired level, by adding more shells and therefore slabs.

Apart from the nonadiabatic jumps occuring at the density–discontinuities, such jumps can occur also at any MSW resonance in the earth. The formalism presented above is capable of handling this. One simply replaces eq.(4.12) for $M^{(n)}$ for that transition by an appropriate Landau–Zener formula[12].

As before we parametrize the mixing matrix U in vacuum as $U = U^{23}(\psi)U^{13}(\phi)U^{12}(\omega)$ where $U^{ij}(\theta_{ij})$ is the two flavor mixing matrix between the ith and the jth mass eigenstates with the mixing angle θ_{ij}, neglecting CP violation. In the solar neutrino problem ψ drops out [12, 24]. The mass differences in vacuum

are defined as $\delta_{21} = \mu_2^2 - \mu_1^2$ and $\delta_{31} = \mu_3^2 - \mu_1^2$. It has been shown [22, 28] that the simultaneous solution of both the solar and the atmospheric neutrino problems requires the mass hierarchy $\delta_{31} \gg \delta_{21}$ and under this condition δ_{31} also drops out. The rediagonalization of the mass matrix in the presence of matter (in the sun or earth) under the hierarchy condition leads to the following results [22]

$$\tan 2\omega_m = \frac{\delta_{21} \sin 2\omega}{\delta_{21} \cos 2\omega - A \cos^2 \phi}, \tag{4.16}$$

$$\sin \phi_m = \sin \phi, \tag{4.17}$$

$$\delta_{21}^m = \delta_{21} \cos 2(\omega - \omega_m) - A \cos^2 \phi \cos 2\omega_m, \tag{4.18}$$

where A is the Wolfenstein term $A = 2\sqrt{2} \, G_F \, N_e \, E$ (N_e is the number density of electrons and E is the neutrino energy). We note that $\delta_{31} \gg A$, for A evaluated at any point in the sun or the earth. In eqs (5.17) - (5.19), the "m" stands for matter and in using these equations, one must use the appropriate density of matter that is required at the various points along the trajectory of the neutrino.

All the probabilities $P_{\alpha\beta}^N$, $P_{\alpha j}^S$ and $P_{j\beta}^E$ satisfy the normalization conditions, as for instance, $\sum_j P_{j\beta}^E = 1$. For three flavors, use of these conditions allows us to express P_{ee}^N in terms of P_{ee}^D, P_{1e}^E, P_{2e}^E and P_{e3}^S as

$$
\begin{aligned}
P_{ee}^N = &[P_{ee}^D(P_{1e}^E - P_{2e}^E) - \cos^2 \phi(\sin^2 \omega P_{1e}^E - \cos^2 \omega P_{2e}^E) \\
&- P_{e3}^S((3\cos^2 \phi \cos^2 \omega - 1)P_{2e}^E - (3\cos^2 \phi \sin^2 \omega - 1)P_{1e}^E \\
&- \cos^2 \phi \cos^2 \omega)]/(\cos^2 \phi \cos 2\omega).
\end{aligned} \tag{4.19}
$$

Simplifications arise from the mass heirarchy condition.

First M_{ij}^S is nonzero for $i, j = 1, 2$ only. (This approximation was used in analyzing the solar neutrino problem in chapter 2) So $P_{\alpha j}^S$ becomes $|U_{e3}^C|^2$, which is just $\sin^2 \phi_C \approx \sin^2 \phi$. And hence we can replace P_{e3}^S in eq(4.19) by $\sin^2 \phi_C$. $|M_{12}^S|^2$ is taken to be the modified Landau- Zener jump probability for an exponentially varying solar density [12]. Further from eq.(4.4), we get

$$M^{(n)} = \begin{bmatrix} \cos \theta & \sin \theta & 0 \\ -\sin \theta & \cos \theta & 0 \\ 0 & 0 & 1 \end{bmatrix}, \tag{4.20}$$

where $\theta = \omega_n - \omega_{n-1}$. That is $M^{(n)}$ are basically reduced to 2×2 matrices. So nonadiabatic effects even in the crossing at the surface of the earth, is only between

the first and the second mass eigenstates. As a result, we get the simple formulae from eq(4.8), valid for $x < 0.84$:

$$P_{1e}^E = \cos^2\phi[\cos^2\omega_E - \sin 2\omega_E \sin 2(\omega_E - \omega)\sin^2\Phi_{12}] \tag{4.21}$$

$$P_{2e}^E = \cos^2\phi[\sin^2\omega_E + \sin 2\omega_E \sin 2(\omega_E - \omega)\sin^2\Phi_{12}], \tag{4.22}$$

where ω_E is the mixing angle, just below the surface of the earth. Using eqns(19) and (20) in eqn(18), we get the following simple expression for P_{ee}^N

$$P_{ee}^N = P_{ee}^D + \frac{[1 - 2P_{ee}^D - \sin^2\phi(2 - \sin^2\phi)]}{\cos 2\omega \cos^2\phi}$$
$$\times (P_{2e}^E - \sin^2\omega\cos^2\phi). \tag{4.23}$$

The above goes over to the one given in [64] for for two flavors by setting $\phi = 0$.

4.3   Calculations and results

We first present some details about the different neutrino trajectories during the night. The neutrino samples different amounts of matter in the earth during a single night and also during a year. The distance d travelled by the neutrino inside the earth during night, as a function of time t, is given by

$$d = 2R(\sin\phi_l \sin\delta + \cos\phi_l \cos\delta \cos(\frac{2\pi t}{T_D})), \tag{4.24}$$

$$\sin\delta = \sin 23.5° \sin(\frac{2\pi t}{T_Y}). \tag{4.25}$$

Here R is the radius of the earth, ϕ_l is the latitude of the location of the detector, T_D is the length of the day, T_Y is the length of the year and zero of t is chosen at midnight on autumnal equinox. The time variation of $x = (\frac{d}{2R})$ during the night and year are illustrated in Fig.(4.1a). If the data collected during successive nights are accumulated at the corresponding x- bins, the calculation of neutrino rates per unit bin will require the function $f(x)$ defined as the time duration per unit interval of x [60]. $f(x)$ for different locations are plotted in Fig.(4.1b), which shows the relative merits of the detectors for exposure to regions of x.

The neutrino detection rates for a Super–Kamioka type of detector is given by

$$R = \int \phi\sigma P_{ee}dE + \frac{1}{6}\int \phi\sigma(1 - P_{ee})dE, \tag{4.26}$$

where the second term is the neutral current contribution and $\phi(E)$ is the solar neutrino flux as a function of the neutrino energy E and $\sigma(E)$ is the cross section from neutrino electron scattering and we integrate from $5MeV$ onwards. The cross section is taken from [14] and the flux from [15]. The rates for the night and day R_N and R_D are calculated using P_{ee}^N and P_{ee}^D respectively. We define the day–night asymmetry ratio as $A = (R_N - R_D)/(R_N + R_D)$. We can multiply R_N and R_D by the function $f(x)$ displayed in Fig.(4.1) to get the rates per unit interval in x. Note that $f(x)$ cancels in the asymmetry ratio calculated theoretically. However, the experimentalists have to weight the day rate R_D with $f(x)$ before comparing their data with our theoretical curves.

In Figs.(4.2) and (4.3) we have plotted A as a function of x, the fractional distance travelled by the neutrino inside the earth for various values of the neutrino parameters δ_{21}, ω and ϕ. Different values of these parameters have distinguishable characteristics. Some gross features which may enable us to specify their approximate domains are the following:

• For small angle ω there is a gradual increase of the asymmetry with x, whereas for large ω the oscillations in x start showing up. For $x < 0.84$ (*i.e.* trajectories through mantle only) there is a very clear discrimination between the small ω and large ω, irrespective of δ_{21} and ϕ.

• As ϕ increases, the asymmetry at any x decreases.

• The amplitude of the oscillatory pattern is largest for small δ_{21} and decreases steadily as δ_{21} increases.

• For small ω and large δ_{21}, asymmetry is appreciable only in the core and is a sensitive function of δ_{21}.

The reasons for nonzero ϕ diluting the asymmetry are twofold.
1) Unitarity demands that $\sum_i P_{ie}^E = 1$. This means that in three flavors P_{2e}^E is always less than its value in the two flavor case.
2) The resonance condition in the case of three flavors has the form

$$A \cos^2 \phi = \delta_{21} \cos 2\omega. \tag{4.27}$$

A resonance which occurs at a given energy, in the core of the earth in the two flavor case $\phi = 0$ will either occur at a higher energy or it may not occur at all in the three flavor case. Since the boron neutrino flux falls rapidly with energy, resonance occuring at a higher energy is not as effective as resonance occuring at lower energies. Another point to be noted from eq.(5.24), is that if one fixes the energy at which resonance takes place in two flavors, then in the three flavor case depending on the value of ϕ, the resonance will be shifted to a higher density, which may not be available in the earth. Thus overall the resonance effect is supressed in the case of three flavors. So a nonzero ϕ dilutes the asymmetry. Our numerical results include the effect of any adiabatic MSW resonances that may occur inside the earth. For $\phi = 0$, as pointed out recently [61, 58], MSW resonances do occur in the earth's core. However, for large ϕ they disappear and this is another reason for the regeneration efect to be smaller for large ϕ, in the core.

In Fig.(4.3) we have chosen a few parameter sets for which A is very small (< 0.15) since they are possible solutions to the solar and atmospheric neutrino problems [22, 28, 21]. But we cannot rigorously exclude other values of the neutrino parameters at the present stage of knowledge. Day–night effect must be studied in an unbiased manner, especially because the ratio A is relatively independent of the uncertainties of the solar models.

4.4 Eclipse effect

In this section we will discuss two possibilities : (1) Neutrinos detected during a solar eclipse which pass through the moon. (2) Neutrinos detected at the far side of the earth during a solar eclipse pass through the moon and the earth. We shall call this scenario (2) a *double eclipse*. Two previous works [65, 66] have discussed scenario (1), however both are incomplete in many respects. We do a proper analysis of the above mentioned possibilities.

We first present some astronomy relevant to the eclipse effect. Solar neutrinos are produced within the solar core whose radius is of order 1/10 of the solar radius and we shall approximate this by a point at the centre of the sun. What is required

for our purpose is that the lunar disc must cover this point at the centre of the sun and so as far as the neutrino radiation is concerned , the solar eclipse is more like an occultation of a star or a planet by the moon.

Astronomers characterize the solar eclipse by the optical coverage C which is defined as the ratio of the area of the solar disc covered by the lunar disc to the total area of the solar disc. For neutrino physics we require the distance d_M travelled by the neutrino inside the moon. Defining the fraction $x = \dfrac{d_M}{2R_M}$ where R_M is the lunar radius, x can be given in terms of C by the following formulae:

$$x = \sqrt{(4z(2-z)-3)}, \tag{4.28}$$

$$C = \frac{2}{\pi}\left(\cos^{-1}(1-z)-(1-z)\sqrt{z(2-z)}\right). \tag{4.29}$$

Eqn(4.29) can be inverted to get the parameter z for a given C and this z can be substituted in eqn(4.28). The relationship between x and C so obtained is plotted in Fig.(4.4). When the lunar disc passes through the centre of the sun, C is 0.39 and the neutrino eclipse starts at this value of C. When the optical coverage increases above 39%, x rises sharply from zero and reaches 0.6 and 0.95 for optical coverage of 50% and 80% respectively.

For any point of observation of the usual solar eclipse (which we shall call *single eclipse*) there is a corresponding point on the other side of the earth where a double eclipse occurs. With the coordinates labeled as (latitude, longitude), the single eclipse point (α, β) is related to the double eclipse point (λ, σ) by the relations (see Fig.(4.5)):

$$\lambda = \alpha + 2\delta$$
$$\sigma = \pi - 2\Theta_{UT} - \beta \tag{4.30}$$

where

$$\sin\delta = \sin 23.5° \sin(\frac{2\pi t}{T_Y}). \tag{4.31}$$

T_Y is the length of the year , zero of time t is chosen at midnight of autumnal equinox *i.e.*Sept. 21, and Θ_{UT} is the angle corresponding to the Universal Time – UT.

During a double eclipse, the neutrinos travel through the earth in addition. The distance d_E travelled by the neutrino inside the earth along the chord between the points (α, β) and (λ, σ) as a function of time t, is given by

$$d_E = 2R_E(\sin \lambda \sin \delta + \cos \lambda \cos \delta \cos(\frac{2\pi t}{T_D})), \tag{4.32}$$

where R_E is the radius of the earth and T_D is the length of the day. This is the same distance that needs to be calculated in the study of the day–night effect and a plot of this distance as a function of t is given earlier in this chapter.

Present and upcoming high statistics neutrino detectors expect to collect a few solar neutrino events every hour. As discussed in Secs. 4.4.1 and 4.4.2, single and double eclipse can lead to enhancements of rates by upto two and a half times. Even with such large enhancements during the eclipse the signal may not exceed statistical errors, since each solar eclipse lasts only for a few hours. However they occur fairly often. As many as 32 solar eclipses are listed to occur during the 14 year period 1996 through 2010. Global maps and charts are available[67] for location and duration of both the umbral and penumbral coverage. In the planning of sites for neutrino–detectors of the future, these locations may be kept in mind.

The eclipses during the 2 year period 1997 through 1999 are the following:

1997 **March 9** – Total Solar Eclipse

1997 **Oct 12** – Partial Solar Eclipse

1998 **Feb 26** – Total Solar Eclipse

1998 **Aug 22** – Annular Solar Eclipse

1999 **Feb 16** – Annular Solar Eclipse

1999 **Aug 11** – Total Solar Eclipse

We have analyzed the five total/annular eclipses. We have not examined the partial solar eclipse of 1997 October 12, since we have not so far been able to procure the data for this eclipse from the references cited in [67]. It is important to remark

here that although partial solar eclipses are not so useful to astronomers they are nevertheless relevant for neutrino physics as long as C is above 0.39.

A study of the global maps of the five total/annular eclipses listed above shows that only three of them can occur as a single or a double eclipse at any of the three existing detector sites Kamioka, Sudbury and Gran Sasso with coordinates $(36.4°N, 140°E)$, $(46.5°N, 81°W)$ and $(42.5°N, 13.5°E)$ respectively. Approximate estimates are presented below for the duration and optical coverage of the relevant detectors at these sites:

1997 March 9 – This eclipse was a single eclipse for the Super–Kamioka, with an approximate duration of two and a half hours and a maximum optical coverage of just over 60%. In addition, there was a double eclipse at the Gran–Sasso, the site of Borexino, at almost the same time as at Kamioka and for the same duration, with a 70% optical coverage.

1998 Feb 26 – Though Sudbury has an optical eclipse the coverage is less than 39% and so no neutrino–eclipse occurs. However, a double eclipse occurs at Gran–Sasso with a maximum coverage of 70% to 80%. This corresponds to the single eclipse at $(31°N, 45°W)$.

1999 Aug 11 – This eclipse will provide one of the best opportunities, as a single eclipse with 90% optical coverage and almost 3 hour duration at Gran-Sasso. In addition Super–Kamioka site will also get a double eclipse with 90% to 100% optical coverage, corresponding to the single eclipse at approximately $(36°N, 40°E)$

4.4.1 Single eclipse

We now describe a straightforward way of obtaining the neutrino regeneration effect in the moon by using a model of moon of constant density (3.33gms/cc). Our starting point is the same as in the previous section. Let a neutrino of flavor α be produced at time $t = t_0$ in the core of the sun. Its state vector is

$$|\Psi_\alpha(t_0)\rangle = |\nu_\alpha\rangle = \sum_i U^S_{\alpha i}|\nu^S_i\rangle,$$

where $|\nu_i^S\rangle$ are the matter dependent mass eigenstates with mass eigenvalues μ_i^S and $U_{\alpha i}^S$ are the matrix elements of the matter dependent mixing matrix in the core of the sun. We use Greek index α to denote the three flavors e, μ, τ and Latin index i to denote the mass eigenstates i = 1,2,3. The neutrino propagates in the sun adiabatically upto t_R (the resonance point), makes non-adiabatic transitions at t_R, propagates adiabatically upto t_1 (the edge of the sun) and propagates as a free particle upto t_2 when it enters the moon. So the state vector at t_2 is

$$
\begin{aligned}
|\Psi_\alpha(t_2)\rangle &= \sum_{j,i} |\nu_j\rangle exp\left(-i\varepsilon_j(t_2 - t_1)\right) exp\left(-i\int_{t_R}^{t_1} \varepsilon_j^S(t)dt\right) M_{ji}^S \\
&\times exp\left(-i\int_{t_0}^{t_R} \varepsilon_i^S(t)dt\right) U_{\alpha i}^S,
\end{aligned}
\tag{4.33}
$$

where $\varepsilon_i^S(t)(\equiv E + (\mu_i^S(t))^2/2E)$ are the matter dependent energy eigenvalues in the sun, ε_i and $|\nu_i\rangle$ are the energy eigenvalues and the corresponding eigenstates in vacuum and M_{ji}^S is the probability amplitude for the non-adiabatic transition $i \to j$. We multiply the right hand side of eq.(4.33) by $\sum_k |\nu_k^M\rangle\langle\nu_k^M|$ (= 1)where $|\nu_k^M\rangle$ (i =1,2,3) is the complete set of matter dependent mass eigenstates inside the moon. The neutrino propagates upto the the other end of the moon at t_3, and the state vector at t_3 is

$$
\begin{aligned}
|\Psi_\alpha(t_3)\rangle &= \sum_{k,j,i} |\nu_k^M\rangle exp\left(-i\varepsilon_k^M(t_3 - t_2)\right) \langle\nu_k^M|\nu_j\rangle \\
&\times exp\left(-i\varepsilon_j(t_2 - t_1) - i\int_{t_R}^{t_1} \varepsilon_j^S(t)dt\right) \\
&\times M_{ji}^S exp\left(-i\int_{t_0}^{t_R} \varepsilon_i^S(t)dt\right) U_{\alpha i}^S \\
&= \sum_{k,j,i} |\nu_k^M\rangle exp\left(-i\varepsilon_k^M(t_3 - t_2)\right) M_{kj}^M \\
&\times exp\left(-i\varepsilon_j(t_2 - t_1) - i\int_{t_R}^{t_1} \varepsilon_j^S(t)dt\right) \tag{4.34} \\
&\times M_{ji}^S exp\left(-i\int_{t_0}^{t_R} \varepsilon_i^S(t)dt\right) U_{\alpha i}^S. \tag{4.35}
\end{aligned}
$$

We have introduced the probability amplitude M_{kj}^M for non-adiabatic transitions $j \to k$ due to the abrupt change in density when the neutrino enters the moon. It is given by

$$
M_{kj}^M = \langle\nu_k^M|\nu_j\rangle = \sum_\gamma \langle\nu_k^M|\nu_\gamma\rangle\langle\nu_\gamma|\nu_j\rangle = \sum_\gamma U_{\gamma k}^M U_{\gamma j}^*, \tag{4.36}
$$

where $U_{\gamma j}$ is the mixing matrix in vacuum . We multiply the right hand side of eq.(4.3) by $\sum_l |\nu_l\rangle\langle\nu_l|$ where $|\nu_l\rangle$ (l =1,2,3) is the complete set of vacuum mass eigenstates. The neutrino leaves the other end of the moon at $t = t_3$ and propagates upto the surface of the earth, which it reaches at t_4 .So the state vector at t_4 is

$$
\begin{aligned}
|\Psi_a(t_4)\rangle &= \sum_{k,j,i,l} |\nu_l\rangle exp\left(-i\varepsilon_k^M(t_3-t_2)\right)\langle\nu_l|\nu_k^M\rangle \\
&\quad \times M_{kj}^M exp\left(-i\varepsilon_j(t_2-t_1)-i\int_{t_R}^{t_1}\varepsilon_j^S(t)dt\right) \\
&\quad \times M_{ji}^S exp\left(-i\int_{t_0}^{t_R}\varepsilon_i^S(t)dt\right)U_{\alpha i}^S exp\left(-i\varepsilon_l(t_4-t_3)\right) \\
&= \sum_{k,j,i,l} |\nu_l\rangle M_{kj}^M M_{kl}^{M*} M_{ji}^S U_{\alpha i}^S exp\left(-i\Phi_{ijkl}\right),
\end{aligned}
\tag{4.37}
$$

where

$$
\Phi_{ijkl} = \varepsilon_k^M(t_3-t_2) + \varepsilon_l(t_4-t_3) + \varepsilon_j(t_2-t_1) + \int_{t_R}^{t_1}\varepsilon_j^S(t)dt + \int_{t_0}^{t_R}\varepsilon_i^S(t)dt. \tag{4.38}
$$

We have used the fact that the the probability amplitude for non-adiabatic transitions $k \to l$ due to the abrupt change in density when the neutrino leaves the moon is

$$
\langle\nu_l|\nu_k^M\rangle = M_{kl}^{M*}. \tag{4.39}
$$

The probability of detecting a neutrino of flavor β at t_4 is

$$
\begin{aligned}
|\langle\nu_\beta|\Psi_a(t_4)\rangle|^2 &= \sum U_{\beta i}^* U_{\beta i'} M_{kj}^M M_{k'j'}^{M*} M_{kl}^{M*} M_{k'l'}^M M_{ji}^S M_{j'i'}^{S*} U_{\alpha i}^S U_{\alpha i'}^{S*} \\
&\quad \times exp\left(-i(\Phi_{ijkl}-\Phi_{i'j'k'l'})\right),
\end{aligned}
\tag{4.40}
$$

where the summation is over the set of indices i,j,k,l,i',j',k',l' Averaging over t_R leads to $\delta_{ii'}\delta_{jj'}$ and this results in the desired incoherent mixture of mass eigenstates of neutrinos reaching the surface of the moon at t_2. Calling this averaged probability as $P_{\alpha\beta}^M$ (the probability for a neutrino produced in the sun as ν_α to be detected as ν_β in the earth after passing through the moon), we can write the result as

$$
P_{\alpha\beta}^M = \sum_j P^S(\alpha \to j)P^M(j \to \beta), \tag{4.41}
$$

where

$$
P^S(\alpha \to j) = \sum_i |M_{ji}^S|^2 |U_{\alpha i}^S|^2 \tag{4.42}
$$

$$
\begin{aligned}
P^M(j \to \beta) &= \sum_{l,k,l',k'} U_{\beta i}^* U_{\beta l'} M_{kj}^M M_{k'j}^{M*} M_{kl}^{M*} M_{k'l'}^M \\
&\quad \times exp\left(-i(\varepsilon_k^M-\varepsilon_{k'}^M)d_M - i(\varepsilon_l-\varepsilon_{l'})r\right).
\end{aligned}
\tag{4.43}
$$

In eqn.(4.43) we have replaced $(t_3 - t_2)$ by d_M, the distance travelled by the neutrino inside the moon, and $(t_4 - t_3)$ by r the distance travelled by the neutrino from the moon to the earth. If there is no moon , we put $d_M = 0$, so that $P^M(j \to \beta)$ becomes $|U_{\beta j}|^2$ and so eqn.(4.41) reduces to the usual [13, 22] averaged probability for ν_α produced in the sun to be detected as ν_β in the earth :

$$P_{\alpha\beta}^D = \sum_{i,j} |U_{\beta j}|^2 |M_{ji}^S|^2 |U_{\alpha i}^S|^2.$$

4.4.2 Double eclipse

We use a model of earth of constant density (5.52gms/cc). The variation of density can be taken into account by using the analytical formulation of Ref.[68]. This is for the future. We start with $\Psi_\alpha(t_4)$ given by eq.(4.37) and multiply the right hand side by $\sum_p |\nu_p^E\rangle\langle\nu_p^E|$ $(= 1)$ where $|\nu_p^E\rangle$ $(i = 1, 2, 3)$ is a complete set of mass eigenstates inside the earth. The neutrino enters the earth at time $t = t_4$ and is detected at time $t = t_5$ inside the earth. The state vector at time $t = t_5$ is

$$|\Psi_\alpha(t_5)\rangle = \sum_{k,j,i,l,p} |\nu_p\rangle M_{pl}^E M_{kj}^M M_{kl}^{M*} M_{ji}^S U_{\alpha i}^S \exp\left(-i\Phi_{ijklp}\right), \qquad (4.44)$$

where we have introduced the probability amplitude M_{pl}^E for non adiabatic transitions $l \to p$ due to the abrupt change in density when the neutrino enters the earth. It is given by

$$M_{pl}^E = \langle\nu_p^E|\nu_l\rangle = \sum_\sigma U_{\sigma p}^E U_{\sigma l}^* \qquad (4.45)$$

and

$$\begin{aligned}
\Phi_{ijklp} &= \varepsilon_p^E(t_5 - t_4) + \varepsilon_k^M(t_3 - t_2) + \varepsilon_l(t_4 - t_3) + \varepsilon_j(t_2 - t_1) \\
&\quad + \int_{t_R}^{t_1} \varepsilon_j^S(t)dt + \int_{t_0}^{t_R} \varepsilon_i^S(t)dt.
\end{aligned} \qquad (4.46)$$

The probability of detecting a neutrino of flavor β at t_5 is

$$\begin{aligned}
|\langle\nu_\beta|\Psi_\alpha(t_5)\rangle|^2 &= \sum U_{\beta p}^{E*} U_{\beta p'}^E M_{pl}^E M_{p'l'}^{E*} M_{kj}^M M_{k'j'}^{M*} M_{kl}^{M*} M_{k'l'}^M M_{ji}^S M_{j'i'}^{S*} U_{\alpha i}^S U_{\alpha i'}^{S*} \\
&\quad \times \exp\left(-i(\Phi_{ijklp} - \Phi_{i'j'k'l'p'})\right),
\end{aligned} \qquad (4.47)$$

where the summation is over the set of indices $i, j, k, l, p, i', j', k', l', p'$ Again averaging over t_R and calling this averaged probability as $P_{\alpha\beta}^{ME}$ (the probability for a neutrino produced in the sun as ν_α to be detected as ν_β in the earth after passing through the moon and the earth), we can write the result as

$$P_{\alpha\beta}^{ME} = \sum_j P^S(\alpha \to j) P^{ME}(j \to \beta), \qquad (4.48)$$

where

$$P^{ME}(j \to \beta) = \sum_{l,k,p,l',k',p'} U_{\beta p}^{E*} U_{\beta p'}^E M_{pl}^E M_{p'l'}^{E*} M_{kj}^M M_{k'j}^{M*} M_{kl}^{M*} M_{k'l'}^M$$
$$\times exp\left(-i(\varepsilon_p^E - \varepsilon_{p'}^E)d_E - i(\varepsilon_k^M - \varepsilon_{k'}^M)d_M - i(\varepsilon_l - \varepsilon_{l'})r\right) (4.49)$$

Here again we have replaced $(t_5 - t_4)$ by d_E, the distance travelled by the neutrino inside the earth, $(t_3 - t_2)$ by d_M, the distance travelled by the neutrino inside the moon and $(t_4 - t_3)$ by r the distance travelled by the neutrino from the moon to the earth.

For the sake of completeness, we state that if we put $d_M = 0$ in eqn.(4.49) we get the regeneration in earth alone:

$$P_{\alpha\beta}^E = \sum_j P^S(\alpha \to j) P^E(j \to \beta), \qquad (4.50)$$

where

$$P^E(j \to \beta) = \sum_{k,k'} U_{\beta k}^{E*} U_{\beta k'}^E M_{kj}^E M_{k'j}^{E*} exp\left(-i(\varepsilon_k^E - \varepsilon_{k'}^E)d_E\right). \qquad (4.51)$$

Eqns(4.50) and (4.51) were used in the previous section on day–night effect [68]. We again emphasise that that the factorization of probabilities seen in eqs(4.41),(4.48) and (4.50) is valid only for mass eigenstates in the intermediate state.

The parametrization of the three flavor parameters, in vacuum and matter is exactly the same as in the previous section on day-night effect. We again work in the hierarchy $\delta_{31} \gg \delta_{21}$.

4.5   Calculations and results

The neutrino detection rates for a Super–Kamoika type of detector is given by

$$R = \int \phi(E)\sigma(E)P_{ee}dE + \frac{1}{6}(\int (\phi(E)\sigma(E)(1-P_{ee})dE) \qquad (4.52)$$

where the second term is the neutral current contribution and $\phi(E)$ is the solar neutrino flux as a function of the neutrino energy E and $\sigma(E)$ is the cross section from neutrino electron scattering and we integrate from $5MeV$ onwards. The cross section is taken from [14] and the flux from [15]. The rates for a single eclipse, double eclipse and without eclipse (at day–time) R_M, R_{ME} and R_D are calculated using P_{ee}^M, P_{ee}^{ME} and P_{ee}^D from eqns.(4.41),(4.48) and (4.4.1) respectively. We define the enhancement factors F and G for a single and double eclipse respectively:

$$F = \frac{R_M - R_D}{R_D} \qquad (4.53)$$

$$G = \frac{R_{ME} - R_D}{R_D}. \qquad (4.54)$$

It is easy to see that F and G have to be less than 5 and this theoretical maximum value occurs when $P_{ee}^O = 0$ and P_{ee}^M and P_{ee}^{ME} are put 1. If one imposes the constraint that the observed [69] neutrino rate is 0.51 ± 0.07 of the prediction of the standard solar model, the maximum possible enhancement is reduced to about 1.40 (at 90% C.L.).

We calculate the enhancement factors F and G for various values of the neutrino parameters, ω, δ_{21}, and ϕ. We show the results as contour plots in the δ_{21}–ω plane for different values of ϕ. Figs. (4.6) and (4.7) show the F–contours for $\phi = 0°$ and $\phi = 30°$ respectively. For each ϕ we show the contours for different distances of travel of the neutrino through the moon. Fig.(4.8) shows the G–contours for $\phi = 0$ for the maximum distance of travel of the neutrino inside the moon and the earth. The main features of the results are as follows:

- As the distance travelled by the neutrino inside the moon increases one can see an appreciable increase in the enhancement factor F. It increases from less than 10% to about almost 100% when the neutrino travels the whole diameter of the moon in the case of two flavor mixing i.e $\phi = 0$.

- Large ($> 40\%$) values of F occur for ω between $20°$ and $30°$ and $\delta_{21} \sim 10^{-6} eV^2$ This is true even for nonzero ϕ.

- The effect of a non zero "13" mixing angle ϕ, is to dilute the enhancement factor F for all values of distance travelled through the moon.(In fact for $\phi \approx 45°$, F is practically zero and so we have not plotted this case.)

- If large enhancement F is seen for values of $x \leq 0.6$, it immediately signals a very small value of ϕ. On the other hand, if no enhancement is seen for small x but there is enhancement only for $x \geq 0.8$ it signals an appreciable value of ϕ.

- For a double eclipse there are considerable enhancements even for small values of ω. There is enhancement throughout the range of ω from small angles till about $40°$. In fact the regions of largest enhancement ($> 100\%$) are for ω between $5°$ to $20°$.

- The region of maximum enhancement factor G is centered around a value of δ_{21} which is a little above $10^{-6} eV^2$, this being the value for maximum in F. This can be traced to the fact : $A^E > A^M$. However sizeable enhancement occurs over a wide range of δ_{21}.

- If enhancement is not seen, then certain regions of the neutrino parameter space can be excluded.If no enhancement is seen for single eclipse, a panel of ω between $5 - 25°$ and $\delta_{21} \approx 2 \times 10^{-7} - 2 \times 10^{-6} eV^2$ for $\phi = 0$ can be ruled out. If it is not seen for a double eclipse, a larger region can be ruled out.

4.5.1 Remarks

We have studied the effect on the solar neutrinos of their passage through the moon as well as the moon together with the earth. Although the numerical results presented in the paper cover only a representative sample of the set of various parameters, our analytical expressions can be used for more extensive calculations depending on the requirement. Also one can go beyond the hierarchy : $\delta_{31} \gg \delta_{21}$.

We now offer a few concluding remarks:

- Together with the day-night effect, the eclipse effects provide us with the tools for studying solar neutrinos, in a way independent of the uncertainties of the solar models.

- If the neutrino mass differences are really very small ($\delta_{21} < 10^{-5} eV^2$) there is no way of pinning down the neutrino parameters other than using the astronomical objects such as the moon or the earth for the "long-base-line experiments".

- It is important to stress that even the demonstrated absence of any eclipse effect would provide us with definitive information on neutrino physics.

- Accumulation of data over many eclipses may be needed for good statistics. However, it may be possible to see the effect even during one single eclipse if the large Borex detector with neutrino counting rates of about 40 per hour[30] or other such large detectors are built.

- It appears that Nature has chosen the neutrino parameters in such a way that the sun affects the propagation of solar neutrinos. It may be hoped that Nature has similarly chosen "lucky" parameters so that the moon and the earth too can affect the neutrinos !

- Finally, we stress the novelty of the whole phenomenon, and urge the experimentalists to look for and study the eclipse effects in an unbiased manner. They may even discover some surprises, not predicted by our calculations !

FIGURES FOR ECLIPSE EFFECT :

Fig.(4.4). The fractional distance travelled by the neutrino inside the moon $x(= \dfrac{d_M}{2R_M})$ is plotted against the optical coverage C of the solar eclipse.

Fig.(4.5). Geometry relating the double eclipse point (λ, σ) to the single eclipse point (α, β). (a) Section of the earth passing through (α, β) and perpendicular to the ecliptic. (b) Section passing through (α, β) and parallel to the equator.

Fig.(4.6). Contour plots of the enhancement factor for single eclipse $F(= \dfrac{R_M - R_O}{R_O})$ in the $\omega - \delta_{21}$ plane for $\phi = 0°$ and for four values of x ($x = 0.4$, 0.6, 0.8 and 1.0). The enhancement factor (regarded as a percentage) increases by 10% for every adjacent ring, as we move inwards towards the centre of the plot.

Fig.(4.7). Contour plots of the enhancement factor for single eclipse $F(= \dfrac{R_M - R_O}{R_O})$ in the $\omega - \delta_{21}$ plane for $\phi = 30°$ and $x = 0.6$, 0.8 and 1.0. The enhancement factor (regarded as a percentage) increases by 10% for every adjacent ring, as we move inwards towards the centre of the plot.

Fig.(4.8). Contour plot of the enhancement factor for double eclipse $G(= \dfrac{R_{ME} - R_O}{R_O})$ for $\phi = 0$ and $x = 1.0$. The distance travelled by the neutrino inside the earth is also taken to be the full earth diameter. The enhancement factor increases by 20% as we move inwards.
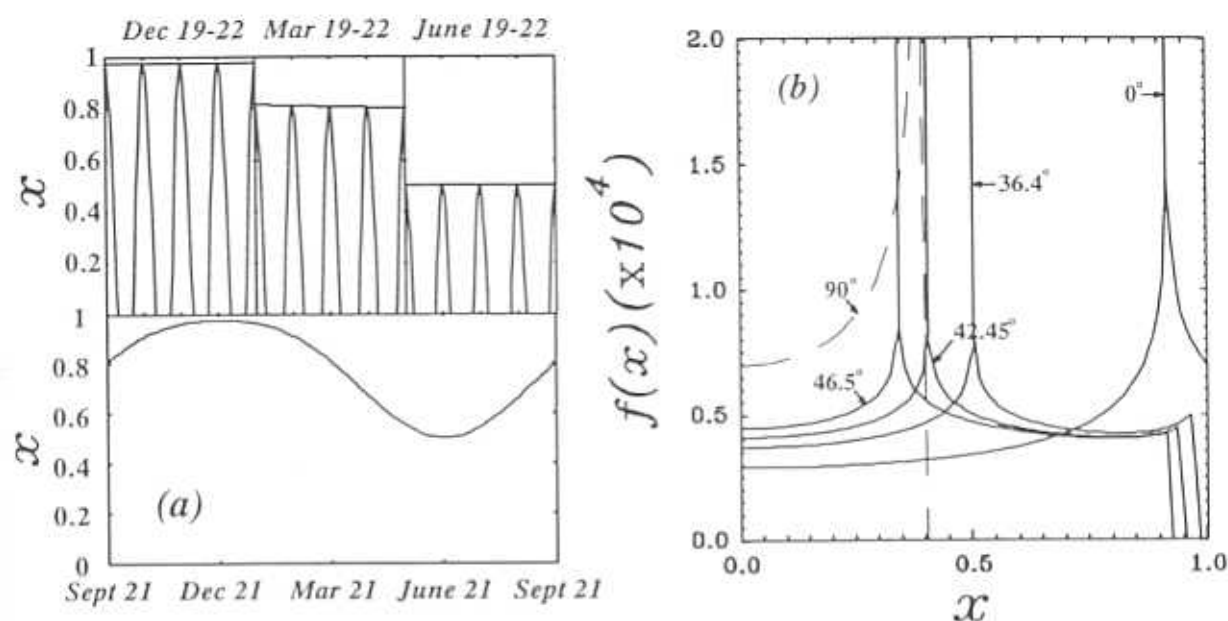
Figure 4.1: (a)The fractional distance x travelled by the neutrino inside the earth during night is plotted against time for the latitude (36.4°) of the Super–Kamioka detector. The lower figure gives the envelope of the 365 maxima during the year. As examples of the actual curves, those for a few nights during three specific seasons of the year are shown in the upper figure. The function $f(x)$ in hours per unit x is plotted for various latitudes: Super–Kamioka (36.4°), Borexino (42.45°), SNO (46.5°), equator (0.0°), pole (90°).
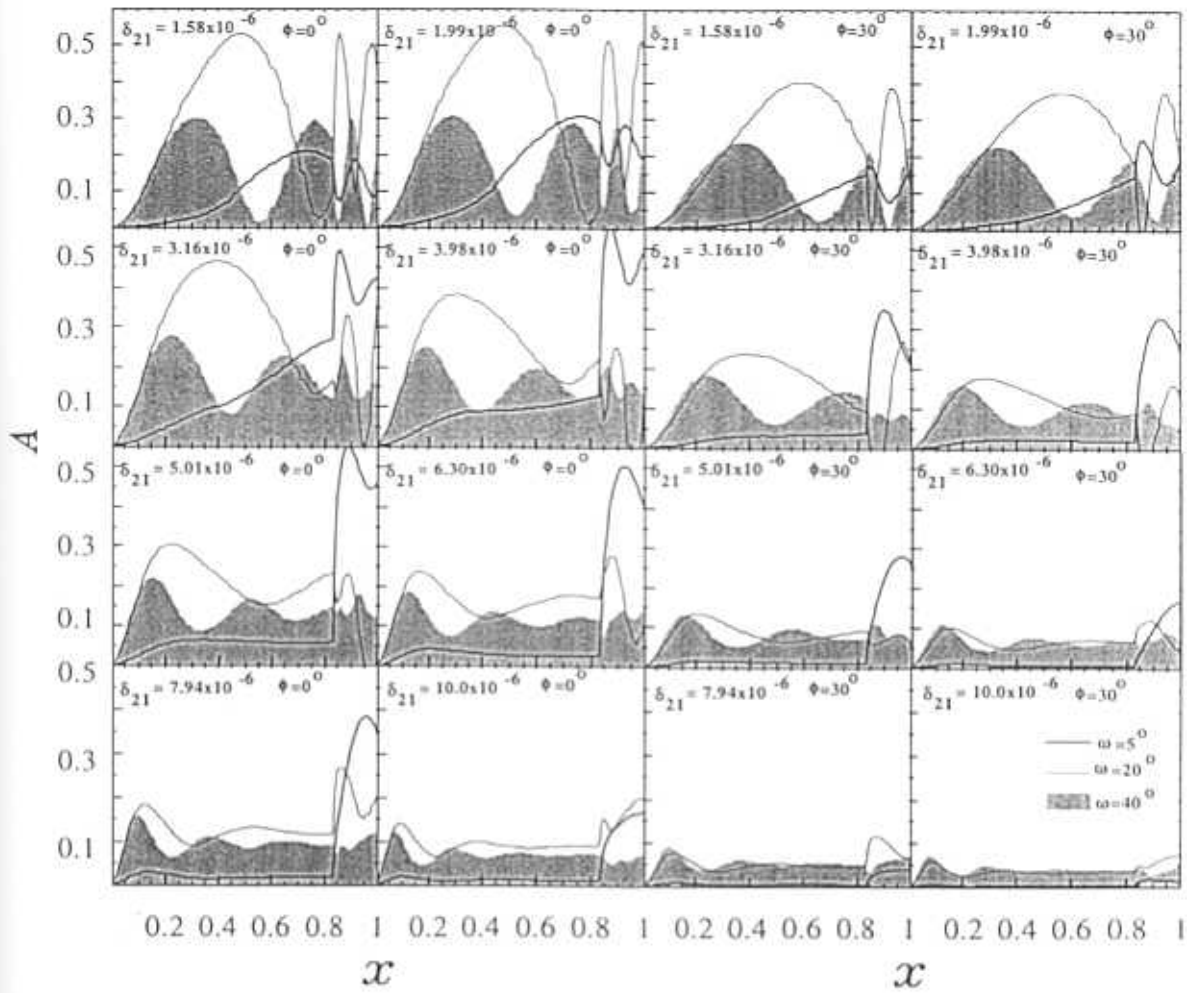
Figure 4.2: A as a function of x, the fractional distance travelled by the neutrino, for stated values of ω, δ_{21} (in eV^2) and ϕ.
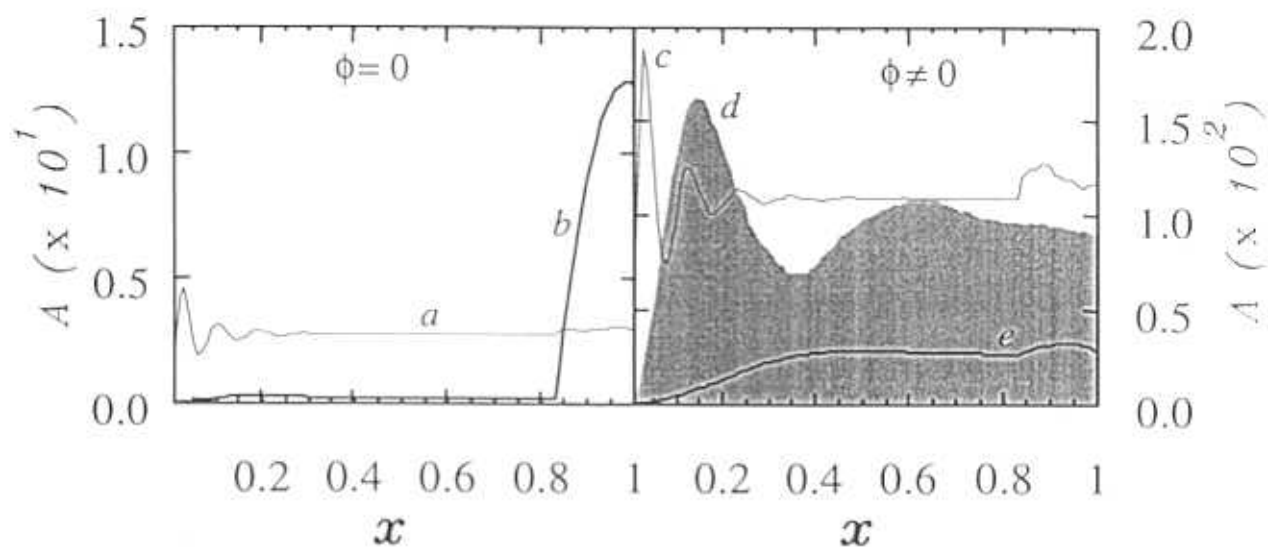
Figure 4.3: A as a function of x, for (a) $\delta_{21} = 3 \times 10^{-5}$ eV^2, $\omega = 28°$, $\phi = 0$; (b) $\delta_{21} = 6 \times 10^{-6}$, $\omega = 2.5°$, $\phi = 0$; (c) $\delta_{21} = 2.5 \times 10^{-5}$, $\omega = 20°$, $\phi = 32°$; (d) $\delta_{21} = 6.3 \times 10^{-5}$, $\omega = 18°$, $\phi = 45°$; (e) $\delta_{21} = 2.5 \times 10^{-6}$, $\omega = 6°$, $\phi = 50°$.
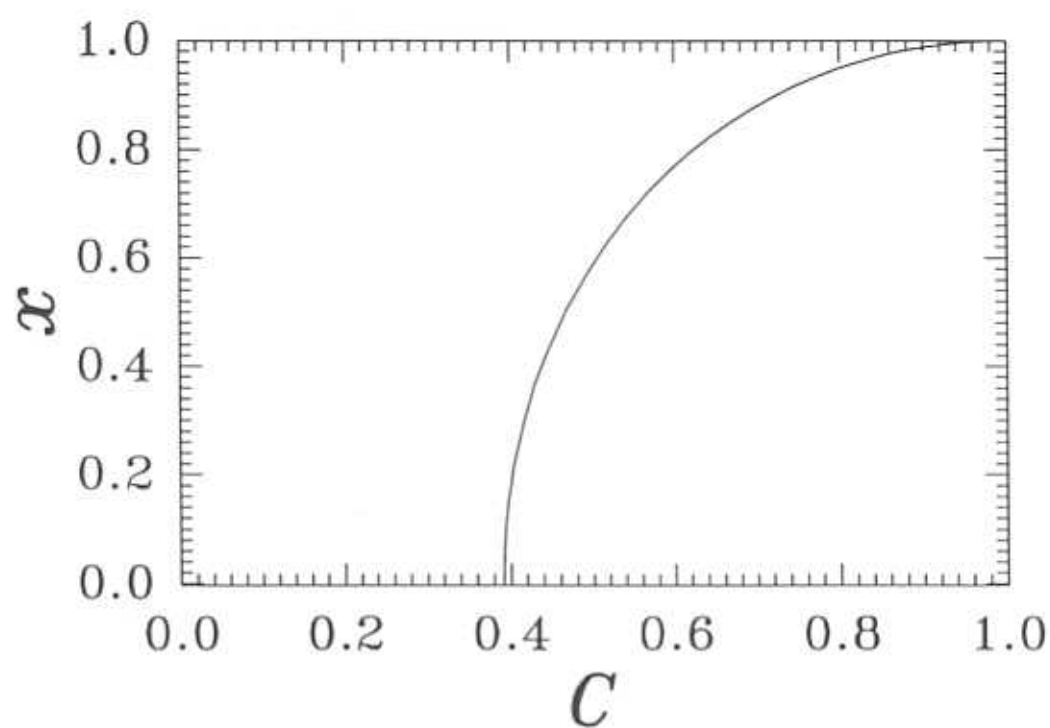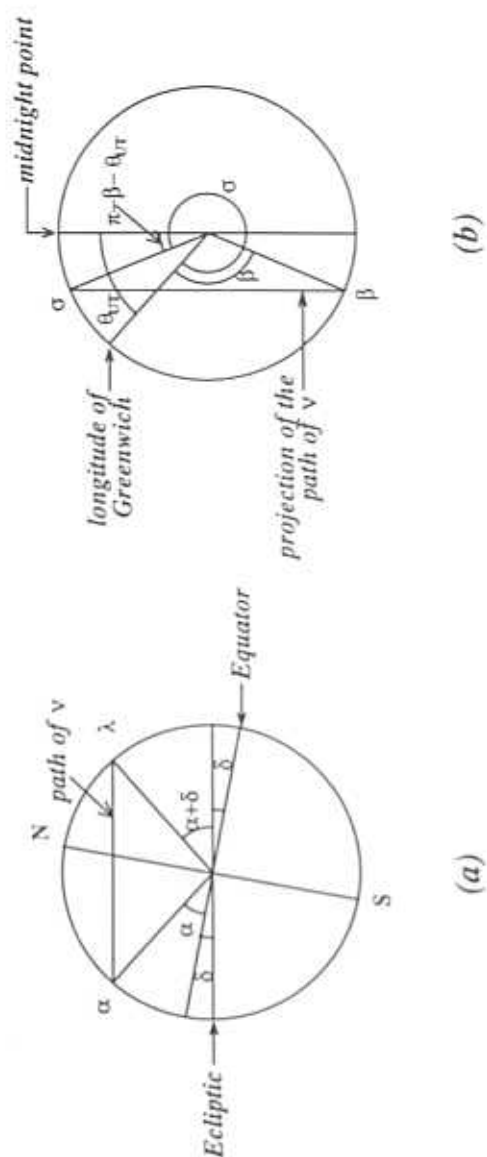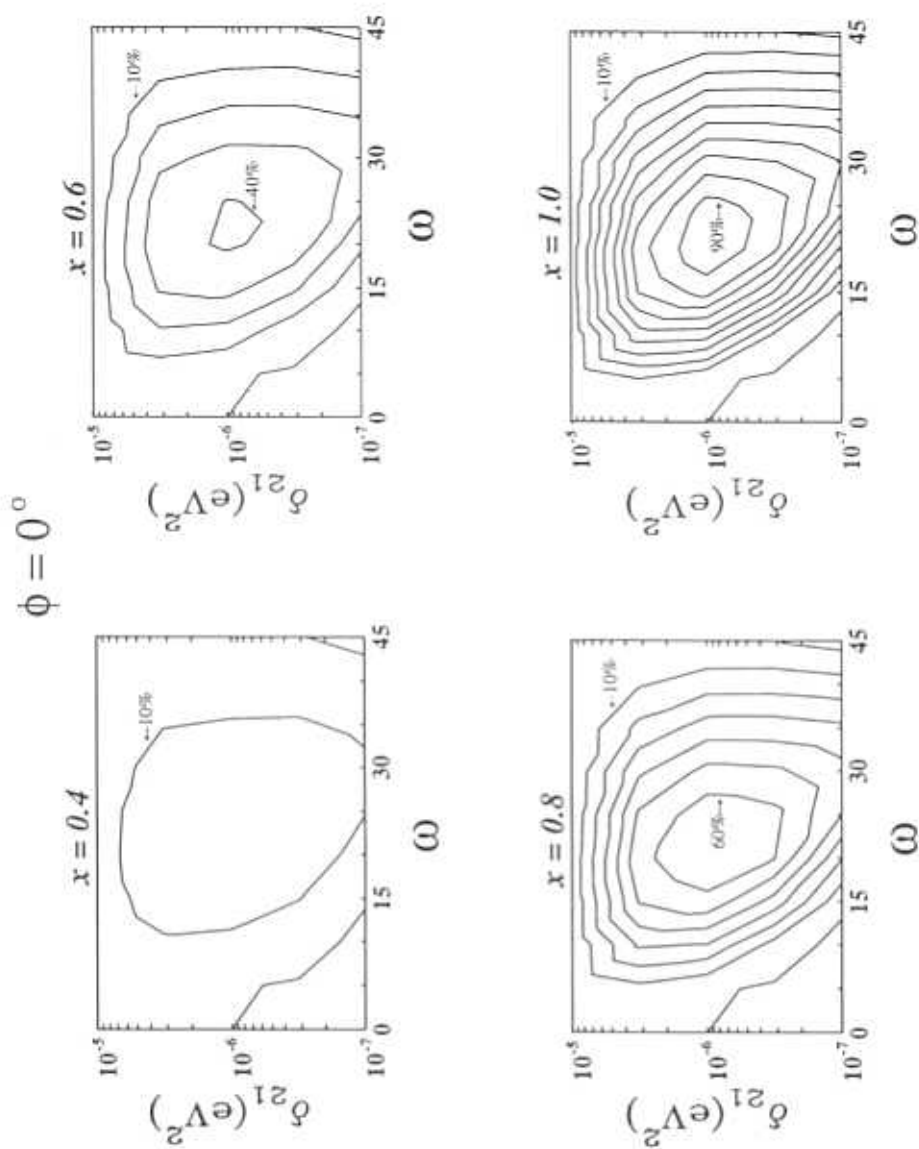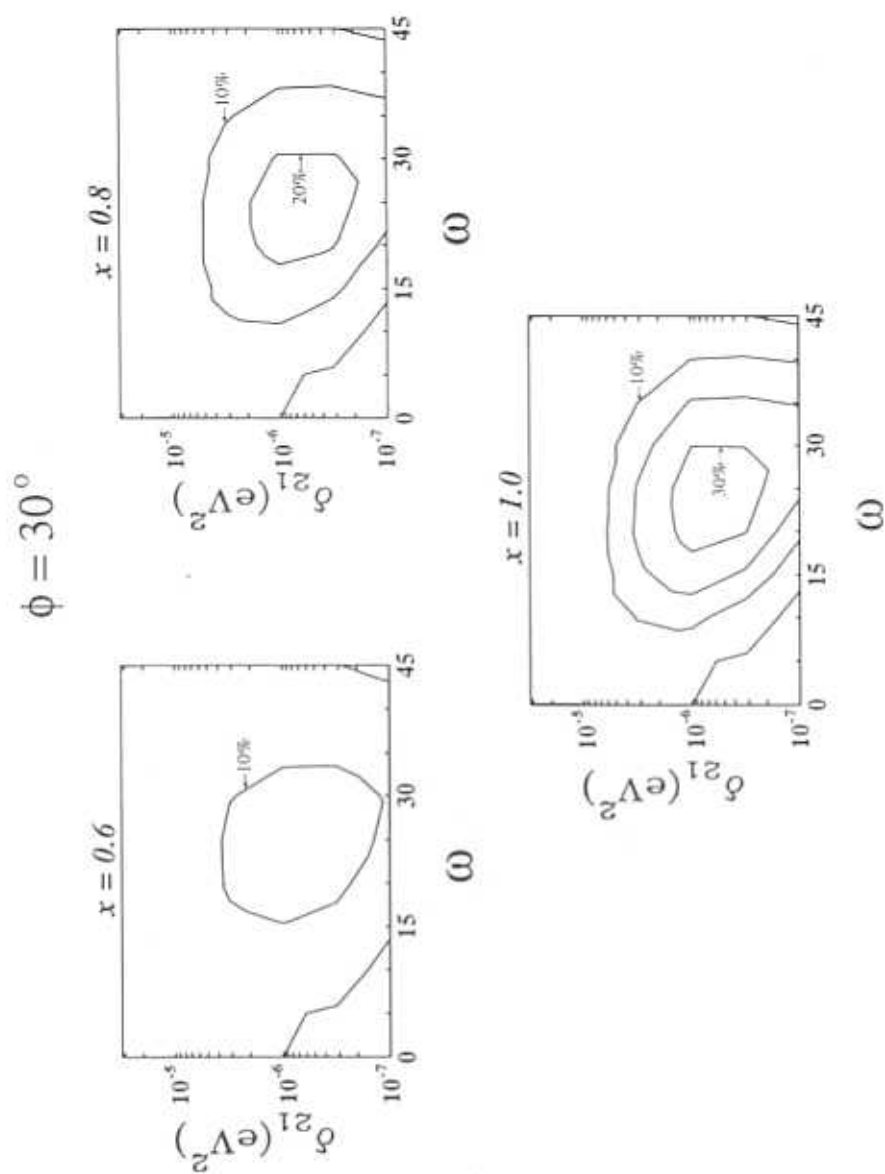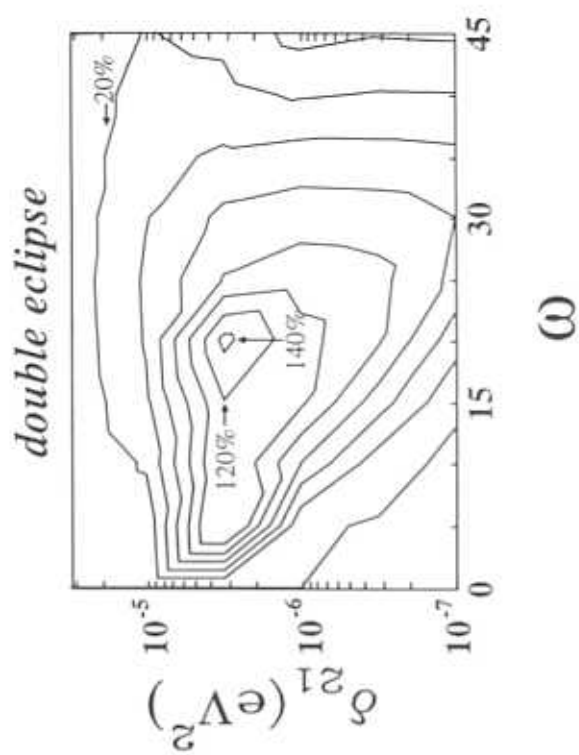
Figure 4.4:

Figure 4.5:

Figure 4.6:

Figure 4.7:

Figure 4.8:

Chapter 5

Terrestrial experiments and future experiments

5.1 Introduction

Until now we have discussed the implications of neutrino oscillations for the solar and the atmospheric neutrino anomalies. A combined solution to both these problems requires at least three flavors of neutrinos, and hence we have a three flavor parameter space spanned by five parameters. The constraints arising from these solutions have implications for laboratory neutrino experiments. Laboratory neutrino beams from reactors and accelerators are ideal sources to look for signals for neutrino oscillations. This is because the composition as well as the spectrum of the beam is very much under control. This is to be contrasted with the case of "natural" sources like solar and atmospheric neutrino beams, where one has absolutely no control over the beams, and one has to rely on elaborate Monte Carlo methods for determining the initial beam spectrum.

Reactor beams are mostly made up of electron antineutrinos ($\bar{\nu}_e$) as they are produced during the decay of neutrons which are copiously produced in reactors. These neutrinos have energies in the range $1 - 10 MeV$. Since the neutrino energy is too low to produce μ or τ, it is only possible to look for $\bar{\nu}_e \to \bar{\nu}_e$ oscillations

(survival) and $\bar{\nu}_e \to \bar{\nu}_x$ oscillations (disappearance). That is one looks for a possible attenuation in the original flavor as a signal for flavor oscillations. Accelerator neutrinos are mostly made up of muon antineutrinos ($\bar{\nu}_\mu$). These neutrinos have energies from tens of MeV to a few GeV. Therefore for accelerator neutrinos it is possible to look for signals in the appearance mode of the other flavor, i.e $\bar{\nu}_\mu \to \bar{\nu}_x$ oscillations. Here x can be either e or τ. For a good review of reactor and accelerator based experiments see [70].

Neutrino oscillation experiments with laboratory beams can be broadly classified into short baseline and long baseline experiments. In a short baseline experiment the source to detector distance is typically less than 1 km. For the long baseline experiments the distance is hundreds of km. As stated in chapter.1, the survival probability, i.e the probability that the neutrino retains its original flavor denoted by P_{ee} (we consider electron neutrinos and only two flavors as an example) after travelling a distance x is given by

$$P_{ee} = 1 - \sin^2 2\theta \sin^2\left(\frac{\delta m^2}{4E} x\right).$$

In usual units the formula for P_{ee} can be written as

$$P_{ee} = 1 - \sin^2 2\theta \sin^2\left(\frac{1.27\delta m^2(eV^2)x(m)}{E(MeV)}\right) \tag{5.1}$$

and

$$P_{e\mu} = \sin^2 2\theta \sin^2\left(\frac{1.27\delta m^2(eV^2)x(m)}{E(MeV)}\right), \tag{5.2}$$

where the distance x is measured in meters, δm^2 in eV^2 and E is in MeV.

One sees from the above two equations that for a given value of δm^2 and $\sin^2 2\theta$, the sensitivity of a baseline experiment to possible oscillations is controlled by the factor $\frac{x}{E}$. Example if δm^2 is very small, then one needs large values of $\frac{x}{E}$ to observe oscillations with fine tuning.

All the laboratory experiments performed so far (with one exception which we shall discuss in detail later) have been short baseline experiments. For a review see [71]. The range of $\frac{x}{E}$ accessible to these experiments has been from about $10^{-2} - 10$ (in units of $m MeV^{-1}$). None of these experiments has found any evidence for neutrino oscillations (with the sole exception of the controversial LSND signal

which was discussed in chapter.3). Also these experiments have not been able to probe the actual parameter space allowed by the atmospheric neutrino problem. The next generation of proposed accelerator neutrino experiments will have very long source to detector distances. For example

- 730 km for the Fermilab to Soudan experiment (MINOS) [72] .

- 250 km for the KEK-PS to Super-Kamiokande experiment [73] .

- 68 km for the Brookhaven National Laboratory experiment E889 [74].

- 732 km for the CERN to Gran Sasso experiment, with ICARUS [75], RICH [76], or NOE [77] as candidate detectors.

Very recently the CHOOZ collaboration [78], a reactor based experiment which searches for signals of $\bar{\nu}_e \rightarrow \bar{\nu}_x$ oscillations, where x can be any other flavor, in the disappearance mode of the original flavor has reported the results of its first run [78]. Even though the source to detector distance for CHOOZ is only about 1 km, it mimics a long baseline experiment. This is because the beam energy being very low ($\approx 3MeV$) the average value of $\frac{x}{E}$ is equal to 300. Hence it can probe mass squared differences as low as $10^{-3}eV^2$, an order of magnitude lower than previous reactor experiments. The collaboration sees no evidence of oscillations of the original flavor. They have analyzed their results assuming two flavor oscillations between ν_e and another flavor and gave an exclusion plot in the parameter space spanned by the mass squared difference Δm^2 and the mixing angle θ. Their main result is that for $\Delta m^2 > 3 \times 10^{-3}eV^2$, $\sin^2(2\theta)$ must be less than 0.18 [78]. We analyze the CHOOZ result in a realistic framework where mixing between all the three flavors of neutrinos are taken into account. We show that it is possible to deduce on which of the three mixing angles, the CHOOZ constraint actually applies. Also we demonstrate that this has dramatic repurcussions on the parameter space allowed as solutions to the solar and atmospheric neutrino problems.

Among the next generation of solar neutrino experiments, SNO and Borexino will play a pivotal role in furthering our understanding of neutrino physics. In this

chapter we do a detailed analyses of the physics prospects of Borexino in a three flavor framework. We also make a few remarks regarding SNO.

5.2 Three flavor analysis of CHOOZ result

We begin by recapitulating the relation between the flavor and mass eigenstates in vacuum. The flavor eigenstates are related to the mass eigenstates by

$$
\begin{bmatrix} \nu_e \\ \nu_\mu \\ \nu_\tau \end{bmatrix} = U \begin{bmatrix} \nu_1 \\ \nu_2 \\ \nu_3 \end{bmatrix}.
$$

Here we can take, without loss of generality, that $m_3 > m_2 > m_1$. The unitary matrix U can be parametrized as

$$
U = U^{23}(\psi) \times U^{phase} \times U^{13}(\phi) \times U^{12}(\omega),
$$

where $U^{ij}(\theta_{ij})$ is the two flavor mixing matrix between the ith and jth mass eignes-tates with the mixing angle θ_{ij}. For simplicity, we neglect the CP violation and set $U^{phase} = I$. The vacuum oscillation probability for a neutrino of flavor α to oscillate into a neutrino of flavor β is given by

$$
\begin{aligned}
P^0_{\alpha\beta} &= (U_{\alpha1}U_{\beta1})^2 + (U_{\alpha2}U_{\beta2})^2 + (U_{\alpha3}U_{\beta3})^2 + 2\,U_{\alpha1}U_{\alpha2}U_{\beta1}U_{\beta2}\cos\left(2.53\frac{d\,\delta_{21}}{E}\right) + \\
&\quad 2\,U_{\alpha1}U_{\alpha3}U_{\beta1}U_{\beta3}\cos\left(2.53\frac{d\,\delta_{31}}{E}\right) + 2\,U_{\alpha2}U_{\alpha3}U_{\beta2}U_{\beta3}\cos\left(2.53\frac{d\,\delta_{32}}{E}\right), (5.3)
\end{aligned}
$$

where d is the distance travelled in meters, E is in MeV, and mass squared differences are in eV^2. We may also note the vacuum oscillation probabilities are same as in eq. (5.3) for the case of antineutrinos because CP violation is neglected. If we assume the hierarchy among the neutrino mass eigenstates $\delta_{31} \gg \delta_{21}$, and that δ_{21} is about $10^{-5}eV^2$, which is required to fit solar neutrino data [21], then the oscillatory term involving δ_{21} can be set to one. The oscillation probability relevant for the CHOOZ experiment is the electron neutrino survival probability P_{ee} which is easily computed from eq. (5.3) to be

$$
P_{ee} = 1 - \sin^2 2\phi \sin^2\left(1.27\frac{d\,\delta_{31}}{E}\right). \tag{5.4}
$$

Notice the interesting point that this involves only the (13) mixing angle ϕ, and because of the heirarchy the (12) mixing angle ω disappears from the probability. So we reinterpret the CHOOZ result [78], to be that for $\delta_{31} > 3 \times 10^{-3}$, $\sin^2(2\phi)$ must be less than 0.18, i.e $\phi < 12.5°$. At this point we wish to emphasise again the importance of a three flavor analysis. The fact it is the (13) mixing angle which is constrained by CHOOZ can be seen only in a three flavor analysis.

We have discussed the atmospheric neutrino anomaly in detail in chapter.(3). We saw that in a three flavor analysis, both $e - \mu$ and $e - \tau$ oscillations contribute to the observed double ratio. Using the three flavor interpretation of the CHOOZ result we can now estimate the maximum contribution of the $e - \mu$ channel to the atmospheric neutrino anomaly. Since the relevant δ_{31} is about $10^{-2}eV^2$, matter effects are negligible for the problem [51]. Hence the relevant probability is the vacuum $\nu_e \leftrightarrow \nu_\mu$ oscillation probability,

$$P_{\bar{\mu}e} = P_{\mu e} = \sin^2 2\phi \sin^2 \psi \sin^2 \left(1.27 \frac{d\ \delta_{31}}{E} \right). \tag{5.5}$$

Note that both ϕ and ψ have to be non-zero for $P_{\mu e}$ to be non-zero, and also the oscillation length corresponding to δ_{21} does not contribute to the atmospheric neutrino problem [51]. Now solutions to Kamiokande atmospheric neutrino data [51, 22] require a value of $\psi \geq 45°$. The average contribution of the oscillatory term is 0.5. Therefore using the CHOOZ result that the maximum value of $\sin^2(2\phi)$ allowed is 0.18 we get

$$P_{\mu e}^{max} \leq 1.0 \times 0.18 \times 0.5 = 0.09 \tag{5.6}$$

which is less than 9 percent. Hence the atmospheric neutrino anomaly is driven almost completely by $\nu_\mu \leftrightarrow \nu_\tau$ oscillations. In our previous analysis of the atmospheric neutrino problem [51] we found that matter effects play a negligible role in the solution to even binned Multi-GeV data. Hence the θ dependence of data can be simply explained by the distance dependence of various oscillation probabilities.

In three flavors since ν_e can oscillate into ν_τ also we compute the $e - \tau$ conversion. The $\nu_e \leftrightarrow \nu_\tau$ conversion probability is given by

$$P_{\bar{e}\tau} = P_{e\tau} = \sin^2 2\phi \cos^2 \psi \sin^2 \left(1.27 \frac{d\ \delta_{31}}{E} \right). \tag{5.7}$$

Since $\psi > 45°$, we find that the $e - \tau$ conversion probability is less than 5 percent, i.e there is very little $e - \tau$ oscillations. Therefore the electron neutrino flux is more or less close to the Monte Carlo (no oscillations) prediction, which is what is experimentally observed.

Lastly we incorporate the CHOOZ constraints on our previous fits to solar and atmospheric neutrino data, and so we reproduce the plots from our earlier works, with the constraints coming from the CHOOZ results shown on them. In Fig.(5.1), the light contours enclose the parameter region in $\phi - \psi$ plane allowed by the binned multi-GeV data of Kamiokande with 1.6 σ error bars. The present CHOOZ constraint has been shown as a thick vertical line, with the region to the right of it being excluded. Fig.(5.2) shows the allowed region in the $\phi - \delta_{31}$ plane from the same analysis, with the CHOOZ constraint again being shown as a thick vertical line [51]. Fig.(5.3) and Fig.(5.4) show the previously allowed regions by the solar neutrino data in $\phi - \omega$ and $\phi - \delta_{21}$ planes respectively along with the new constraint [22]. One sees that the CHOOZ constraint as properly interpreted in a three flavor framework drastically cuts into the parameter space which was previously allowed. Note the fact that ϕ being the angle which connects the solar neutrino parameter space spanned by ω, ϕ, and δ_{21} with the atmospheric neutrino space spanned by ϕ, ψ, and δ_{31}, the constraint on ϕ also translates into a strong constraint in the solar neutrino parameter space. Now observe what is probably the most important consequence of the CHOOZ result. The fact that ϕ, the link between the solar and the atmospheric neutrino problems is constrained to be small implies that *the solar neutrino problem can be essentially viewed as a two flavor $\nu_e \leftrightarrow \nu_\mu$ oscillation phenomena, and the atmospheric neutrino problem essentially as a two flavor $\nu_\mu \leftrightarrow \nu_\tau$ oscillation phenomena even in a three flavor framework.*. We mention that this remarkable result implies that for the solar neutrino problem there is essentially only the small angle and the large solutions. See Fig from chapter.(2) where the parameter space for $\phi = 10°$ is shown. There is no discernible change as compared to the $\phi = 0°$ case. So the Super-Kamioka constraint on the two flavor parameter space which comes from the absence of day-night effect, even though it comes from a two flavor analysis is really a very strong constraint.

Lastly we analyze the consequences of the CHOOZ result for the tentative signal reported earlier by the LSND collaboration. In the ref. [51] the results of the LSND Collaboration [52] were analyzed in the same three flavor framework, along with the atmospheric neutrino problem. It was found that there is a small region of overlap between the respective parameter spaces allowed by each experiment. Hence one could account for the solar neutrino problem, the atmospheric neutrino problem and the LSND results in a three flavor framework. This is no longer possible if one takes the CHOOZ result into account. If the CHOOZ constraint $\phi \leq 12.5°$ is imposed, then the lower limit on δ_{31} from LSND goes upto about 0.1 eV^2, which is larger than the maximum allowed value from the atmospheric neutrino analysis. Hence it is not possible to explain the solar and the atmospheric neutrino problems and at the same time satisfy the results of the CHOOZ and LSND experiments in a three neutrino flavor framework.

Hence in conclusion the recent CHOOZ result enables us to draw the following conclusions.

- It establishes the fact that the atmospheric neutrino anomaly is mainly driven by $\nu_\mu \leftrightarrow \nu_\tau$ i.e vacuum oscillations.

- It demonstrates that even in a three flavor analysis, the solar and the atmospheric neutrino problems approximately decouple from each other.

- It excludes large parts of the parameter space previously allowed as solutions to solar and atmospheric neutrino data.

- It is not possible to reconcile CHOOZ and LSND signals in a three flavor framework.

5.3 Borexino

5.3.1 Introduction

As described in chapter.(2), neutrino oscillations, with the MSW effect included, provide the best solution to SNP. If one assumes that the electron neutrino ν_e mixes with only one other active flavor, then the corresponding solution has two disjoint viable regions in the parameter space of mass-squared difference (δ_{21}) and the mixing angle ω. In the region characterized by small mixing angle, the entire flux of ^7Be neutrinos, which has a line spectrum with $E_\nu = 0.861$ MeV, is converted into the other flavor. In the large mixing angle region, only about half of the ^7Be neutrinos oscillate into the other flavor. In a three flavor analysis, depending on the parameters of the three flavor mixing, especially the mixing angles, the flux of ^7Be neutrinos can vary between 0% to 50% of its SSM value [22]. Hence, an accurate measurement of ^7Be flux is of paramount importance in determining the neutrino oscillation parameters. Further the accurate measurement of ^7Be flux has important implications for the SSM.

Borexino is a real time solar neutrino detector[30], which can measure ^7Be flux quite accurately because the signal rate due to these neutrinos is about 50 events per day for SSM flux. The detection of neutrinos is via $\nu - e$ scattering. The recoil energy of the electrons scattered by the monoenergetic ^7Be neutrinos is expected to be in the range $0.25 - 0.66$ MeV. Hence a kinematic cut on the electron energy in the range $0.25 - 0.80$ MeV, selects events which are almost entirely due to the ^7Be neutrinos [30]. This unique ability to measure the signal due to only the ^7Be neutrinos enables Borexino to distinguish between the different values of the neutrino oscillation parameters, which are currently viable but which predict different suppression factors for the ^7Be neutrinos. Because of its very high statistics, Borexino is an ideal tool to look for day-night effects in solar neutrino signals (which could be a very small effect for some values of the neutrino parameters), and hence probe an appreciable part of the neutrino parameter space, with no dependence at all on the absolute prediction of the ^7Be flux. An evidence for day-night effect from Borexino will be an unambigious signal for neutrino mixing and oscillations. Further if

day-night asymmetry is there Borexino will be able to map out the asymmetry as a function of the distance travelled by the neutrino in the earth during night at a single neutrino energy which will single out a very small region in the neutrino parameter space. Borexino will also be sensitive to the ^8B flux, though 90 percent of its signal will be due to the ^7Be line. In this chapter, we calculate the rates which Borexino will measure, assuming oscillations among all the three active neutrino flavors and arbitrary mixing among the three flavors. We also compute the signals for day-night effect which Borexino can measure for various ranges of the neutrino parameters including those which are preferred solutions to the solar neutrino problem. Day-night effect for Borexino has been analyzed previously [79] and recently in [80] but both have been done in a two flavor framework. We demonstrate that the inclusion of the third flavor can substantially change the results of the two flavor analysis. In particular we point out how the binned asymmetry can give a strong pointer towards the neutrino parameters and show characteristic effects of the third flavor.

5.3.2 Theory

The theoretical framework for Borexino is similar to that of the other solar neutrino experiments with the important difference that there is no energy integration over the neutrino energy, as the dominant contribution is from a line spectrum. Because of this we recall the main features of the theory below. We first analyze the recoil spectrum measured during the day from which one can calculate the total scattering rate.

Let ϕ be the ^7Be flux from the sun as given by the standard solar model. In the absence of neutrino oscillations, we can write number of electrons scattered with energy T

$$N(T) = \frac{d\sigma}{dT}\phi, \qquad (5.8)$$

where $\frac{d\sigma}{dT}$ = electroweak cross-section for $\nu - e$ elastic scattering and N(T) is the spectrum of recoil electrons. The Total scattering rate is given by

$$R = \phi \int_{0.25}^{0.8} \frac{d\sigma}{dT} dT = R_{SSM}. \qquad (5.9)$$

With oscillations one has

$$N(T) = \frac{d\sigma}{dT}\phi P_{ee} + \frac{d\sigma'}{dT}\phi(1 - P_{ee}), \tag{5.10}$$

where P_{ee} is the electron neutrino survival probability (we shall discuss this in detail later) as a function of the neutrino energy ($E_\nu = 0.861 MeV$) and $\sigma' = \nu_x - e$ elastic scattering cross-section, where $x \neq e$.

The total scattering rate R is

$$R = \phi P_{ee} X + \phi(1 - P_{ee})Y, \tag{5.11}$$

where

$$X = \int_{0.25}^{0.8} \frac{d\sigma}{dT} dT$$

and

$$Y = \int_{0.25}^{0.8} \frac{d\sigma'}{dT} dT.$$

Since

$$R_{SSM} = \phi X,$$

we get

$$\frac{R}{R_{SSM}} = P_{ee} + \frac{Y}{X}(1 - P_{ee}). \tag{5.12}$$

Hence, the ratio $\frac{R}{R_{SSM}}$ allows one to directly extract P_{ee}, and hence strongly constrain the vacuum parameters. Note that R_{SSM} involves the SSM flux of ^7Be, and therefore even though one can extract P_{ee} from the experimental number, it is still dependent on the SSM flux. The major gain with respect to other detectors is the fact that one can get P_{ee} at a single neutrino energy as there is no integration over the neutrino spectrum. Also note that the recoil spectrum (i.e $N(T)$ vs T) as well as the total rate just scale with respect to the SSM expectations.

We now focus on the day-night effect. We define the day-night asymmetry as

$$A = \frac{N - D}{N + D}, \tag{5.13}$$

where D is the usual day time scattering rate defined previously (R), and N is the scattering rate at night after the neutrino has travelled a distance x through the

earth (x is dimensionless , expressed as a fraction of the earths diameter).

$$N = \frac{d\sigma}{dT}\phi P_{ee}^N + \frac{d\sigma'}{dT}\phi(1 - P_{ee}^N),$$ (5.14)

where P_{ee}^N is the electron neutrino survival probability after travelling a distance x through the earth. Note that P_{ee}^N differs from P_{ee}^D since the neutrinos travel through the solar matter as well as through the earth. For some parameter ranges this second travel may introduce drastic changes. i.e P_{ee}^N is a function of E_ν, x as well as of the vacuum parameters. So A becomes

$$A = \frac{P_{ee}^N - P_{ee}^D}{P_{ee}^N + P_{ee}^D + \frac{2X}{X-Y}}$$ (5.15)

where P_{ee}^D is the same P_{ee} defined previously in eq.(5.10). Note that the day-night asymmetry unlike the ratio $\frac{R}{R_{SSM}}$ is completely independent of the SSM fluxes, and is dependent only on the particle physics aspect i.e., only on the oscillation probabilities and the scattering cross sections. This is where Borexino has an advantage over the other real time detectors. The average asymmetry is defined as

$$<A> = \frac{<N> - <D>}{<N> + <D>}$$ (5.16)

where $<N>$ means the night rate integrated over all the x bins.

As before we parametrize the neutrino mixing matrix U in vacuum as $U = U^{23}(\psi)U^{13}(\phi)U^{12}(\omega)$ where $U^{ij}(\theta_{ij})$ is the two flavor mixing matrix between the ith and the jth mass eigenstates with the mixing angle θ_{ij}, neglecting CP violation. In the solar neutrino problem ψ drops out [12, 24]. The mass differences in vacuum are defined as $\delta_{21} = \mu_2^2 - \mu_1^2$ and $\delta_{31} = \mu_3^2 - \mu_1^2$. It has been shown [22, 28] that the simultaneous solution of both the solar and the atmospheric neutrino problems requires the mass hierarchy $\delta_{31} \gg \delta_{21}$ and under this condition δ_{31} also drops out. The rediagonalization of the mass matrix in the presence of matter (in the sun or earth) under the hierarchy condition leads to the following results [22]

$$\tan 2\omega_m = \frac{\delta_{21} \sin 2\omega}{\delta_{21} \cos 2\omega - A \cos^2 \phi},$$ (5.17)

$$\sin \phi_m = \sin \phi,$$ (5.18)

$$\delta_{21}^m = \delta_{21} \cos 2(\omega - \omega_m) - A \cos^2 \phi \cos 2\omega_m ,$$ (5.19)

where A is the Wolfenstein term $A = 2\sqrt{2}\, G_F\, N_e\, E$ (N_e is the number density of electrons and E is the neutrino energy) . We note that $\delta_{31} \gg A$, for A evaluated at any point in the sun or the earth. In eqs (5.17) - (5.19), the "m" stands for matter and in using these equations, one must use the appropriate density of matter that is required at the various points along the trajectory of the neutrino.

The probability for an electron neutrino produced in the solar core to be detected as an electron neutrino on earth at day (in the heirarchy defined above) , averaged over the time of emission and the time of absorption, has been shown to be[22]

$$
\begin{aligned}
P_{ee}^D &= \cos^2\phi\cos^2\phi_m\left(\cos^2\omega\cos^2\omega_m + \sin^2\omega\sin^2\omega_m\right) + \sin^2\phi\sin^2\phi_m \\
&\quad - x_{12}\cos^2\phi\cos^2\phi_m\cos 2\omega\cos 2\omega_m.
\end{aligned}
\tag{5.20}
$$

Where x_{12} is the Landau Zener jump probability between the first and second mass eigenstates, for a exponentially varying density profile, which is taken from [12]. Note this expression for P_{ee}^D is derived in a different framework in [68]. In [68], one averages the exact formula for P_{ee}^D only over the resonance width to get the formula in eq.(5.20), i.e., does not have to average over the time of absorption.

The derivation of P_{ee}^N is quite complicated and is given in the previous chapter on day-night effect. For example for trajectories that pass only through the mantle we get

$$
P_{ee}^N = P_{ee}^D + \frac{[1 - 2P_{ee}^D - |U_{e3}|^2(2 - |U_{e3}|^2)]}{(|U_{e1}|^2 - |U_{e2}|^2)} \times (P_{2e}^E - |U_{e2}|^2),
\tag{5.21}
$$

where U_{ei} are elements of the first row of the vacuum neutrino mixing matrix and P_{2e}^E is the probability of the second mass eigenstate oscillating to the electron flavor at the point of detection. It is given by

$$
P_{2e}^E = \cos^2\phi[\sin^2\omega_E + \sin 2\omega_E\sin 2(\omega_E - \omega)\sin^2\Phi_{12}].
\tag{5.22}
$$

Here ω_E is the mixing angle in matter evaluated at the point of detection, and Φ_{12} is given by

$$
\Phi_{12} = \frac{1}{2}\int_{t_1}^{t_2}(\varepsilon_1^E(t) - \varepsilon_2^E(t))dt,
\tag{5.23}
$$

where ε^E are mass eigenvalues in earth, and t_1 refers to the time when the neutrino mass eigenstate hits the surface of the earth from the core of the sun, and t_2 refers to point of detection in the earth. The equation is much more complicated for

trajectories that cross the core of the earth also. The method of computing it, as well as other details about the day-night effect is outlined in the previous chapter. For Borexino in a year less than 5 percent of the events pass through the core, so core events are very small in number as compared to events that go through mantle only.

5.3.3   Results and discussions

We first compute the recoil spectrum during day. We calculate the recoil spectrum for various values of the vacuum parameters including those which are the favoured solutions to the solar neutrino problem. The crosssections are taken from [14]. Then we compute A, and $< A >$ for a range of vacuum parameters including those which are favoured solutions to the solar neutrino problem.

In Fig.(5.5) we show the recoil spectrum of the scattered electrons (during day time) for various values of the vacuum parameters. The top curve is for the SSM, i.e., no oscillation case. The curve labelled (a) corresponds to the small angle solution to the solar neutrino problem, while that labelled (b) corresponds to the large angle solution. The curve labelled (c) is a three flavor solution to the solar neutrino problem. One sees that the recoil spectrum, and hence the total rate basically just scale w.r.t the SSM (i.e no oscillation) recoil spectrum. So just knowing the scale factor gives one a strong pointer towards the vacuum parameters.

We show the average asymmetry as a function of the vacuum parameters in the form of a contour plot. Fig.(5.6) is the plot for $\phi = 0.0°$ i.e a two flavor case. The enhancement factor (regarded as a percentage) increases by 10% for every adjacent ring, as we move inwards towards the centre of the plot. Note the large enhancement region ($\approx 20 - 30$) percent are for $\delta_{21} < 10^{-6} eV^2$. This is simply a reflection of the low energy of the ^7Be line (0.861 MeV) i.e the Wolfenstein term A in the earth at the energy of the ^7Be line is order of $10^{-7} eV^2$, and hence if δ_{21} is close to A one can get large enhancement in the matter mixing angle, and so a large asymmetry. Note that our result agrees very well with that of Bahcall. This clearly illustrates the robustness of our analytic approach vis a vis numerical integration. Figs. (5.7),

The reason for nonzero ϕ diluting the asymmetry is twofold.

1) Unitarity demands that $\sum_i P_{ie}^E = 1$. This means that in three flavors P_{2e}^E is always less than its value in the two flavor case.

2) The resonance condition in the case of three flavors has the form

$$A \cos^2 \phi = \delta_{21} \cos 2\omega. \tag{5.24}$$

Since, for Borexino the neutrino energy is fixed, a resonance which occurs at a given density in the core of the earth in the two flavor case $\phi = 0$ will either occur at a higher density or it will not occur at all. Thus the resonance effect is suppressed in the case of three flavors. Note that for the region of δ_{21} favoured by the solar neutrino solutions, $(10^{-6}$ to $10^{-4} eV^2)$ day-night effect is rather small even while it is nonzero. Therefore from the contours for various values of ϕ it is obvious that if Borexino sees small day-night effect, it either points to a large (13) mixing irrespective of δ_{21} and ω, or small (13) mixing with δ_{21} in the region favoured by the MSW solutions to the solar neutrino problem . Conversely a large day-night effect would point to small (13) admixture and δ_{21} small i.e $< 10^{-6} eV^2$. One also sees that from the day-night contours the above conclusions are valid for a large range of ω. So to get further constraints on the vacuum parameters one needs further information which is provided by looking at the day-night asymmetry as a function of the distance travelled by the neutrino during night, i.e., one needs to look at binned asymmetries.

In Figs. (5.10) and (5.11) we show the day-night asymmetry as a function of x for some representative values of the neutrino parameters. Fig.(5.10) is for $\phi = 0.0°$ and Fig.(5.11) is for $\phi = 30.0°$. In each panel in the above figures, small dashes correspond to $\omega = 5°$, large dashes to $\omega = 40°$ and solid line to $\omega = 20°$ all for a fixed value of δ_{21}.

Different values of these parameters have distinguishable characteristics. Some gross features which may enable us to specify their approximate domains are the following:

- For small (12) mixing angle ω there is a gradual increase of the asymmetry with x, whereas for large ω the oscillations in x start showing up. For $x < 0.84$ (i.e.

trajectories through mantle only) there is a very clear discrimination between the small ω and large ω, irrespective of δ_{21} and ϕ.

- For $\phi = 0$ and $\delta_{21} > 2.51 \times 10^{-6}eV^2$, the asymmetry is negligible. So null day-night effect at Borexino implies that for $\phi = 0$ or very small, δ_{21} is in the range given by the MSW solutions to the solar neutrino problem.

- Note that for $\delta_{21} > 10^{-6}eV^2$, there is hardly any asymmetry for the small ω, while for large ω, it shows up as regular oscillations with a oscillation wavelength which is close to the vacuum oscillation length. The reason being that for $\delta_{21} > 10^{-6}eV^2$, the Wolfenstein term is quite small compared to δ_{21}. If $\varepsilon = \frac{A}{\delta_{21}}$, then it is easy to show that (for $\phi = 0$)

$$\delta_{21}^m \approx \delta_{21}(1 - \varepsilon(x)\cos(2\omega)) \tag{5.25}$$

and

$$\Phi_{12} = \int \delta_{21} \frac{(1 - \varepsilon(x)\cos(2\omega))}{2E} dx, \tag{5.26}$$

where δ_{21}^m denotes differences of mass eigenvalues in matter. Hence the mass squared difference in matter is almost the same as the vacuum mass squared difference which results in the oscillation wavelength in matter being close to the vacuum oscillation length, with the approximation becoming more exact as ω increases. Here we see an intriguing feature, i.e there is day-night asymmetry, hence matter effect(although small), but the oscillations in matter being controlled by the vacuum oscillation length. The above conclusion holds for nonzero ϕ also with the difference that the asymmetry is less than that for $\phi = 0$.

- As ϕ increases, the asymmetry at any x decreases.

- The amplitude of the oscillatory pattern is largest for small δ_{21} and decreases steadily as δ_{21} increases.

- For small ω and large δ_{21}, asymmetry is appreciable only in the core and is a sensitive function of δ_{21}.

Lastly as remarked before, in light of the CHOOZ result, one essentially has only the large or the small angle solution to the solar neutrino problem. So the Borexino measurement of the ^7Be can really pick out the solution to the solar neutrino problem. Hence in conclusion the Borexino measurements could be some of the most decisive results in neutrino physics.

We now briefly point out the importance of the Sudbury Neutrino Observatory (SNO) [29], which is expected to begin operating in the near future.

The Sudbury Neutrino Observatory (SNO) [29] is high statistics real time detector like Super-Kamiokande with an expected threshold of $5MeV$. The target material in SNO is deuterium instead of water which is what is used in Super-Kamioka. Hence unlike Super-Kamioka which measures the solar neutrino flux only via neutrino electron scattering, in SNO it will also be possible to study the following two reactions *seperately* [81].

$$\nu_x + D \rightarrow n + p + \nu_x \qquad (5.27)$$

where x can be e, μ or τ, and

$$\nu_e + D \rightarrow p + p + e^-. \qquad (5.28)$$

Observe that eq.(5.27), which is the neutrino dissociation of the deuteron is a neutral current process. This reaction is flavor blind, and hence all flavors of neutrinos can contribute. Therefore this reaction will measure the total neutrino flux. Eq.(5.28) which is a charged current reaction is accessible only for the electron type of neutrinos. Therefore this reaction will measure the total electron neutrino flux. If this measurement is different from that of the total flux, then one has a signal for neutrino oscillations *independent of the SSM flux predictions*. Thus SNO is another experiment which can conclusively confirm the phenomenon of neutrino oscillations.
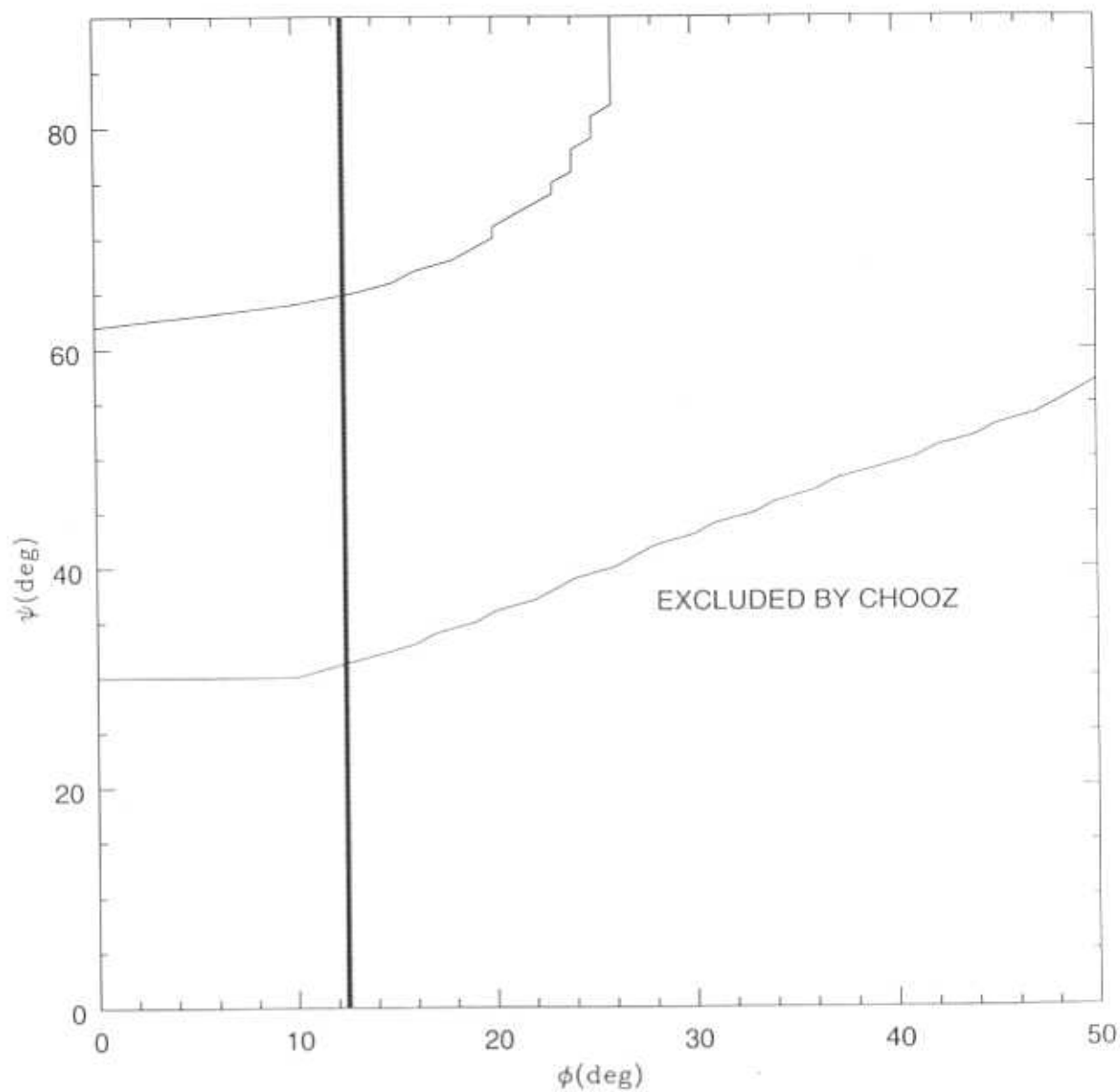
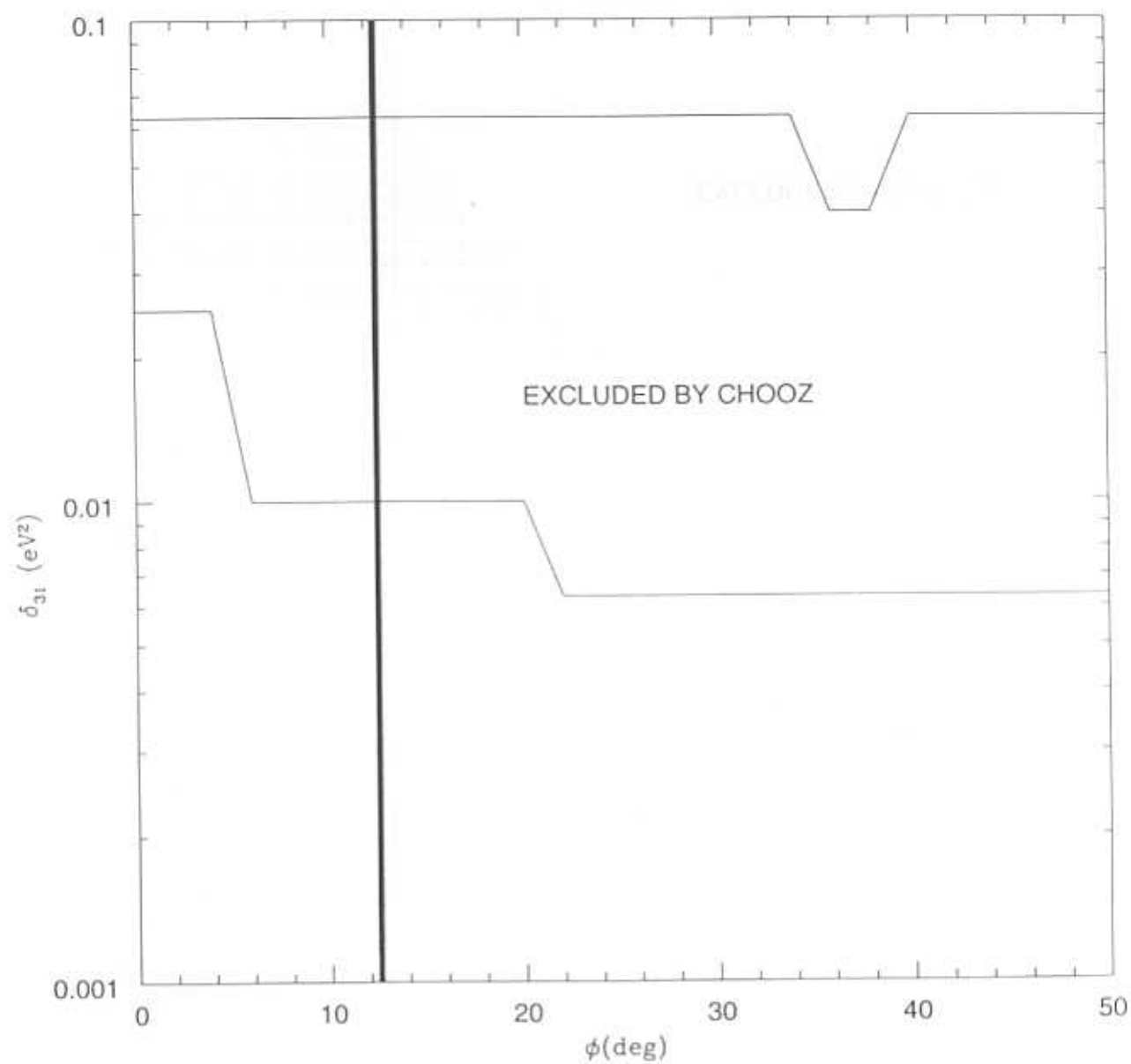Figure 5.1: Allowed region in $\phi - \psi$ plane by the sub-GeV data

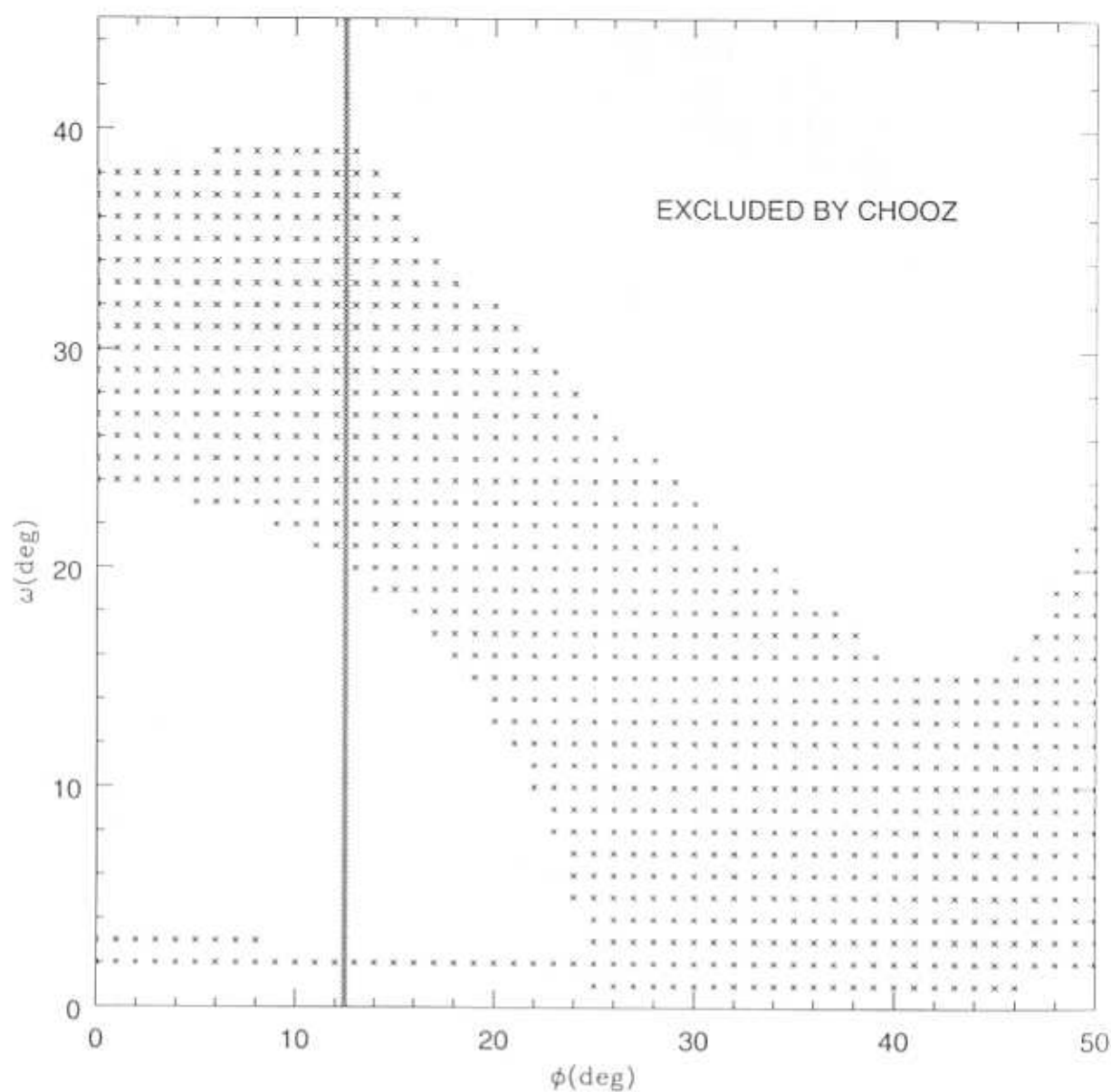Figure 5.2: Allowed region in $\phi - \psi$ plane by the sub-GeV data

117

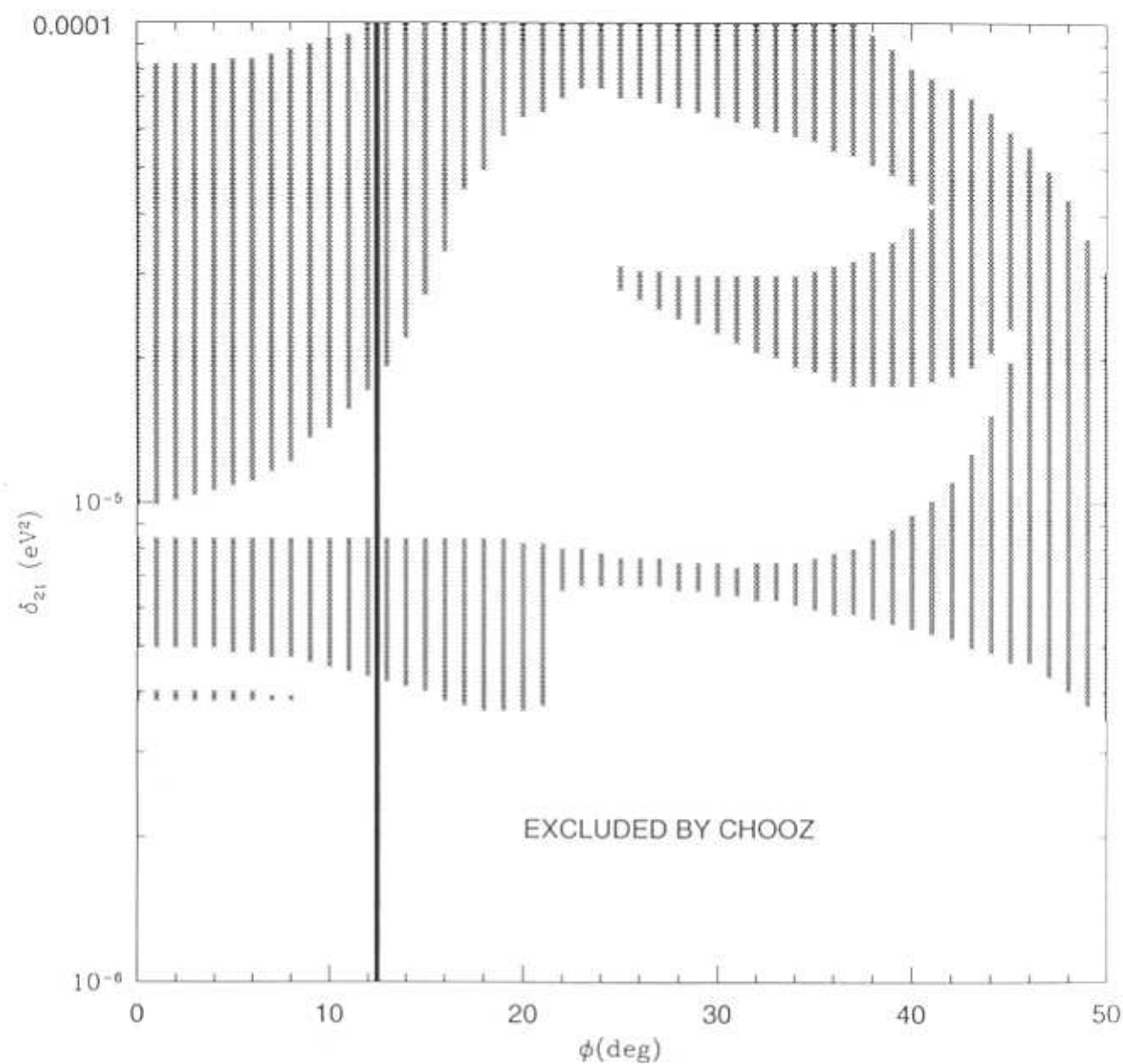Figure 5.3: Allowed region in $\phi - \psi$ plane by the sub-GeV data

Figure 5.4: Allowed region in $\phi - \psi$ plane by the sub-GeV data
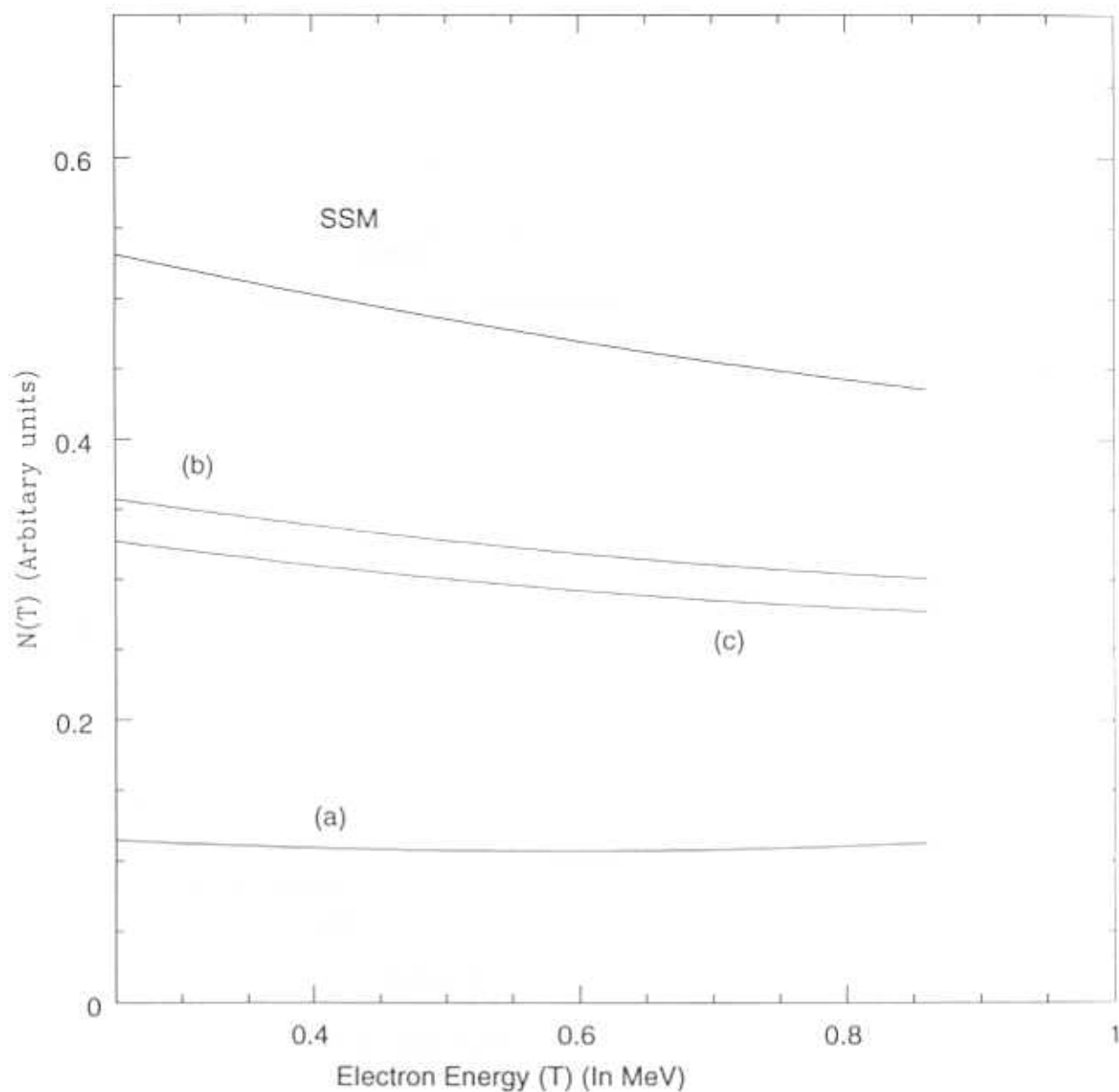
Figure 5.5: Recoil spectrum of the scattered electrons. (a) $\delta_{21} = 6.0 \times 10^{-6}, \omega = 2.5°, \phi = 0.0°$; (b) $\delta_{21} = 3.0 \times 10^{-5}, \omega = 28.0°, \phi = 0.0°$; (c) $\delta_{21} = 9.0 \times 10^{-5}, \omega = 24.5°, \phi = 24.0°$;
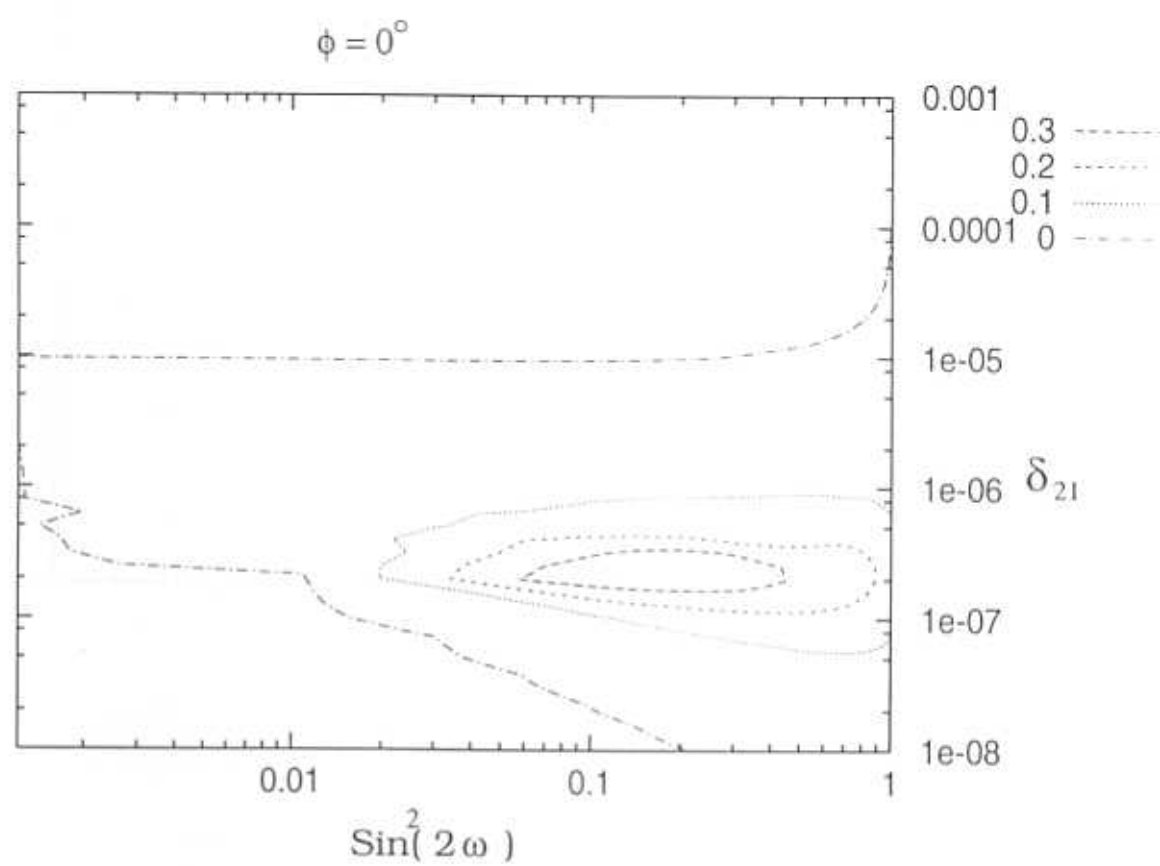
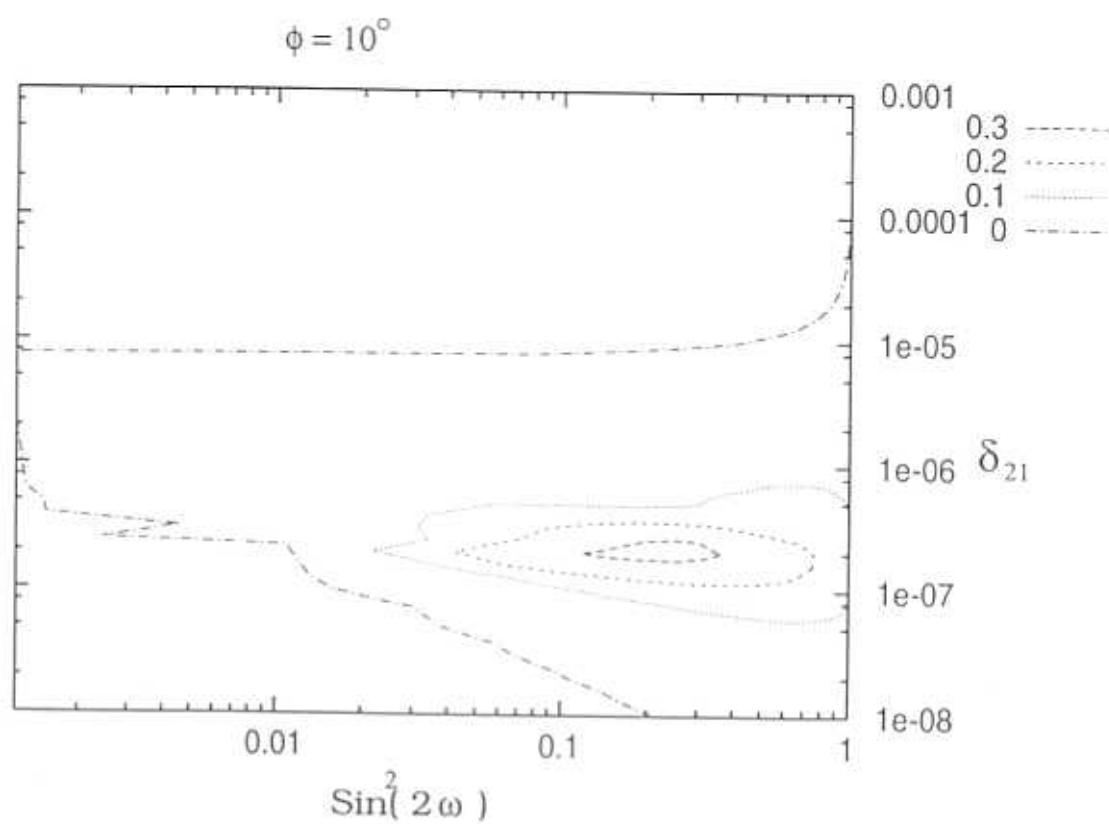Figure 5.6: Average Asymmetry for $\phi = 0.0^o$ (δ_{21} is in eV^2).

Figure 5.7: Average Asymmetry for $\phi = 10.0°$ (δ_{21} is in eV^2).
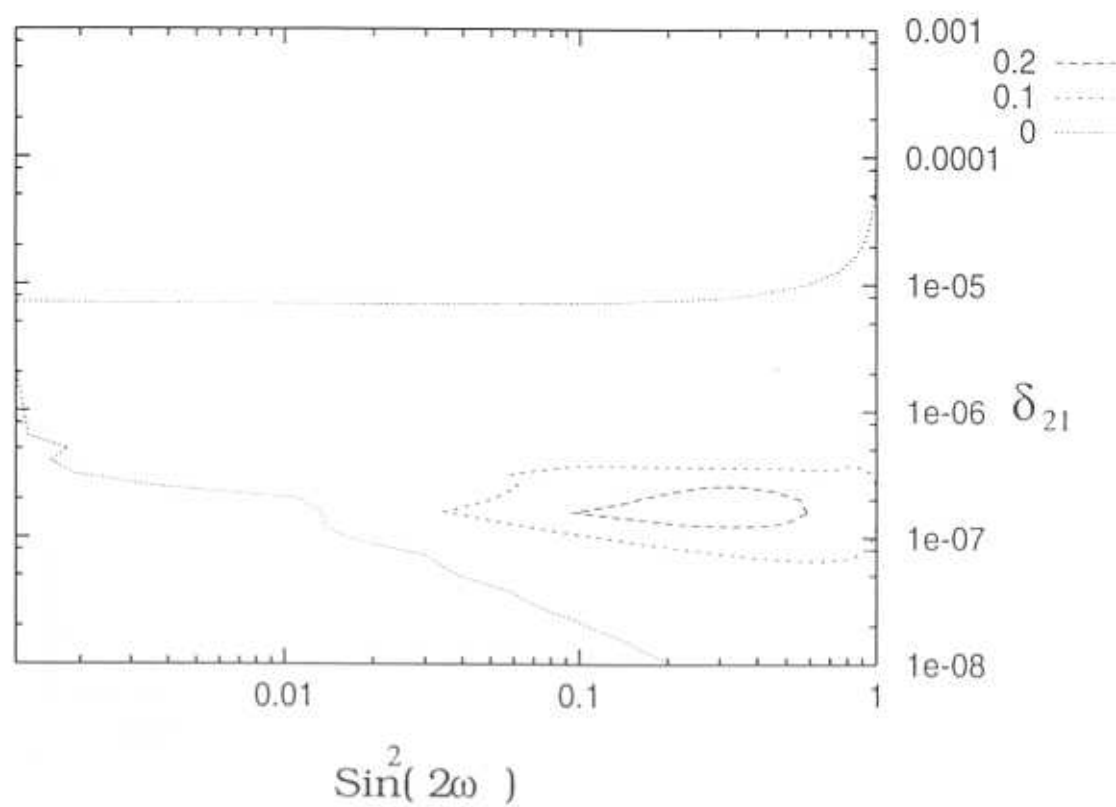
$\phi = 30^\circ$

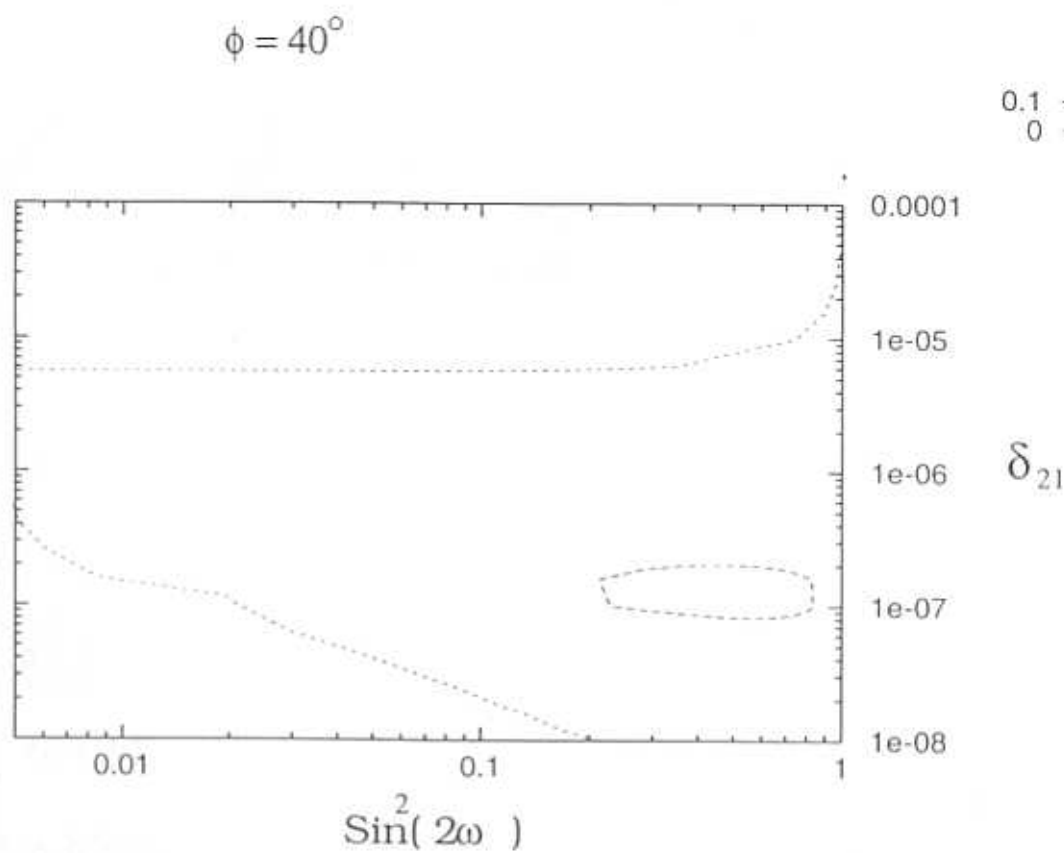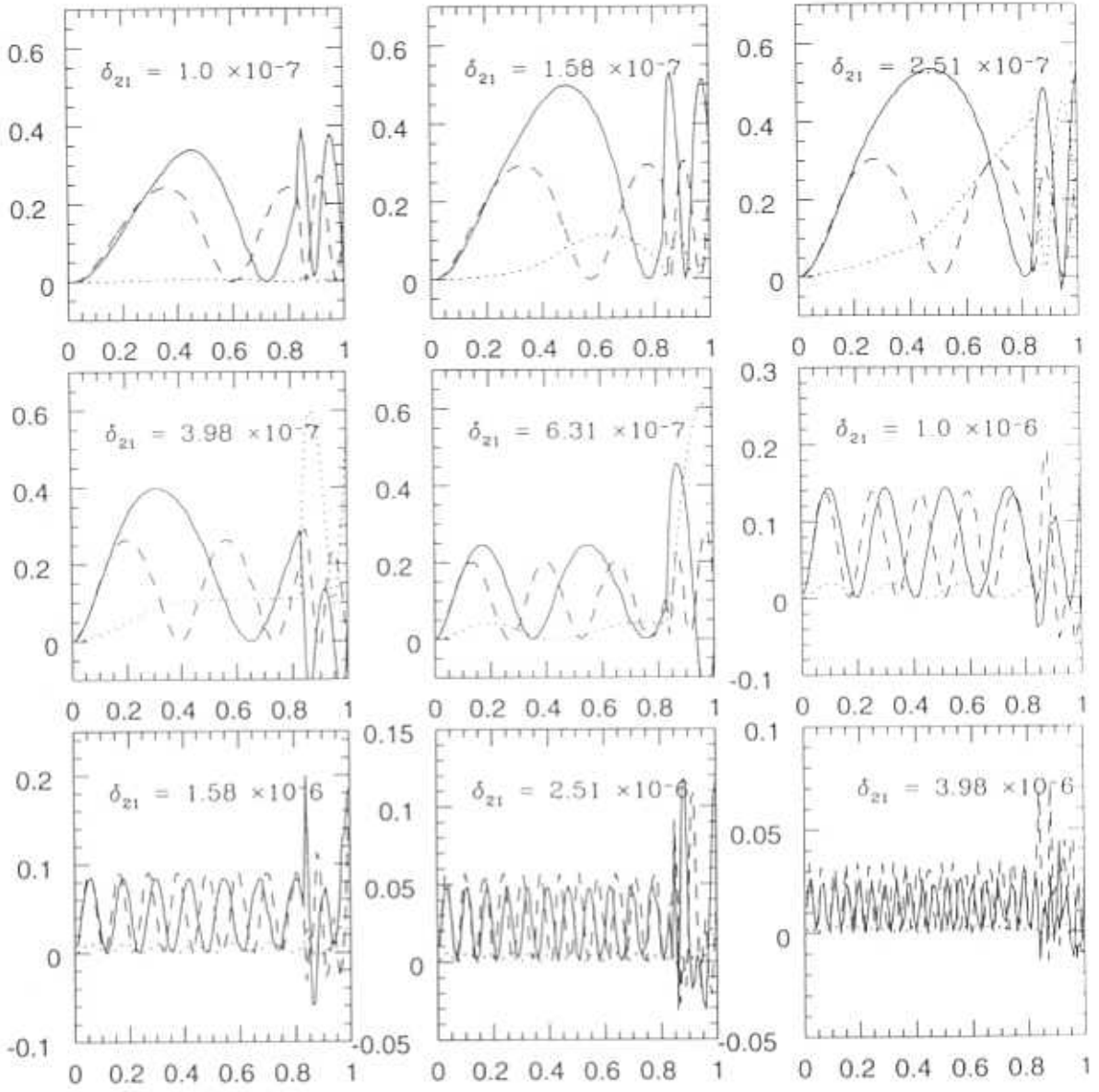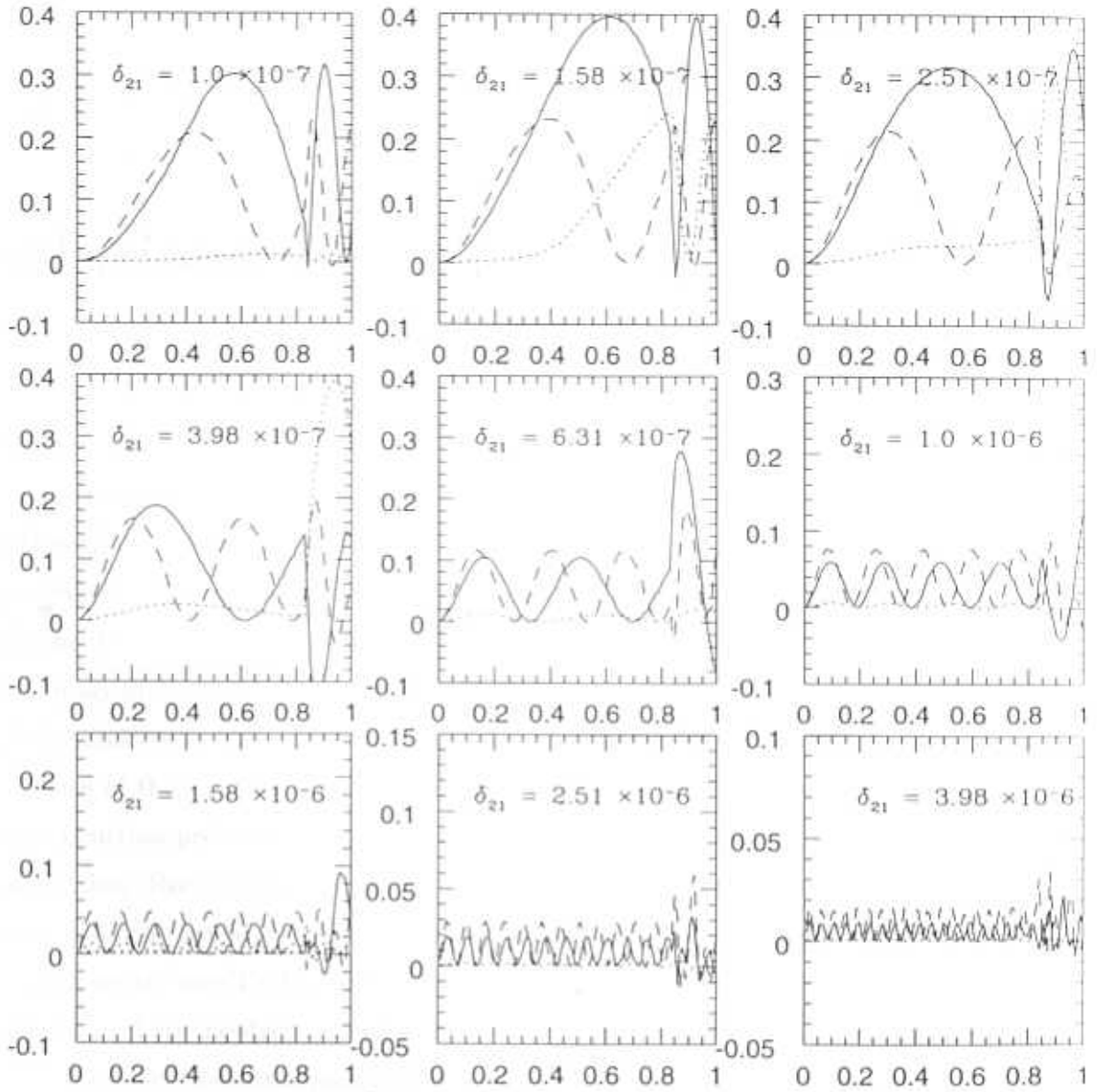Figure 5.8: Average Asymmetry for $\phi = 30.0^\circ$ (δ_{21} is in eV^2).

Figure 5.9: Average Asymmetry for $\phi = 40.0°(\delta_{21}$ is in $eV^2)$.

Figure 5.10: Binned asymmetry for $\phi = 0.0^\circ$

Figure 5.11: Binned asymmetry for $\phi = 30.0°$

Chapter 6

Conclusions

The Solar neutrino problem has been an persistent problem in neutrino physics for more than three decades. The discrepancy between experiment and the standard solar model estimates first seen in the Davis experiment has been confirmed by three other experiments. Thus the observation of the deficit in the neutrino flux dubbed as the solar neutrino problem is a real problem. At present astrophysical solutions seem to be highly disfavoured, hence pointing to some nonstandard neutrino physics as a possible solution to this anomaly. The idea of nonstandard neutrino physics being the cause of the solar neutrino deficit has been given further impetus by the atmospheric neutrino problem, which was reported by the Kamioka as well as the IMB collaboration. Recently Super-Kamioka, an upgraded version of Kamioka with much higher counting rates, has also confirmed the deficit in the atmospheric neutrino flux with better sensitivity. The zenith dependence of the suppression in the Multi-GeV atmospheric neutrino events, observed by Kamioka is also a very significant event. Together these two problems constitute a major challenge to neutrino physics and some nonstandard properties of neutrinos are strongly suggested as the possible solution to these anomalies.

One of the most natural extensions of the standard model is to assume that neutrinos are massive. This in turn can lead to mixing and oscillations between the various flavors of neutrinos. In this thesis, we have demonstrated that, if one assumes mixing between the three known flavors of neutrinos, then one can find a

solution to the Solar and the atmospheric neutrino problems in a consistent way. There exists an appreciable region in the three flavor parameter space, which can account for both the solar and the atmospheric neutrino data.

If neutrino oscillation is indeed the cause of the solar and the atmospheric neutrino oscillations, then for some values of the neutrino parameters, there could be significant day-night and eclipse effects. These effects are model independent signatures of neutrino oscillations. The observation of positive signals for these novel effects will have significant impact on the parameter space. Conversely even the absence of such effects constrain some part of the neutrino parameter space. In this thesis we have done a thorough analysis of such effects for the existing as well as for the future high statistics real time detectors in a three flavor framework. The existing detectors are not the ideal ones to observe the day-night effect since the neutrinos for most part of the year travel through the mantle, a detector situated close to the equator will be a boon to the study of day-night effect.

The parameter space allowed by solar and atmospheric neutrino data were completely consistent with all the previously running reactor and accelerator experiments which were short baseline experiments. The recent result from the CHOOZ experiment is the first result of a long baseline experiment. We have shown in this thesis that a three flavor analysis of the CHOOZ result has dramatic consequences for the solar and the atmospheric neutrino problems. An appreciable part of the allowed three flavor parameter space is ruled out by the CHOOZ result when properly analysed in a three flavor framework. Note that these conclusions could not have been reached in a two flavor framework. In fact in a two flavor framework the CHOOZ result is inconsistent with the atmospheric neutrino problem. A three flavor analysis resolves this contradiction. It should be mentioned at this stage that future long baseline experiments will be able to confirm the CHOOZ result, as well as further probing the neutrino parameter space. In fact different parts of the neutrino parameter space can be probed by tuning the neutrino energy and the distance it travels between the source and the detector. While the Solar and the atmospheric neutrino deficits have focussed the attention on the neutrino properties, perhaps the most precise information on neutrino parameters is to be expected from long

baseline experiments in the near future. Since these are lab experiments one has better control on the experiments.

Among the next generation of solar neutrino experiments, SNO and Borexino will play a major role in distinguishing allowed solutions of the solar neutrino problem, and hence as a consequence the atmospheric neutrino problem also. In this thesis we have done a three flavor analysis of the physics prospects of Borexino, and shown that coupled with the CHOOZ result Borexino can narrow down available range for the actual solution to the solar neutrino problem. SNO can in a model independent way test the hypothesis of neutrino oscillations. Together SNO and Borexino can unambiguously demonstrate neutrino oscillations as the cause of the solar neutrino problem.

In conclusion neutrino oscillations between the three known flavors of neutrinos provide a robust solution to the solar and the atmospheric neutrino problems. The allowed region in the three flavor parameter space will be severely constrained by the next generation of experiments, notably by the long baseline experiments, Borexino and SNO.

Now if one accepts neutrino oscillations as the reason for the solar and the atmospheric neutrino anomalies, then it is natural to look for the dynamical origin of these masses and mixing angles. Various extensions of the standard model can give rise to such masses and mixing angles. There have been enough effort in recent years in this direction, but all these models are rather fine tuned and have met only with very limited success. So one of the most challenging problems in neutrino physics will be to construct a mass model which is consistent with what is allowed today in the three neutrino parameter space. Another important issue is the question of CP violation in the lepton sector, which can arise from the complex phase in the neutrino mixing matrix. CP violation can in principle be determined by using data from long baseline experiments. Recently there have been efforts to analyse CP violation effects, in long baseline experiments though more refined analyses are called for.

Neutrinos by virtue of being one of the most favoured candidates for hot dark matter (HDM) can play a major role in Cosmology. Neutrinos are also emitted by

supernovae. (In fact Kamioka was the first experiment to detect neutrino bursts from a supernova). It will an interesting exercise to see what repurcussions, the values of the neutrino parameters allowed by present solar, atmospheric and long baseline data have for the role of neutrinos in cosmology.

Bibliography

1. F. Reines and C. L. Cowan, Phys. Rev. **90**, 492 (1953).

2. G. Danby *et al*, Phys. Rev. Lett. **9**, 36, (1962).

3. Particle Data Group, Phys. Rev. **D50**, (1994).

4. The upper limit of $7.3eV$ is the so called "PDG" upper limit, the average value of different experiments. See "Review of Particle Properties by Particle Data Group", Phys. Rev. **D45**, (1992).

5. R. Abela *et al*, Phys. Lett. **B146**, 431, (1984).

6. H. Albrecht *et al*, Phys. Lett. **B163**, 404, (1985).

7. A. Balysh *et al* (Heidelberg-Moscow Experiment), Phys. Lett. **B356**, 450, (1995).

8. B. Pontecorvo, Zh. Eksp. theor. Fiz. **33**, 549 (1957) [JETP. **6**, 439 (1958)], *ibid*. **53**, 1717 (1969) [JETP **26**, 989 (1967)].

9. H. A. Bethe, Phys. Rev. Lett. **56**, 1305 (1986).

10. L. Wolfenstein, Phys. Rev. **D17**, 2369 (1978); **D20**, 2634 (1979)

11. S. P. Mikheyev and A. Yu. Smirnov, Yad. Fiz. **42**, 1441 (1985) [Sov. J. Nucl. Phys. **42**, 913 (1985)]; Nuovo Cimento, **9C**, 17 (1986).

12. T. K. Kuo and J. Pantaleone, Rev. Mod. Phys. **61**, 937 (1989).

13. Stephen Parke, Phys.Rev.Lett. **57**, 1275(1986).

14. J. Bahcall, *Neutrino Astrophysics*, Cambridge University Press.

15. J. N. Bahcall and M. H. Pinsonneault, Rev. Mod. Phys. **67**, 781 (1995).

16. K. Lande, (Homestake Collabaration), in the 4th international Solar Neutrino conference, Heidelberg, Germany, 1997, to appear in the proceedings.

17. Y.Fukuda *et al*, (kamiokande Collabaration), Phys. Rev. Lett. **77**, 1683 (1996)

18. SAGE Collabaration, in LP'97, 28th International Symposium on Lepton Photon Interactions, Hamburg, Germany, 1997, to appear in the proceedings.

19. M.Cribier (GALLEX Collabaration), in TAUP' 97 5th International Workshop on Topics in Astroparticle and Underground Physics, Laboratori Nazionali del Gran Sasso , Assergi, Italy, 1997, to appear in the proceedings.

20. Y. Totsuka (Super-Kamioka Collabaration), in LP'97, 28th International Symposium on Lepton Photon Interactions, Hamburg, Germany, 1997, to appear in the proceedings.

21. N. Hata and P. Langacker, Phys. Rev. **D56**, 6107 (1997).

22. M. Narayan, M. V. N. Murthy, G. Rajasekaran and S. Uma Sankar, Phys. Rev. **D53**, 2809 (1996).

23. T. K. Kuo and J. Pantaleone, Phys. Rev. **D35**, 3432 (1987).

24. A. S. Joshipura and M. V. N. Murthy, Phys. Rev. **D37**, 1374 (1988).

25. Kamiokande Collabaration: K. S. Hirata *et al*, Phys. Lett. **B280**, 146 (1992).

26. Kamiokande Collabaration: Y. Fukuda *et al*, Phys. Lett. **B335**, 237 (1994).

27. L. D. Landau and E. M. Lifshitz, *Non-relativistic Quantum Mechanics*, 3rd Edition (1977), Pergamon Press.

28. G. Fogli, E. Lisi and D. Montanino, Phys. Rev. **D49**, 3626 (1994); *ibid.* **D54**, 2048 (1996).

29. G. T. Ewan et al., Sudbury Neutrino Observatory Proposal, Pub.No.SNO-87-12 (1987).

30. "Borexino at Gran Sasso", Proposal for a real time detector for low energy solar neutrinos, Edited by G. Bellini, M. Campanella, D. Guigni and R. S. Raghavan (1991)

31. M. Honda *et al*, Phys. Rev. **D52**, 4985 (1995).

32. Agrawal *et al*, Phys. Rev. **D53**, 1314 (1996).

33. IMB Collaboration: D. Casper *et al.*, Phys. Rev. Lett. **66**, 2561(1991); R. Becker-Szendy *et al.*, Phys. Rev. **D46**, 3720(1992).

34. IMB Collaboration observed a deficit of muon-like events in their data compared to the Monte-Carlo prediction as early as 1986 and have speculated whether this deficit is due to non-Standard Physcis. T. J. Haines *et al*, Phys. Rev. Lett. **57**, 1986 (1986).

35. V. Barger *et al*, Phys. Rev. **D22**, 2718 (1980).

36. G. V. Dass and K. V. L. Sarma, Phys. Rev. **D30**, 80 (1984).

37. J. Pantaleone, Phys. Rev. **D49**, R2152 (1994).

38. S. Goswami, K. Kar and A. Raychaudhury, Int. J. Mod. Phys. **A12**,781 (1997).
    S. Goswami, Phys. Rev. **D55**, 2931 (1997). hep-ph/9507212.

39. S. M. Bilenky, C. Giunti and C. W. Kim, hep-ph 9505301.

40. C. Giunti, C. W. Kim and J. D. Kim, Phys. Lett. **352B**, 357 (1995).

41. D. Harley, T. K. Kuo and J. Pantaleone, Phys. Rev. **D47**, 4059 (1993).

42. G. Fogli, E. Lisi and D. Montanino, Astropart. Phys. **4**, 177 (1995).

43. A. S. Joshipura and P. I. Krastev, Phys. Rev. **D 50**, 3484 (1994).

44. O. Yasuda, TMUP-HEL-9603 February 1996, hep-ph/9602342

45. A. K. Mann, Phys. Rev. **D48**, 422 (1993).

46. We thank Prof. T. Kajita of the Kamiokande Collaboration for providing us with the efficiencies for the detection of various types of events.

47. T. K. Gaisser and J. S. O'Connell, Phys. Rev **D34**, 822 (1986).

48. P. Musset and J. P. Vialle, Phys. Rep. **39C**, 1 (1978).

49. Kamiokande Collaboration, in their analysis in Ref. [26], used the fluxes from G. Barr, T. K. Gaisser and T. Stanev, Phys. Rev. **D39**, 3532 (1989) for $E_\nu < 3\ GeV$ and those from L. V. Volkova, Sov. J. Nucl. Phys. **31**, 784

(1980) for $E_\nu > 10$ *GeV*. For energies between 3 and 10 GeV they have smoothly interpolated between the two fluxes.

50. G. L. Fogli, E. Lisi and D. Montanino, Phys. Rev. **D54**, 2048 (1996).

51. M. Narayan, G. Rajasekaran and S. Uma Sankar, Phys. Rev. **D56**, 437 (1997).

52. LSND Collaboration: C. Athanassopoulos *et al*, Phys. Rev. Lett **77**, 3082 (1996).

53. C. Y. Cardall and G. M. Fuller, Phys. Rev. **D53**, 4421 (1996).

54. Kamiokande Collaboration: K.S.Hirata *et al*,Phys. Rev. **D 44**, 2241 (1991).

55. Kamiokande Collaboration: Y.Fukuda *et al*,Phys. Rev. Lett. **77**, 1683 (1996).

56. Y.Totsuka, Nucl. Phys.(Proc. Suppl.) **B48**, 547 (1996); A. Suzuki, in *Physics and Astrophysics of Neutrinos*, edited by M. Fukugita and A. Suzuki (Springer–Verlag, Tokyo, 1994), page 414.

57. R.S. Raghavan, in *Proceedings of the 25th International Conference on High Energy Physics*, Singapore, 1990, edited by K.K. Phua and Y. Yamaguchi (World Scientific, Singapore, (1991), p. 698.

58. J. M. Gelb, W. Kwong, and S. P. Rosen, Phys. Rev. Lett, **78**, 2296 (1997).

59. For earlier work, see [60, 61, 58] and references therein.

60. M. L. Cherry and K .Lande, Phys. Rev, **D36**, 3571 (1987)

61. A. J. Baltz and J. Weneser, Phys. Rev, **D35**, 528 (1987); *ibid*,**D50**,5971 (1994); *ibid*, **D51**, 3960 (1994).

62. Mohan Narayan, G. Rajasekaran and Rahul Sinha. astro-ph/9702395.

63. We have taken the densities from F. D. Stacey, *Physics Of the Earth*, John Wiley & Sons, Inc., New York. (1977).

64. S.P.Mikheyev and A.Yu. Smirnov, in *New and Exotic Phenomena*, Proceedings of the Moriond Workshop, Les Arc Savoie, France, 1987, edited by O.Fackler and J. Tran Thanh Van (Editions Frontie'res, Gif-Sur-Yvette, France,1987), p. 405.

65. M.Narayan, G.Rajasekaran and Rahul Sinha, Current Science, **70**, 848 (1996), and Erratum.

66. B.Mason and Marc Sher, Preprint of College of William and Mary, Williamsburg VA, WM-94-112 (1994)

67. The global maps are available at URL: http://umbra.nascom.nasa.gov/eclipse/, http: //planets .gsfc.nasa.gov/eclipse/eclipse.html and ftp://ftp.univ-rennes1.fr/pub/Images /ASTRO/charts/years95-99.

68. M.Narayan, G. Rajasekaran and Rahul Sinha, Mod. Phys. Lett, **A13**, 1915 (1998).

69. M. Nakahata, Talk at *International Conference on High Energy Physics*, at Glasgow, August 1994.

70. F. Boehm and P. Vogel, *Physics of Massive Neutrinos*, Cambridge university Press.

71. L. Oberauer and F. von Feilitzsch, Rep. Prog. Phys. **55**, 1093 (1992).

72. MINOS Colloboration proposal, Fermilab Reports No.NuMI-L-63 and No. NuMI-L-79 (unpublished).

73. KEK-PS and Super-Kamiokande Collaboration proposal, University of Tokyo report, 1995 (unpublished).

74. E889 Collaboration proposal, Brookhaven National Laboratory Report No. BNL-52459 (unpublished).

75. ICARUS Collaboration proposal, Laboratori Nazionali del Gran Sasso (LNGS, Italy) Reports No. LNGS-94-99 (Vol.1 and 2) and No. LNGS-95-10 (unpublished).

76. T. Ypsilantis *et al*, CERN Report No. CERN-LAA-96-02 (unpublished).

77. NOE Collaboration, Letter of intent to the Scientific Committee of Gran Sasso Laboratory (Dec. 1995), University of Naples Report (unpublished).

78. The CHOOZ Collaboration: M. Apollonio *et al*, Phys. Lett. **B420**, 397 (1998).

79. R.S. Raghavan, A.B. Balantekin, F. Loreti, A.J. Baltz, S. Pakvasa, and J. Pantaleone, Phys. Rev. **D44**, 3786 (1991).

80. J.N.Bahcall and P.I.Krastev, Phys. Rev. **C56**, 2839 (1997).

81. Herbert H. Chen, Phys. Rev. Lett. **55**, 1534 (1985).